出版前言

2011年12月11日是西安交通大学杰出校友钱学森先生的百年诞辰。为缅怀钱学森学长，学习他的科学思想和卓越风范，展示其丰功伟绩和人格魅力，西安交通大学举办了“纪念钱学森诞辰100周年”系列活动：作为制片方之一，参与西部电影集团摄制传记故事片《钱学森》；与中央电视台合作，出品纪录片《实验班的故事——沿着钱学森走过的路》；扩建钱学森生平业绩展馆，向校内外开放；举办钱学森科学与教育思想研讨会；出版发行《钱学森力学手稿》、《钱学森年谱（初编）》、《钱学森第六次产业革命思想探微丛书》等。

钱学森先生在美国深造和工作期间留下大量珍贵手稿，这些手稿真实展示了钱学森先生博大精深的学识、开拓求实的精神和严谨奋进的作风，是钱老勇攀科学高峰和严谨治学的集中体现。这里，我们将部分原稿整理汇集成册，出版《钱学森力学手稿》，作为钱老百年诞辰的献礼。

《钱学森力学手稿》共10卷，包含两部分内容。第一部分是草稿，包括扁壳、球壳和圆柱壳屈曲分析的公式推导和数值演算。在研究圆柱壳轴压屈曲问题时，为了求得圆柱壳体的临界压力，在有关的五百多页草稿中，对多达二十多种可能的屈曲模

态逐一进行公式推演和数值计算，最终才找到满意的并在论文中采用的屈曲模态。仔细观察草稿中的数据列表，每个数字有效位数都长达八位，在手摇机械式计算机作为主要计算工具的年代，这串串数字凝聚着多少现今难以想象的艰辛劳动。

第二部分是手稿，以航空航天工程为核心，涵盖空气动力学、固体力学、火箭技术、工程控制论和物理力学等领域的部分学术论文手稿、打印稿和讲义。

《钱学森力学手稿》是在西安交通大学校领导的大力支持下，由西安交通大学航天航空学院沈亚鹏教授整理完成。图书出版过程中得到了西安交通大学党委宣传部、校友关系发展部、图书馆、航天航空学院等的积极协助，在此深表感谢。

Contents

Section 1

Wind-Tunnel Testing Problem in Superaerodynamics

1 org. 4 carbons
double space

1

Wind-Tunnel Testing Problems in Superaerodynamics

Hsue-shen Tsien
Guggenheim Aeronautical Laboratory
Massachusetts Institute of Technology

Wind-tunnels are, perhaps, the most useful tool in aerodynamic investigations and certainly have contributed much in the modern development of fluid mechanics. It is thus natural, when one turns to the new field of aerodynamics, the aerodynamics of rarefied gases or superaerodynamics, that one should think of using the wind tunnel again. Only here ~~the old faithful tool~~ it has to be adopted to entirely new circumstances and many new problems, both in its design and in its operation, appears. It is the purpose of this paper to discuss some of these problems, so as to gain an orientation in the new field of experimentation.

1. Tunnel Design

To test models in the wind tunnel at its test section, it is of primary importance to obtain a uniform stream at the desired temperature, pressure and velocity. For subsonic wind tunnels with ordinary pressures, this can be achieved without much difficulty. For supersonic wind tunnels at ordinary pressures, the expansion part of the tunnel, or the nozzle, before the test section, is first designed to obtain a uniform stream at its exit without considering the effects of the viscosity of air. Then the boundary layer along the wall of the nozzle is calculated with the pressure gradient thus determined. Finally the thickness of the boundary layer, or rather the ~~enlarged~~ needed space for the boundary layer flow at lower velocity is provided by ~~making~~ the nozzle larger than the dimensions first determined by the calculated amount. (Ref 1) This design procedure is found to give satisfactory nozzles for supersonic wind tunnels.

However when one tries to use the same design procedure to the superaerodynamics windtunnel, one is immediately confronted with the difficulty of extremely large viscous effect. In other words, the boundary layer will be so thick as to occupy the main portion of the nozzle passage. To demonstrate this effect, let us consider that the length of the test section is L and the width of the square test section be b, then the Reynolds number based upon the conditions in the test section is $Re = \frac{UL}{\nu}$ where

U is the velocity in the test section. If, as a rough estimate, we take the thickness of the boundary layer to be zero at the beginning of the test section and equal to a value δ calculated by the well-known Blasius formula for a flat plate at the end of the test section, then

$$\delta = 3.65 L \frac{1}{\sqrt{Re}} \qquad (1)$$

Now if this boundary layer actually occupies half the tunnel width b/2, then

$$\delta = \frac{b}{2} = 3.65 L \frac{1}{\sqrt{Re}} \qquad (2)$$

On the other hand, the ratio of the mean free path l and the boundary layer thickness δ is known (Ref. 2) to be equal to

$$\frac{l}{\delta} = \frac{1.255\sqrt{\gamma}}{3.65} \frac{M}{\sqrt{Re}} \qquad (3)$$

where γ is the ratio of specific heats and can be taken as 1.4, M is the Mach number in the test section. By combining (2) and (3), we have

$$\left(\frac{l}{\delta}\right)\left(\frac{L}{b}\right) = 0.0557 M \qquad (4)$$

This relation is shown in Fig. 1. Thus for a Mach number M equal to 2, and L/b = 2, the boundary layer will completely fill up

the test section, if the mean free path is equal to 5.6% of the boundary layer thickness or 2.8% of the tunnel width. This means that the extremely strong viscous effect at low densities, makes the ordinary concept of designing a wind tunnel totally inapplicable.

The same fact can be also demonstrated by calculating the ratio of frictional loss on the walls of the test section and the shock loss in the diffuser after the test section. Consider the diffuser to be a straight tube of approximately the same cross-section area as the test section, then the pressure loss due to friction, Δp_1 is

$$\Delta p_1 = \frac{\text{Frictional force}}{b^2}$$

$$= \frac{\rho U^2}{2} 4bL \cdot C_f \frac{1}{b^2}$$

Taking C_f to be Blasius value again or $C_f = \frac{1.328}{\sqrt{Re}}$, we have

$$\Delta p_1 = 2\rho U^2 \left(\frac{L}{b}\right) \frac{1.328}{\sqrt{Re}} \qquad (5)$$

Now the shock loss can be estimated as that due to a normal shock with no recovery after the shock. Then if p is the pressure in the test section, the pressure loss due to shock Δp_2 is

$$\Delta p_2 = \left[\left\{1 + \frac{\gamma-1}{2} M_1^2\right\}^{\frac{\gamma}{\gamma-1}} - \left\{\frac{2\gamma}{\gamma+1} M^2 - \frac{\gamma-1}{\gamma+1}\right\}\right] p \qquad (6)$$

By combining (5) and (6), the ratio of these two pressure losses is

$$\frac{\Delta p_1}{\Delta p_2} = \frac{2\gamma M^2 \left(\frac{L}{b}\right) \frac{1.328}{\sqrt{Re}}}{\left[\left\{1 + \frac{\gamma-1}{2} M^2\right\}^{\frac{\gamma}{\gamma-1}} - \left\{\frac{2\gamma}{\gamma+1} M^2 - \frac{\gamma-1}{\gamma+1}\right\}\right]} \qquad (7)$$

Introducing the mean free path ratio given by (3), we have

$$\left(\frac{\Delta p_1}{\Delta p_2}\right) = \left(\frac{L}{b}\right)\left(\frac{l}{\delta}\right) \frac{3.264 \times 2\gamma M}{\left[\left\{1+\frac{\gamma-1}{2}M^2\right\}^{\frac{\gamma}{\gamma-1}} - \left\{\frac{2\gamma}{\gamma+1}M^2 - \frac{\gamma-1}{\gamma+1}\right\}\right]} \quad (8)$$

This relation is plotted in Fig. 2. Therefore if the Mach number M is 2, and $L/b = 2$ as before, then when the ratio l/δ is 0.056, the ratio of frictional loss to shock loss is 0.628. Therefore the frictional loss and the shock loss is of the same order of magnitude.

These elementary calculations makes it clear that for the design of the nozzle and test section for a superaerodynamics windtunnel, it is no longer possible to separate the compressibility effects and the viscous effect. In fact, the concept of boundary layer is also of doubtful value due to the extremely small Reynolds number encountered. Therefore to actually design such a nozzle to obtain the nearest approximation to the ideal uniform flow, it will be necessary to use the exact Navier-Stokes equations instead of the approximate boundary layer equations. Of course, it may be argued that for superaerodynamics, the Navier-Stokes equations for no more exact and additional corrections must be added (Ref. 2). However, recent investigations by R. Schamberg (Ref. 3) have shown that these additional corrections are small in case of slip-flows concerned here and will not essentially alter the flow pattern. Hence for a first approximation, just like the non-viscous isentropic flow as a first approximation for ordinary supersonic nozzles, we can use the Navier-Stokes equations. The simplest case to be considered is certainly the axially symmetric nozzles. If x is the coördinate in the axial direction, r the coördinate in the radial direction and u and v are the corresponding velocity components (Fig. 3), the equations are:

$$\frac{1}{r}\frac{\partial}{\partial r}(rv) + \frac{\partial u}{\partial x} = 0 \quad (9)$$

$$\rho \frac{Du}{Dt} = -\frac{\partial p}{\partial x} - \text{Grad}(\tau)_x \tag{9}$$

$$\rho \frac{Dv}{Dt} = -\frac{\partial p}{\partial r} - \text{Grad}(\tau)_r \tag{10}$$

$$\rho \frac{D}{Dt}\left(\frac{u^2+v^2}{2} + c_p T\right) = \Phi - \left\{u \,\text{Grad}(\tau)_x + v \,\text{Grad}(\tau)_r\right\}$$

$$+ \frac{\partial}{\partial x}\left(\lambda \frac{\partial T}{\partial x}\right) + \frac{1}{r}\frac{\partial}{\partial r}\left(\lambda r \frac{\partial T}{\partial r}\right) \tag{12}$$

where $\frac{D}{Dt} = u\frac{\partial}{\partial x} + v\frac{\partial}{\partial r}$

Φ = dissipation function

τ = stresses tensor

(9), (10), (11) + (12) together with the equation of state

$$\frac{p}{\rho} = RT \tag{13}$$

then determines the five unknowns u, v, p, ρ and T. Of course, the actual process of making this calculation will be extremely tedious and some approximation method of solution may have to be developed. One possibility would be to adopt the Kármán-Pohlhausen method for boundary layer to this case: We integrate the differential equations once with respect to r and thus only try to satisfy the equations "on the average" over the cross-section of the nozzle. The "distribution" of u, v over the cross-section will then be set in the form of a polynomial in r. Critical study in this procedure is already made by S. A. Schaaf (Ref. 4) at the suggestion of the author.

For ordinary supersonic diffuser, high efficiency of pressure recovery can be generally achieved by using a long diffuser. However, for superaerodynamics wind tunnel, due to the extremely large loss through friction, long diffusers are undesirable. In fact,

the pressure loss can be reduced by using a shortest possible diffuser.

2. Flow Measurement

The quantities which determine the flow field are two out of the three variables p, ρ, T and the velocity components. The quantities p, ρ, T are related by the equation of state and therefore only two is necessary for the determination of all three. Generally for windtunnel work, the quantities actually measured are p, ρ and q, the magnitude of the velocity.

For the measurement of pressure, a manometer is used. For ordinary pressure, one uses a fluid manometer filled with water, alcohol or mercury. However for the extremely low pressure encountered in the superaerodynamic flow, some other form of manometer is necessary. One of the most used type is the Pirani gauge. The conventional form of Pirani gauges has a pressure sensitivity of about 10^{-2} micron.* It utilizes the change of temperature of a wire heated with constant energy caused by a change in the pressure of the gas surrounding it. The temperature change is measured by the change in the resistance of the wire. The wire is located in a small chamber which is connected to the point of measurement by a hole, flush with the gas stream, if static pressure is to be measured. The question of best design of the connecting tube for quick response is studied by S. A. Schaaf. (Ref. 5)

To measure the density ρ, the conventional method utilizes the difference in the velocity of light rays in mediums of different density. With different optical arrangements, we have the shadowgraph method, the schlieren method and the interferometer method. However, if the density of the medium is very low as the case of superaerodynamic flow, the sensitivity of these methods become extremely poor. For instance, in case of schlieren method, the percentage change in illumination I by passing through

* 1000 micron = 1 mm. Hg.

a region of thickness b in air is given by

$$\frac{\Delta I}{I} = k\frac{f}{\varepsilon}\ 0.000294\left(\frac{\rho}{\rho_0}\right)\left[\frac{b}{\rho}\frac{\Delta\rho}{\Delta n}\right] \qquad (14)$$

where ρ_0 is the air density at 32°F and 1 atmosphere pressure, and $\Delta\rho/\Delta n$ is the density gradient normal to the light ray, f and ε are the focal length and the normal, unobscured width of the light source image perpendicular to the knife edge. k is factor of order 1, determined by the particular optical path used. Therefore the sensitivity of the schlieren method decreases with the factor (ρ/ρ_0). Some improvement can be made by altering the quantities f and ε, but practical limitations and diffraction difficulties do not allow the increase of sensitivity to satisfactory values.

A new approach to this problem density measurement is the method of absorption. It is found for instance, that oxygen at low pressures shows a strong absorption band at wave lengths around 1350 Å or ultra-violet light. The percentage absorption is proportional to the number of molecules that meet the light ray and is, therefore, proportional to the density of the gas. The measurement is then similar to that of the interferometer method where the density of gas is determined. A similar method is the utilization of the after-glow of nitrogen. These method are now being studied by R.A. Evans (Ref 6)

The conventional method for the measurement of velocity is through the use of dynamic pressure rise in a Pitot-tube. A straight forward application of this method is, however, difficult for rarefied gases. The formula used is, however, based upon the neglection of viscosity effects. But for rarefied gases, the viscosity effect is of great importance as pointed out in the previous section. Then the dynamic pressure would be quite different than that given by the usual formula. To estimate this effect, let us consider the case of low Mach number so that compressibility effects can be neglected. Then as a first approximation, take the flow field around the

Pitot-tube as that of a source of strength S in non-viscous flow of uniform velocity U. (Fig. 4) The "radius" of the tube a is

$$a = \sqrt{\frac{S}{\pi U}}$$

and the stagnation point is located at

$$r_s = \sqrt{\frac{3S}{4\pi U}} = \frac{\sqrt{3}}{2} a \qquad (15)$$

The velocity introduced by the source is then

$$- U \cdot \frac{3}{4} \frac{a^2}{r^2}$$

By calculating the viscous stress from this approximate disturbance velocity, we have for flow along the axis

$$u \frac{\partial u}{\partial r} + \frac{1}{\rho} \frac{\partial p}{\partial r} = + \nu U a^2 \frac{3}{2 r^4} \qquad (16)$$

Hence if p_0 is the stagnation pressure and p^0 the ~~free stream~~ static pressure,

$$p_0 - p^0 = \frac{1}{2} \rho U^2 + \mu U a^2 \frac{3}{2} \int_{+\infty}^{r_s} \frac{dr}{r^4}$$

$$= \frac{1}{2} \rho U^2 - \frac{1}{2} \mu U a^2 \frac{1}{r_s^3}$$

Or

$$p_0 - p^0 \cong \frac{1}{2} \rho U^2 \left[1 - \frac{8}{3\sqrt{3}} \frac{\nu}{aU} \right] \qquad (17)$$

For rarefied gases, the value of ν / aU or the reciprocal of the Reynolds' number of the Pitot-tube could be of the order of unity. Then the dynamic pressure rise $p_0 - p^0$ is not the usual value $\frac{1}{2} \rho U^2$ but a value much less than that. We shall be seriously in error if we use the ordinary formula to calculate the velocity U.

When the velocity of flow is high, we have the added complication due to the shock. The conventional Rayleigh formula for Pitot tubes in supersonic flow is based upon the assumption of very thin shock wave ahead of the Pitot tube. Now the thickness of the shock is proportional to the mean free path. Hence in rarefied flows, the

thickness of the shock will be so increased as to cause interference with flow in the neighborhood of the Pitot-tube. This together with the viscous effect mentioned in previous paragraph definitely show the inapplicability of the Rayleigh formula for supersonic velocity of rarefied gases.

With these great complications in applying the conventional velocity measuring device to superaerodynamic flows, one is naturally lead to the thought of other avenues of approach. One possibility is the use of hot-wire. If the wire diameter is of the order of 0.0008 inches, and if the pressure of the gas stream is approximately 100 microns, the ratio of the mean free path to the wire diameter will be approximately 180. Therefore the flow around the wire is definitely the free molecular flow. (Ref. 2) We have thus a simple physical situation. If θ is the inclination of the solid surface to a gas stream of velocity U, and if the molecular velocity distribution is assumed to be Maxwellian, then the translational energy of molecules $E_{i_{tr.}}$ incident upon the unit area is

$$E_{i_{tr.}} = \rho \frac{c}{2\sqrt{\pi}} \left\{ e^{-\frac{U^2}{c^2}\sin^2\theta} (c^2 + \tfrac{1}{2}U^2) + \sqrt{\pi}\,\frac{U}{c}\sin\theta \left(\tfrac{5}{4}c^2 + \tfrac{1}{2}U^2\right)\left[1 + \operatorname{erf}\left(\frac{U}{c}\sin\theta\right)\right] \right\} \quad (18)$$

where $c^2 = 2RT$, T temperature of the gas stream. For the sake of simplicity let us consider a surface in the direction of flow, $\theta = 0$, then

$$E_{i_{tr.}} = \rho \frac{c}{2\sqrt{\pi}} (c^2 + \tfrac{1}{2}U^2), \quad \theta = 0$$

The total incident energy per unit area is then

$$E_i = \rho \frac{c}{2\sqrt{\pi}} \left[\tfrac{1}{2}U^2 + (\tfrac{1}{2}R + c_v)T \right] \quad (19)$$

where c_v is the specific heat of the gas at constant volume. If T_w is the wall temperature, and α the accommodation coefficient the difference between the energy E_i incident upon the surface and the energy E_r carried by the molecules re-emitted from the surface is given by

$$E_i - E_r = \alpha (E_i - E_w)$$

where E_w is the energy that would be carried away by the molecules if the re-emission were at the temperature of the wall T_w. Therefore

$$E_i - E_r = \alpha \rho \frac{\sqrt{RT}}{\sqrt{2\pi}} \left\{ \left(\tfrac{1}{2}R + c_v\right)(T - T_w) + \tfrac{1}{2}U^2 \right\} \qquad (20)$$

The energy radiated from the surface is $\varepsilon \sigma T_w^4$ where ε is the emissivity, and σ the Stefan-Boltzmann constant.

Now let the hot wire be a ribbon of width c. Then the energy balance requires

and resistance r, heated by a current i

emissivity

start →

$$2c\left[\varepsilon \sigma T_w^4 - \alpha \rho \frac{\sqrt{RT}}{\sqrt{2\pi}} \left\{ \left(\tfrac{1}{2}R + c_v\right)(T - T_w) + \tfrac{1}{2}U^2 \right\}\right] = i^2 r \qquad (21)$$

If β is the temperature coefficient of the resistance of the wire referred to the air temperature T, then

$$r = r_0 \left[1 + \beta (T_w - T)\right] \qquad (22)$$

where r_0 is the resistance of the wire at the air temperature T. By eliminating T_w from (21) and (22), we have

$$\frac{1}{2}M^2 = \frac{1}{2\gamma}\frac{\gamma+1}{\gamma-1}\frac{1}{(\beta T)}\left(\frac{r}{r_0} - 1\right) + \left[\frac{\varepsilon \sigma T^4}{\alpha \rho \frac{\sqrt{RT}}{\sqrt{2\pi}} \gamma R T}\right]\left\{1 + \frac{1}{(\beta T)}\left(\frac{r}{r_0} - 1\right)\right\}^4$$

$$- \left[\frac{i^2 r_0}{2c\alpha \rho \frac{\sqrt{RT}}{\sqrt{2\pi}} \gamma R T}\right]\left(\frac{r}{r_0}\right) \qquad (23)$$

where M is the Mach number of the gas stream, γ the ratio of specific heats. This is then the performance equation of the hot wire.

To be more specific, let us assume that the wire current be maintained at a constant value i such that when the air velocity is zero, $T_w = T$ or $r = r_0$. Then

$$\frac{1}{2} M^2 = \frac{1}{2\gamma} \frac{\gamma+1}{\gamma-1} \frac{1}{\beta T} \left(\frac{r}{r_0} - 1 \right) + \left[\frac{\varepsilon \sigma T^4}{\alpha \rho \frac{\sqrt{RT}}{\sqrt{2\pi}} \gamma R T} \right] \left[\left\{ 1 + \frac{1}{\beta T} \left(\frac{r}{r_0} - 1 \right) \right\}^4 - \frac{r}{r_0} \right] \quad (24)$$

Now for platinum wire at $T \cong 500°R$, $\beta T \cong 1$. (γ is equal to 1.4) Furthermore if we assume appropriate values for ε, α and take for the density a value corresponds to 100 micron pressure. Then the first factor of the last term to the right of (24) is approximately equal to unity. Therefore the performance of such a ribbon hot wire is given by

$$\frac{1}{2} M^2 = 2.14 \left(\frac{r}{r_0} - 1 \right) + \left(\frac{r}{r_0} \right)^4 - \left(\frac{r}{r_0} \right) \quad (25)$$

This equation is plotted in Fig. 5. It is seen that the sensitivity of such an instrument is quite satisfactory.

We have chosen the ribbon wire only for simplicity of calculation. For practical application, a round wire will be used and the relation between gas velocity U, gas temperature T and gas density ρ and the resistance r will be obtained by direct calibration. But nevertheless the sensitivity of the instrument will be of the same order as shown above. Therefore these preliminary investigations seem to indicate the desirability of further research on the hot wire anemometer for rarefied gases.

3. <u>Parameters of Flow</u>

The two parameters that are directly connected with the flow field are the Reynolds number Re, defined as

$$Re = \frac{UL}{\nu^0}$$

where ν^0 is the kinematic viscosity, L the typical linear dimension of the body; and the Mach number M^0 of the free stream. This

is true even for slip flows and free molecule flows due to the fact that the ratio of mean free path to the typical dimension can be also expressed in terms of the Reynolds' number and the Mach number.

However, as the pressure or density is reduced, the solid boundary of the flow enters actively into the flow conditions by requiring not only that the macroscopic stream velocity be tangential to the surface but that the interaction of the molecules and the wall be considered and that the radiation of energy to and from the wall be taken into account. The interaction of the molecules with the wall is so far expressed through the fraction s of molecules that are diffusely re-emitted from the wall and the accommodation coefficient α. We have reasons to believe that both s and α are functions of the temperature of the wall and the molecular velocity distribution. Therefore the interaction of the molecules with the wall is the same only if the wall temperature, the gas temperature and the Mach number of the gas above the wall is the same. These considerations seem to indicate then that for the model test to be similar to the prototype, the model must be made of same surface material as the prototype, and the fluid must be the same, and furthermore the following parameters must be the same:

1) Reynolds number Re
2) Mach number M^0
3) free stream temperature, T^0

The radiation heat loss from the surface is equal to $\varepsilon\sigma T_w^4$ per unit area. However, if the model is surrounded by the walls of the test chamber, there is also an heat input due to radiation from walls of the test section to the model. Let us call this quantity q_c. Then the net heat loss per unit area of the surface of the model is $\varepsilon\sigma T_w^4 - q_c$. This quantity can be rendered non-dimensional by dividing it by $\rho^0 U (C_p T^0)$. Call this new parameter Λ_m, then

$$\Lambda_m = \left[\frac{\varepsilon\sigma T_w^4 - q_c}{\rho^0 U (C_p T^0)}\right]_m \qquad (25)$$

For the prototype, the heat from the walls of the test chamber is absent but there may be solar radiation and the radiation from the earth and surrounding atmosphere (Ref. 7). Denoting this amount by q, then the parameter Λ for the prototype is

$$\Lambda = \left[\frac{\varepsilon \sigma T_w^4 - q}{\rho^0 U (c_p T^0)} \right]_m \tag{26}$$

In order for the flow to be similar also with respect to the radiation heat transfer,

$$\Lambda = \Lambda_m . \tag{27}$$

Because of the previous conditions on the Reynolds number and free stream temperature, (27) is the same as

$$\frac{\varepsilon \sigma T_w^4 - q}{\varepsilon \sigma T_w^4 - q_c} = \frac{L_m}{L} \tag{28}$$

where L_m is the typical linear dimension of the model and L is the typical linear dimension of the prototype. This means that the wall temperature of the test chamber must be so controlled that q_c satisfies (28).

This set of rather strict similarity rules for model testing in superaerodynamic flows is certainly difficult to satisfy. In what way these rules can be relaxed is the problem of future research.

References

1) A.E. Puckett, "Supersonic Nozzle Design"
Journal of Applied Mechanics (ASME), Vol. 13, p. A-265
(1946)

2) H. S. Tsien, "Superaerodynamics, Mechanics of Rarefied Gases"
J. Aero. Sciences, Vol. 13, p. 653 (1946)

3) R. Schamberg, "The Fundamental Differential Equations and the Boundary Conditions for High Speed Slip-Flow, and Their Application to Several Specific Problems"
Thesis, California Institute of Technology, (1947)

4) S.A. Schaaf, "Viscosity Effects in Wind Tunnel No.2"
University of California, Department of Engineering,
Report No. HE-150-16, (1947)

5) S.A. Schaaf, "The Theory of Minimum Response Time for Vacuum Gages"
University of California, Department of Engineering,
Report No. HE-150-21 (1947)

6) R.A. Evans, "Flow Visualization at Low Pressures"
University of California, Department of Engineering,
Report No. HE-150-25, (1947)

7) H.A. Johnson, ~~H.W. [illegible], F.M. [illegible], E.G. [illegible]~~, L. Posner
"A Design Manual for Determining the Thermal Characteristics of High Speed Aircraft" Chapter 4, AAF Technical Report No. 5632 (1947)

Table 1

The Functions F_1 and F_2 (cf equation 21)

U/c	F_1	F_2
0	1.77245	0
0.2	1.73751	0.07020
0.4	1.63880	0.27269
0.6	1.49248	0.58566
0.8	1.32021	0.97843
1.0	1.14328	1.42053
1.2	0.97825	1.88555
1.4	0.83480	2.35492
1.6	0.71628	2.81812
1.8	0.62153	3.27117
2.0	0.54683	3.71356
2.2	0.48790	4.14672
2.4	0.44090	4.57300
2.6	0.40268	4.99395
2.8	0.37100	5.41117
3.0	0.34420	5.87498

Appendix

Evaluation of the functions F_1 and F_2

For the function F_1,

$$F_1(z) = \frac{1}{\sqrt{\pi}} \int_{-\frac{\pi}{2}}^{\frac{\pi}{2}} e^{-z^2 \sin^2\theta} \, d\theta = \frac{2}{\sqrt{\pi}} \int_0^{\frac{\pi}{2}} e^{-\frac{z^2}{2}(1-\cos 2\theta)} \, d\theta$$

$$= \frac{1}{\sqrt{\pi}} e^{-\frac{z^2}{2}} \int_0^{\pi} e^{+\frac{z^2}{2}\cos\varphi} \, d\varphi = \sqrt{\pi}\, e^{-\frac{z^2}{2}} I_0\left(\frac{z^2}{2}\right)$$

where I_0 is the modified ~~Bessel~~ function of first kind and order zero. The last step is made possible by the substitution $2\theta = \varphi$.

For the function F_2,

$$F_2(z) = \int_{-\frac{\pi}{2}}^{\frac{\pi}{2}} (z \sin\theta) \left\{ 1 + \mathrm{erf}(z \sin\theta) \right\} d\theta = \int_{-\frac{\pi}{2}}^{\frac{\pi}{2}} (z \sin\theta)\, \mathrm{erf}(z\sin\theta)\, d\theta$$

By the definition of the error function, we have

$$F_2(z) = \frac{2}{\sqrt{\pi}} \int_{-\frac{\pi}{2}}^{\frac{\pi}{2}} z \sin\theta \left(\int_0^{z\sin\theta} e^{-s^2} ds \right) d\theta$$

This form can be simplified by partial integration. Thus

$$F_2(z) = \frac{4}{\sqrt{\pi}} z^2 \int_0^{\frac{\pi}{2}} \cos^2\theta \; e^{-z^2\sin^2\theta} \, d\theta$$

$$= \frac{2}{\sqrt{\pi}} z^2 \int_0^{\frac{\pi}{2}} (1 + \cos 2\theta)\, e^{-z^2 \sin^2\theta} \, d\theta$$

$$= \sqrt{\pi}\, z^2 e^{-\frac{z^2}{2}} I_0\left(\frac{z^2}{2}\right) + \frac{1}{\sqrt{\pi}} z^2 e^{-\frac{z^2}{2}} \int_0^{\pi} \cos\varphi \; e^{+\frac{z^2}{2}\cos\varphi} \, d\varphi$$

Therefore

$$F_2(z) = \sqrt{\pi}\, z^2 e^{-\frac{z^2}{2}} \left[I_0\left(\frac{z^2}{2}\right) + I_1\left(\frac{z^2}{2}\right) \right]$$

where I_1 is the modified Bessel function of first kind and order one.

COPY

Wing-Tunnel Testing Problem in Superaerodynamics

Hsue-shen Tsien

Guggenheim Aeroanutical Laboratory

Massachusetts Institute of Technology

Wind-tunnels are, perhaps, the most useful tool in aerodynamic investigations and certainly have contributed much in the modern development of fluid mechanics. It is thus natural, when one turns to a new field of aerodynamics, the aerodynamics of rarefied gases or superaerodynamics, that one should think of using the wind tunnel again. Only here it has to be adopted to entirely new circumstances and many new problems, both in its design and in its operation, appear. It is the purpose of this paper to discuss some of these problems, so as to gain an orientation in the new field of experimentation.

1. Tunnel Design

To test models in the wind tunnel at its test section, it is of primary importance to obtain a uniform stream at the desired temperature, pressure and velocity. For subsonic wind tunnels with ordinary pressures, this can be achieved without much difficulty. For supersonic wind tunnels at ordinary pressure, the expansion part of the tunnel before the test section or the nozzle is first designed to obtain a uniform stream at its exit without considering the effects of the viscosity of air. Then the boundary layer along the wall of the nozzle is calculated with the pressure gradient thus determined. Finally the displacement thickness of the boundary layer, or the needed space for the boundary layer flow at lower velocity is provid-

ed by making the nozzle larger than the dimensions first determined by the calculated amount. (Ref. 1) This design procedure is found to give satisfactory nozzles for supersonic wind tunnels.

However when one tries to use the same design procedure to the super-aerodynamics wing tunnel, one is immediately confronted with the difficulty of extremely large viscous effect. In other words, the boundary layer will be so thick as to occupy the main portion of the nozzle passage. To demonstrate this effect, let the length of the test section be L and the width of the square test section be b. Then the Reynolds number based upon the conditions in the test section is $Re = \frac{UL}{\nu}$ where U is the velocity in the test section. If, as a rough estimate, we take the thickness of the boundary layer to be zero at the beginning of the test section and equal to a value calculated by the well-known Blasius formula for a flat plate at the end of the test section, then

$$\delta = 3.65\ L/\sqrt{Re} \tag{1}$$

Now if this boundary layer actually occupies half the tunnel width b/2, then

$$\delta = \frac{b}{2} = 3.65\ L/\sqrt{Re} \tag{2}$$

On the other hand, the ratio of the mean free path ℓ and the boundary layer thickness δ is known (Ref. 2) to be equal to

$$\frac{\ell}{\delta} = \frac{1.255\sqrt{\gamma}}{3.65}\ \frac{M}{\sqrt{Re}} \tag{3}$$

where γ is the ratio of specific heats and can be taken as 1.4, M is the Mach number in the test section. By combining (2) and (3), we have

$$\left(\frac{\ell}{\delta}\right)\left(\frac{L}{b}\right) = 0.0557\ M \tag{4}$$

This relation is shown in Fig. 1. Thus for a Mach number equal to 2, and L/b = 2, the boundary layer will completely fill up the test section, if the mean free path is equal to 5.6% of the boundary layer thickness or 2.8% of the tunnel width. This means that the extremely strong viscous effect at low derivities makes the ordinary concept of designing a wind tunnel totally inapplicable.

The extremely thick boundary layer where the velocity increases from a small value near the wall to some supersonic velocity at the center of the nozzle, also gives subsonic velocities in a rather large portion of the nozzle. Since pressure disturbances downstream can be transmitted upstream in subsonic flows, the flow in the test section of a low pressure tunnel will be sensitive to changes in the diffuse even if the main stream velocity at the center of the nozzle is supersonic. This is of course a new phenomenon is superaerodynamics tunnel not found in conventional supersonic wind tunnels.

The large viscous effects can be also demonstrated by calculating the ratio of frictional loss on the walls of the test section and the shock loss in the diffuser after the test section. Consider the diffuser to be a straight tube of approximately the same cross-sectional area as the test section, then the pressure loss due to friction Δp_1, is

$$\Delta p_1 = \frac{\text{Frictional Force}}{b^2}$$

$$= \frac{\rho U^2}{2} 4bL\, C_f \frac{1}{b^2}$$

Taking C_f to be Blasius value or $C_f = \frac{1.328}{\sqrt{Re}}$ we have

$$\Delta p_1 = 2\rho U^2 \left(\frac{L}{b}\right) \frac{1.328}{\sqrt{Re}} \tag{5}$$

Now if is the static pressure in the test section, then the pressure by ideal isentropic compression in the diffuser is . If the actual pressure rise in the diffuser is estimated as that due to a normal shock without further recovery, then the actual pressure rise is Therefore the pressure loss due to shock is

(6)

By combining (5) and (6), the ratio of these two pressure losses is

(7)

Introducing the mean free path ratio given by (3), we have

(8)

This relation is plotted in Fig. 2. Therefore if the Mach number is 2, and L/b = 2 as before, then when the ratio ( ) is 0.056, the ratio of frictional loss to shock loss is 0.628. Hence the frictional loss and the shock loss is of the same order of magnitude.

These large viscous effects are fully confirmed by the recent tests on the 1" x 1" low pressure wind tunnel at the University of California.* The test nozzle (Fig. 3) was designed for Mach number without considering the viscous effect of the medium. During test, the static pressure on the

---

* Experimental work done under contact with the Office of Naval Research. The author is deeply indebted to Professors R. G. Folsom and E. D. Kane for permission to use their unpublished results.

wall at the exit of the nozzle is measured. This pressure is equal to 175 microns* for the two tests presented in Figs. 4 and 5. The apparant Mach number "M" is the Mach number calculated from the dynamic pressure measured by a Pitot tube by using the Rayleigh formula. Since there is the complication of large viscous effect in the Pitot tube reading as shown in the following section, this apparant Mach number is only quantitative and cannot be taken as the exact value. However it is apparant from Figs. 4 and 5 that the boundary layer in the test section is indeed very thick, and fills up the whole space. This large boundary layer thickness makes this space available for the expansion of the central potential flow if it exists, very small. Therefore the maximum Mach number reached at the center of the nozzle is very much smaller than the design Mach number of 4. At the lower pressure, the influence of slip at the wall is also evident. This has the tendency to make the flow more uniform. However the very low Mach number at the test section indicates again the strong viscous effect in converting much of the pressure energy into heat energy.

These elementary calculations and preliminary test results makes it clear that for the design of the nozzle and test section for a superaerodynamics wind tunnel, it is no longer possible to separate the compressibility effects and the viscous effect. In fact, the concept of boundary layer is also of doubtful value due to the extremely small Reynolds number encountered. Therefore to actually design such a nozzle to obtain the nearest approximation to the ideal uniform flow it will be necessary to use the exact Navier-Stokes equations instead of the approximate boundary layer equations. Of course, it may be argued that for superaerodynamics, the Navier-Stokes equations for no more exact and additional corrections must be added (Ref. 2). However, recent investigations by

---

* 1000 microns = 1 mm Hg_1 one atmosphere = 0.760 x 10^6 microns.

R. Schamberg (Ref. 3) have shown that these additional corrections are small in case of slip-flows concerned here and will not essentially alter the flow pattern. Hence for a first approximation just like the non-viscous isentropic flow as a first approximation for ordinary supersonic nozzles, we can use the Navier-Stokes equations. The simplest case to be considered is certainly the axially symmetric nozzles. If x is the coordinate in the axial direction,

the coordinate in the radial direction and u and v are the corresponding velocity components, the equations are:

(9)

(10)

(11)

(12)

where

=

= dessipation function

= stresses tensor

(9), (10), (11) and (12) together with the equation of states

= R T (13)

then determines the five unknown u, v, , and T. Of course, the actual process of making this calculation will be extremely tedious and some approximation method of solution may have to be developed. One possibility would be to adopt

the Karman-Polhausen method for boundary layer to this case: We integrate the differential equations once with respect to r and thus only try to satisfy the equations "on the average" over the cross-section of the nozzle. The "distribution" of u, v over the cross-section will then be set in the form of a polynomical in r. Initial study in this procedure is already made by S. A. Schaaf (Ref. 4) at the suggestion of the author.

For ordinary supersonic diffuser, high efficiency of pressure recovery can be generally achieved by using a long diffuser. However, for superaerodynamics wind tunnel, due to the extremely large loss through friction, long diffusers are undesirable. In fact, the pressure loss can be reduced by using a shortest possible diffuser.

2. Flow Measurement

The quantities which determine the flow field are two out of the three variables   ,   , T and the velocity components. The quantities   ,   , T are related by the equation of states and therefore only two is necessary for the determination of all three. Generally for wind tunnel work, the quantities actually measured are   ,   , and   , the magnitude of the velocity.

For the measurement of pressure, a manometer is used. For ordinary pressure, one uses a fluid manometer filled with water, alcohol or mercury. However for the extremely low pressure encountered in the superaerodynamic flow, some other form of manometer is necessary. One of the most successful type is the Pirani gage. The conventional form of Pirani gages has a pressure sensitivity of about 10^{-2} micron. It utilises the change of temperature of a wire heated with constant energy caused by a change in the pressure of the gas surrounding it. The temperature change is measured by the change in the resistance of the wire. The wire is located in a small chamber which is connected to the

point of measurement by a hole, flush with the gas stream if static pressure is to be measured. The question of best design of the connecting tube for quick response is studies by S. A. Schaaf. (Ref. 5).

To measure the density , the conventional method utilizes the difference in the velocity of the light rays in mediums of different density. With different optical arrangements, we have the shadowgraph method, the schlieren method and the interferometer method. However, if the density of the medium is very low as the case of superaerodynamic flow, the sensitivity of these methods become extremely poor. For instance in case of schlieren method, the percentage change in illumination I by passing through a region of thickness b is given by

(14)

where is the air density at 32°F and 1 atmosphere pressure, and is the density gradient normal to the light ray. and are the local length and the normal unobscured width of the light source image perpendicular to the knife edge. k is factor of order 1, determined by the particular optical path used. Therefore the sensitivity of the schlieren method decreases with the factor ( ). Some improvement can be made by altering the quantities f and , but practical limitations and diffraction difficulties do not allow the increase of sensitivity to satisfactory values.

A new approach to this problem density measurement is the method of absorption. It is found for instance, that oxygen at low pressures shows a strong absorption band at wave lengths around 1470° A or ultra-violet light. The percentage absorption is proportional to the number of molecules that meet the light ray and is, therefore, proportional to the density of the gas. The measurement is then similar to that of the interferometer method where the density is determined. A similar method is the utilization of the after-flow of nitrogen. These

methods are now being studied by E. A. Evans (Ref. 6).

The conventional method for the measurement of velocity is through the use of dynamic pressure rise in a Pitot-tube. A straight forward application of this method is, however, difficult for rarefied gases. The formula used is, however, based upon the neglection of viscosity effects. But for rarefied gases the viscosity effect is af great importance as pointed out in the previous section. Then the dynamic pressure would be quite different than that given by the usual formula. To estimate this effect, let us consider the case of low Mach number so that compressibility effects can be neglected. Then as a first approximation, take the flow field around the Pitot-tube as that of a source of strength in non-viscous flow of uniform velocity U. The "radius" of the tube a is

a =

and the stagnation point is located at

(15)

The velocity introduced by the source is then

By calculating the viscous stress from this approximate disturbance velocity, we have for flow along the axis

(16)

Hence if is the stagnation pressure and the static pressure,

Or

(17)

For rarefied gases, the value of or the reciprocal of the Reynold's number of the Pitot-tube could be of the order of unity. Then the dynamic pressure rise - is not the usual values ½ but a value much less than that. In fact previous investigation by Baker (Ref. 7) and F. Homann (Ref. 8) indicate that the Reynolds number where a' is the radius of the mouth of tube, must exceed 30 in order to reach the usual dynamic pressure rise ½

When the velocity of flow is high, we have the added complication due to the shock. The conventional Rayleigh formula for Pitot tubes is supersonic flow is based upon the assumption of very thin shock wave ahead of the Pitot tube. Now the thickness of the shock is proportional to the mean free path. Hence in rarefied flows, the thickness of the shock will be so increased as to cause interference with flow in the neighborhood of the Pitot-tube. This together with the viscous effect mentioned in previous paragraph definitely show the inapplicability of the Rayleigh formula for supersonic velocity of rarefied gases.

3. Hot-Wire Anemometer

With the great complications in applying the conventional velocity measuring device to superaerodynamic flows, one is naturally led to the thought of other avenues of approach. One possibility is the use of hot-wire. If the wire diameter is of the order of 0.0001 inches, and if the pressure of the gas stream is approximately 100 microns, the ratio of the mean free path to the wire diameter will be approximately 180. Therefore the flow around the wire is definitely the free molecule flow (Ref. 2). We have thus a simple physical situation, which is an improvement over the rather uncertain circumstances of mixed dynamic and viscous effects for the measurement of velocity by Pitot tube. It thus seems worthwhile to explore this possibility by a trial calculation of the performance of such a hot-wire anemometer.

If is the inclination of the solid surface to a gas stream which has a macroscopic velocity U and a Maxwellian molecular velocity distribution, the translational energy of molecules incident upon the unit area is,

(18)

where $c^2 = 2\ RT$, T temperature of the gas stream and erf is the error function. Now let r be the radius of the hot-wire. Then the total energy E_i incident upon a unit length of the wire is the sum of translational energy and internal energy. If C_v is the specific heat at constant volume, this total energy per unit length of wire is

(19)

The integrals in equation (19) can be expressed in terms of tabulated functions, (see Appendix) Thus

(20)

where

(21)

(22)

The I_o and I_1 are the modified Bessel functions of the first kind of orders zero and one respectively. The functions F_1 and F_2 are tabulated in Table 1.

If T_w is the wall temperature, and x the accomodation coefficient, the

difference between the energy E_i incident upon the surface and the energy E_r carried by the molecules re-emitted from the surface is given by

$$E_i - E_r = \quad (E_i - E_w)$$

where E_w is the energy that would be carried away by the molecules if the re-emission were at the temperature T_w of the wire. Therefore

$$E_i - E_r = \quad c \; r \quad \tfrac{1}{2} U^2 + (\tfrac{1}{2} R + C_v)\,(T - T_w)\; F_1\left(\frac{U}{c}\right)$$

$$+ \quad \tfrac{1}{2} U^2 + (R + C_v)\,(T - T_w) \quad F_2\left(\frac{U}{c}\right) \qquad (23)$$

This difference of energy is then the net energy input to the wire per unit length of the wire by the air stream.

If i is the electric current heating the wire and   is the resistance of the wire per unit length at the wire temperature, the heat input per unit length of wire by the heating current is i^2 . Heat is lost from the wire by radiation. If   is Stefan-Boltzmann constant and   is the emissivity of the wire surface, the radiation heat loss per unit length is .
Therefore if the wire has reached a steady condition, the heat balance requires

$$(24)$$

This equation can be put into somewhat simpler form by using the relation that

$$R = C_p - C_v = C_v\,(\quad - 1\,) \qquad (25)$$

Furthermore if we take T_o is the reference temperature at which the resistance is , and the corresponding temperature coefficient of the resistance is . Then the resistance can be expressed as

$$= \quad _o \quad 1 + \quad (T_w - T_o) \tag{26}$$

Now let

$$= \tag{27}$$

Then from equation (26)

$$\frac{T_w}{T_o} = \frac{-1}{T_o} + 1 \tag{28}$$

Now introduce $_o$ as the reference density and i_o as the reference heating current, then equation (24) can be written as

(29)

The particular values of the reference temperature T_o, the reference density $_o$ and the reference current i_o are not yet fixed. We fix these quantities now by requiring that

$$T_o = 1 \tag{30}$$

(31)

and (32)

Then equation (29) simplifies into

(33)

This is then the performance equation of the hot-wire in free molecular flow.

Now let us investigate in greater detail the case of a bright platinum wire. To satisfy equation (30),

$$T_o = 492^o \text{ R.}$$

The value for and can be taken to be 0.08 and 0.90 respectively. Then equation (31) gives the corresponding pressure p_o for $_o$ and T_o as

Let the radius r of the wire be 0.0001 inch. Then equation (32) gives the reference heating current i_o as

$$i_o = \text{ ________ } = 0.274 \text{ milliampere.}$$

where the resistivity of the platinum is taken as 10.96×10^{-6} ohms-cms. Therefore the order of magnitude of the different quantities is entirely satisfactory.

If the wire is used with a constant heating current, then equation (33) can be used to calculate the relation between the resistance ratio and the velocity ratio ($\frac{U}{C}$) at constant air stream density and temperature. This is done for $_o = 1$, $T/T_o = 1$ and $i/i_o = 1$* and the result is given in Fig. 6. It is seen that the sensitivity of the instrument is good. Of course, the behavior of the hot-wire anemometer will be actually determined by calibration for any experiment.

---

* The author is indebted to Mr. L. Mack for the numerical computations.

above the wall is the same. These considerations seem to indicate then that for the model test to be similar to the prototype, the model must be made of same surface material as the prototype, and the fluid must be the same, and furthermore the following parameters must be the same:

(1) Reynolds number Re

(2) Mach number M^o

(3) free stream temperature T^o

The radiation heat loss from the surface is equal to per unit area. However, if the model is surrounded by the walls of the test chamber, there is also an heat input due to radiation from walls of the test section to the model. Let us call this quantity . Then the net heat loss per unit area of the surface of the model is . This quantity can be rendered non-dimensional by dividing it by . Call this new parameter , then

(34)

For the prototype, the heat from the walls of the test chamber is absent but there may be solar radiation and the radiation from the earth and surrounding atmosphere. (Ref. 0). Denoting this amount by , then the parameter for the prototype is

(35)

In order for the flow to be same also with respect to the radiation heat transfer,

(36)

Because of the previous conditions on the Reynolds number and free stream temperature, (36) is the same as

(37)

Since the performance of the wire is strongly influenced by the accommodation coefficient as shown by equation (29), it will be necessary to find materials which can hold this coefficient constant for a considerable period of time so that no frequent calibration is required. However the present analysis seems to indicate the feasibility of such an instrument for measurements in rarefied gases and further research is definitely desirable.

4. Parameters of Flow

The two parameters that are directly connected with the flow field are the Reynold's number Re, defined as

$$Re = \frac{UL}{o}$$

where is the kinematic viscosity, L the typical linear dimension of the body; and the Mach number M^o of the free stream. This is true even for slip flows and free molecule flows due to the fact that the ratio of mean free path to the typical dimension can be also expressed in terms of the Reynold's number and the Mach number.

However, as the pressure or density is reduced, the solid boundary of the flow enters actively into the flow conditions by requiring not only that the microscopic stream velocity be tangential to the surface but that the interaction of the molecules and the wall be considered and that the radiation of energy to and from the wall be taken into account. The interaction of the molecules with the wall is so far expressed through the fraction of molecules that are diffusely re-emitted from the wall, and the accommodation coefficient . It is known that both and are functions of the temperature of the wall and we have reasons to believe that they are also functions of the molecular velocity distribution. Therefore the interaction of the molecules with the wall is the same only if the wall temperature, the gas temperature and the Mach number of the gas

Table I

The Functions F_1 and F_2 (cf. equation 21)

U/c	F_1	F_2
0	1.77245	0
0.2	1.73751	0.07020
0.4	1.63880	0.27269
0.6	1.49248	0.58560
0.8	1.32021	0.97843
1.0	1.14328	1.42053
1.2	0.97825	1.88555
1.4	0.83480	2.35492
1.6	0.71628	2.81812
1.8	0.62155	3.27117
2.0	0.54683	3.71356
2.2	0.48790	4.14672
2.4	0.44090	4.57300
2.6	0.40268	4.99395
2.8	0.37100	5.41117
3.0	0.34420	5.87498

COPY

Appendix

Evaluation of the Functions F_1 and F_2

For the function F_1,

where I_o is the modified Bessel function of first kind and under zero. The last step is made possible by the substitution =

For the function F_2,

By the definition of the error function, we have

This form can be simplified by partial integration. Thus

where L_m is the typical linear dimension of the model and L is the typical linear dimension of the prototype. This means that the wall temperature of the test chamber must be so controlled that satisfies (37).

This set of rather strict similarly rules for model testing in super-aerodynamic flows is certainly difficult to satisfy. In what way the rules can be relaxed is the problem of future research.

COPY

Therefore

where I_1 is the modified Bessel function of first kind and order one.

June 12, 1948

Mr. Robert R. Dexter, Secretary
Institute of the Aeronautical Sciences
2 East 64th Street
New York 21, N.Y.

Dear Mr. Dexter:

Enclosed are two manuscripts which I am submitting for consideration of publication in the Journal of the Aeronautical Sciences.

The first paper, "Wind-Tunnel Testing Problem in Superaerodynamics", is the revised form of my paper presented in the Annual Meeting. I apologize for the long delay in getting the manuscript into this form.

The second paper, "Two Dimensional Airfoils in Hypersonic Flows", is written by Mr. Richard D. Linnell and is taken from his Thesis at the Massachusetts Institute of Technology.

Very sincerely yours

H. S. Tsien
Professor of Aerodynamics



INSTITUTE
OF THE
AERONAUTICAL SCIENCES
INC.

2 EAST 64TH STREET
NEW YORK 21, N. Y.

July 20, 1948

Dr. H. S. Tsien
Guggenheim Aeronautical Laboratory
Massachusetts Institute of Technology
Cambridge, Massachusetts

Dear Dr. Tsien:

We are now preparing your paper, "Wind-Tunnel Testing Problems in Superaerodynamics," for publication, and there does not seem to be an abstract or summary included. Since we feel that some sort of an abstract should be published with the paper, I should appreciate your sending one as soon as possible.

Very truly yours,

Berneice H. Jarck

Berneice H. Jarck
Associate Editor

bhj:amb

July 24, 1948

Miss Berneice H. Jarck
Associate Editor
Journal of the Aeronautical Sciences
2 East 64th Street
New York 21, N.Y.

Dear Miss Jarck:

Enclosed is the Summary for my paper, "Wind-Tunnel Testing Problems in Superaerodynamics". This is to answer your request in your letter of July 20, 1948.

Very sincerely yours

H. S. Tsien
Professor of Aerodynamics

Wind-Tunnel Testing Problems in Superaerodynamics

Hsue-shen Tsien

Summary

The problems in the experimentation of rarefied gas are discussed. First the extremely large viscous effects in a wind-tunnel nozzle is shown. Then the difficulties of flow measurement are surveyed, pointing out particularly the unconventional behavior of the Pitot tube in rarefied gas. The performance of a hot-wire anemometer is then studied in some detail to show its feasibility. Finally the rules for achieving complete flow similarity of rarefied gas flow are formulated.

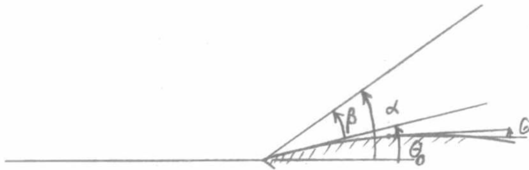
Section 2

Hypersonic Flows $M_1 \rightarrow \infty$

Hypersonic Flow $M_1 \to \infty$

(I) Two Dimensional Case

a) The initial Shock



$$\boxed{\tan\beta = \tan\alpha \cdot \frac{\gamma-1}{\gamma+1}}$$

$$\boxed{p_2 = \frac{2}{\gamma+1} \rho_1 v_1^2 \sin^2\alpha}$$

$$M_2^2 = (1+\cot^2\beta)\frac{\gamma-1}{2\gamma} = \left\{1+\cot^2\alpha \cdot \left(\frac{\gamma+1}{\gamma-1}\right)^2\right\}\frac{\gamma-1}{2\gamma}$$

$$M_2^2 = \frac{\gamma-1}{2\gamma}\frac{1}{\sin^2\alpha} + \frac{2}{\gamma-1}\cot^2\alpha$$

$$= \frac{\gamma-1}{2\gamma}\frac{1}{\sin^2\alpha} + \frac{2}{\gamma-1}\left[\frac{1}{\sin^2\alpha} - 1\right]$$

$$\boxed{M_2^2 = \frac{(\gamma+1)^2}{2\gamma(\gamma-1)}\frac{1}{\sin^2\alpha} - \frac{2}{\gamma-1}}$$

$$\cot\beta = \cot\alpha\left(\frac{\gamma+1}{\gamma-1}\right)$$

b) Subsequent Expansion

We shall use the formula

$$\theta_0 - \theta = \sqrt{\frac{\gamma+1}{\gamma-1}} \tan^{-1}\sqrt{\frac{M^2-1}{\frac{\gamma+1}{\gamma-1}}} - \tan^{-1}\sqrt{M^2-1} - \sqrt{\frac{\gamma+1}{\gamma-1}} \tan^{-1}\sqrt{\frac{M_2^2-1}{\frac{\gamma+1}{\gamma-1}}} - \tan^{-1}\sqrt{M_2^2-1}$$

$$= \sqrt{\frac{\gamma+1}{\gamma-1}}\left[\frac{\pi}{2} - \sqrt{\frac{\gamma+1}{\gamma-1}}\frac{1}{\sqrt{M^2-1}} + \frac{1}{3}\left(\frac{\gamma+1}{\gamma-1}\right)^{3/2}\frac{1}{(M^2-1)^{3/2}} \cdots\right]$$

$$- \left[\frac{\pi}{2} - \frac{1}{\sqrt{M^2-1}} + \frac{1}{3}\frac{1}{(M^2-1)^{3/2}} \cdots\right]$$

$$- \sqrt{\frac{\gamma+1}{\gamma-1}}\left[\frac{\pi}{2} - \sqrt{\frac{\gamma+1}{\gamma-1}}\frac{1}{\sqrt{M_2^2-1}} + \frac{1}{3}\left(\frac{\gamma+1}{\gamma-1}\right)^{3/2}\frac{1}{(M_2^2-1)^{3/2}} \cdots\right]$$

$$+ \left[\frac{\pi}{2} - \frac{1}{\sqrt{M_2^2-1}} + \frac{1}{3}\frac{1}{(M_2^2-1)^{3/2}} \cdots\right]$$

$$= \frac{2}{\gamma-1}\left(\frac{1}{\sqrt{M_2^2-1}} - \frac{1}{\sqrt{M^2-1}}\right) - \frac{1}{3}\frac{4\gamma}{(\gamma-1)^2}\left(\frac{1}{(M_2^2-1)^{3/2}} - \frac{1}{(M^2-1)^{3/2}}\right) \cdots$$

We have the formula

$$1 + \frac{\gamma-1}{2}M^2 = \left(\frac{p_0'}{p}\right)^{\frac{\gamma-1}{\gamma}}, \qquad 1 + \frac{\gamma-1}{2}M_2^2 = \left(\frac{p_0'}{p_2}\right)^{\frac{\gamma-1}{\gamma}}$$

Our aim is to express p/p_2 in terms of $\theta_0 - \theta$.

$$\boxed{\frac{1+\frac{\gamma-1}{2}M^2}{1+\frac{\gamma-1}{2}M_2^2} = \left(\frac{p_2}{p}\right)^{\frac{\gamma-1}{\gamma}}}$$

$$\theta_0 - \theta = \frac{2}{\gamma-1}\frac{1}{\sqrt{M_2^2-1}}\left\{1-\sqrt{\frac{M_2^2-1}{M^2-1}}\right\} - \frac{1}{3}\frac{4\gamma}{(\gamma-1)^2}\frac{1}{(M_2^2-1)^{3/2}}\left\{1-\left(\frac{M_2^2-1}{M^2-1}\right)^{3/2}\right\}\cdots$$

3

$$= \frac{2}{\gamma-1}\frac{1}{(M_2^2-1)^{1/2}}\left\{1-\left(\frac{1-\frac{1}{M_2^2}}{\left(\frac{M}{M_2}\right)^2-\frac{1}{M_2^2}}\right)^{1/2}\right\} - \frac{1}{3}\frac{4\gamma}{(\gamma-1)^2}\frac{1}{(M_2^2-1)^{3/2}}\left\{1-\left(\frac{1-\frac{1}{M_2^2}}{\left(\frac{M}{M_2}\right)^2-\frac{1}{M_2}}\right)^{3/2}\right\}\cdots$$

$$\frac{\frac{1}{M_2^2}+\frac{\gamma-1}{2}\left(\frac{M}{M_2}\right)^2}{\frac{1}{M_2^2}+\frac{\gamma-1}{2}} = \left(\frac{p_2}{p}\right)^{\frac{\gamma-1}{\gamma}}$$

$$\frac{1}{M_2^2}+\frac{\gamma-1}{2}\left(\frac{M}{M_2}\right)^2 = \left(\frac{1}{M_2^2}+\frac{\gamma-1}{2}\right)\left(\frac{p_2}{p}\right)^{\frac{\gamma-1}{\gamma}}, \quad \left(\frac{M}{M_2}\right)^2 = \frac{2}{\gamma-1}\left\{\left(\frac{1}{M_2^2}+\frac{\gamma-1}{2}\right)\left(\frac{p_2}{p}\right)^{\frac{\gamma-1}{\gamma}} - \frac{1}{M_2^2}\right\}$$

$$\left(\frac{M}{M_2}\right)^2 - \frac{1}{M_2^2} = \left\{\frac{2}{(\gamma-1)M_2^2}+1\right\}\left(\frac{p_2}{p}\right)^{\frac{\gamma-1}{\gamma}} - \left(\frac{\gamma+1}{\gamma-1}\right)\frac{1}{M_2^2}$$

$$= \left(\frac{p_2}{p}\right)^{\frac{\gamma-1}{\gamma}} + \frac{1}{\gamma-1}\left\{2\left(\frac{p_2}{p}\right)^{\frac{\gamma-1}{\gamma}} - (\gamma+1)\right\}\frac{1}{M_2^2}$$

$$= \left(\frac{p_2}{p}\right)^{\frac{\gamma-1}{\gamma}}\left[1+\frac{1}{\gamma-1}\left\{2-(\gamma+1)\left(\frac{p}{p_2}\right)^{\frac{\gamma-1}{\gamma}}\right\}\frac{1}{M_2^2}\right]$$

$$\frac{1-\frac{1}{M_2^2}}{\left(\frac{M}{M_2}\right)^2-\frac{1}{M_2}} = \left(\frac{p}{p_2}\right)^{\frac{\gamma-1}{\gamma}}\left[1-\left\{1+\frac{2}{\gamma-1}-\frac{\gamma+1}{\gamma-1}\left(\frac{p}{p_2}\right)^{\frac{\gamma-1}{\gamma}}\right\}\frac{1}{M_2^2}\cdots\right]$$

$$= \left(\frac{p}{p_2}\right)^{\frac{\gamma-1}{\gamma}}\left[1-\frac{\gamma+1}{\gamma-1}\left\{1-\left(\frac{p}{p_2}\right)^{\frac{\gamma-1}{\gamma}}\right\}\frac{1}{M_2^2}\cdots\right]$$

$$\theta_0 - \theta = \frac{2}{\gamma-1}\frac{1}{M_2}\left\{1+\frac{1}{2}\frac{1}{M_2^2}\cdots\right\}\left[1-\left(\frac{p}{p_2}\right)^{\frac{\gamma-1}{2\gamma}}\left\{1-\frac{1}{2}\frac{\gamma+1}{\gamma-1}\left(1-\left(\frac{p}{p_2}\right)^{\frac{\gamma-1}{\gamma}}\right)\frac{1}{M_2^2}\cdots\right\}\right]$$

$$-\frac{1}{3}\frac{4\gamma}{(\gamma-1)^2}\frac{1}{M_2^3}\left\{1+\frac{3}{2}\frac{1}{M_2^2}\cdots\right\}\left[1-\left(\frac{p}{p_2}\right)^{\frac{3(\gamma-1)}{2\gamma}}\left\{1-\frac{3}{2}\frac{\gamma+1}{\gamma-1}\left(1-\left(\frac{p}{p_2}\right)^{\frac{\gamma-1}{\gamma}}\right)\frac{1}{M_2^2}\cdots\right\}\right]$$

$$=\frac{2}{\gamma-1}\frac{1}{M_2}\Bigg[\left\{1+\frac{1}{2}\frac{1}{M_2^2}\cdots\right\}\left\{\left(1-\left(\frac{p}{p_2}\right)^{\frac{\gamma-1}{2\gamma}}\right)+\frac{1}{2}\frac{\gamma+1}{\gamma-1}\left(\frac{p}{p_2}\right)^{\frac{\gamma-1}{2\gamma}}\left(1-\left(\frac{p}{p_2}\right)^{\frac{\gamma-1}{\gamma}}\right)\frac{1}{M_2^2}\cdots\right\}$$

$$-\frac{1}{3}\frac{2\gamma}{\gamma-1}\frac{1}{M_2^2}\left\{1-\left(\frac{p}{p_2}\right)^{\frac{3(\gamma-1)}{2\gamma}}\right\}\cdots\Bigg]$$

$$=\frac{2}{\gamma-1}\frac{1}{M_2}\Bigg[\left\{1-\left(\frac{p}{p_2}\right)^{\frac{\gamma-1}{2\gamma}}\right\}+\frac{1}{2}\Bigg\{\left[1-\left(\frac{p}{p_2}\right)^{\frac{\gamma-1}{2\gamma}}\right]+\frac{\gamma+1}{\gamma-1}\left(\frac{p}{p_2}\right)^{\frac{\gamma-1}{2\gamma}}\left[1-\left(\frac{p}{p_2}\right)^{\frac{\gamma-1}{\gamma}}\right]$$

$$-\frac{1}{3}\frac{4\gamma}{\gamma-1}\left[1-\left(\frac{p}{p_2}\right)^{\frac{3(\gamma-1)}{2\gamma}}\right]\Bigg\}\frac{1}{M_2^2}\cdots\Bigg]$$

Thus

$$\boxed{\theta_0 - \theta = \frac{2}{\gamma-1}\frac{1}{M_2}\left[\left\{1-\left(\frac{p}{p_2}\right)^{\frac{\gamma-1}{2\gamma}}\right\}+\frac{1}{2}\left\{-\frac{\gamma+3}{3(\gamma-1)}+\frac{2}{\gamma-1}\left(\frac{p}{p_2}\right)^{\frac{\gamma-1}{2\gamma}}-\frac{3-\gamma}{3(\gamma-1)}\left(\frac{p}{p_2}\right)^{\frac{3(\gamma-1)}{2\gamma}}\right\}\frac{1}{M_2^2}\cdots\right]}$$

(c) Small θ_0

$$\tan(\alpha-\theta_0) = \frac{\gamma-1}{\gamma+1}\tan\alpha$$

$$\frac{\tan\alpha - \tan\theta_0}{1+\tan\alpha\cdot\tan\theta_0} = \frac{\gamma-1}{\gamma+1}\tan\alpha$$

$$\tan\alpha - \tan\theta_0 = \frac{\gamma-1}{\gamma+1}\tan\alpha + \frac{\gamma-1}{\gamma+1}\tan^2\alpha\cdot\tan\theta_0$$

$$\frac{2}{\gamma+1}\tan\alpha = \tan\theta_0 + \frac{\gamma-1}{\gamma+1}\tan^2\alpha\cdot\tan\theta_0$$

$$\frac{4}{(\gamma+1)^2}\frac{\sin^2\alpha}{1-\sin^2\alpha} = \tan^2\theta_0 + 2\frac{\gamma-1}{\gamma+1}\tan^2\theta_0\frac{\sin^2\alpha}{1-\sin^2\alpha}+\left(\frac{\gamma-1}{\gamma+1}\right)^2\tan^2\theta_0\frac{\sin^4\alpha}{(1-\sin^2\alpha)^2}$$

5

$$\frac{4}{(\gamma+1)^2}\left[\sin^2\alpha - \sin^4\alpha\right] = \tan^2\theta_0\left[1 - 2\sin^2\alpha + \sin^4\alpha\right] + 2\frac{\gamma-1}{\gamma+1}\tan^2\theta_0\left[\sin^2\alpha - \sin^4\alpha\right]$$

$$+ \left(\frac{\gamma-1}{\gamma+1}\right)^2 \tan^2\theta_0 \sin^4\alpha$$

$$\left[\left(1 - \frac{\gamma-1}{\gamma+1}\right)^2 \tan^2\theta_0 + \frac{4}{(\gamma+1)^2}\right]\sin^4\alpha + \left[\left\{2\frac{\gamma-1}{\gamma+1} - 2\right\}\tan^2\theta_0 - \frac{4}{(\gamma+1)^2}\right]\sin^2\alpha$$

$$+ \tan^2\theta_0 = 0.$$

$$\left(\frac{2}{\gamma+1}\right)^2(\tan^2\theta_0+1)\sin^4\alpha - 2\frac{2}{\gamma+1}\left[\tan^2\theta_0 + \frac{1}{\gamma+1}\right]\sin^2\alpha + \tan^2\theta_0 = 0.$$

$$(\tan^2\theta_0+1)\sin^4\alpha - 2\left(\frac{\gamma+1}{2}\right)\left[\tan^2\theta_0 + \frac{1}{\gamma+1}\right]\sin^2\alpha + \left(\frac{\gamma+1}{2}\right)^2\tan^2\theta_0 = 0$$

$$\sin^2\alpha = \cos^2\theta_0\left[\left(\frac{\gamma+1}{2}\right)\left(\tan^2\theta_0 + \frac{1}{\gamma+1}\right) - \sqrt{\left(\frac{\gamma+1}{2}\right)^2\tan^4\theta_0 + \left(\frac{\gamma+1}{2}\right)\tan^2\theta_0 + \frac{1}{4} - \left(\frac{\gamma+1}{2}\right)^2\tan^4\theta_0 - \left(\frac{\gamma+1}{2}\right)^2\tan^2\theta_0}\right]$$

$$= \cos^2\theta_0\left[\frac{\gamma+1}{2}\tan^2\theta_0 + \frac{1}{2} - \sqrt{\frac{1}{4} - \frac{\gamma^2-1}{4}\tan^2\theta_0}\right]$$

$$= \frac{1}{2}\cos^2\theta_0\left[(\gamma+1)\tan^2\theta_0 + 1 - \sqrt{1-(\gamma^2-1)\tan^2\theta_0}\right]$$

$$= \frac{1}{2}\cos^2\theta_0\left[(\gamma+1)\tan^2\theta_0 + 1 - 1 + \frac{\gamma^2-1}{2}\tan^2\theta_0 + \frac{1}{8}(\gamma^2-1)^2\tan^4\theta_0 \cdots\right]$$

$$\sin^2\alpha = \left(\frac{\gamma+1}{2}\right)^2\sin^2\theta_0 + \frac{1}{16}(\gamma^2-1)^2\sin^2\theta_0\cdot\tan^2\theta_0 \cdots$$

$$\sin\theta_0 = \theta_0\left(1 - \frac{1}{6}\theta_0^2 \cdots\right)$$

$$\sin^2\theta_0 = \theta_0^2\left(1 - \frac{1}{3}\theta_0^2 \cdots\right),$$

$$\sin^2\alpha = \left(\frac{\gamma+1}{2}\right)^2\left[\,\theta_0^2\left(1-\frac{1}{3}\theta_0^2\cdots\right)+\frac{1}{4}(\gamma-1)^2\theta_0^4\cdots\right]$$

$$\boxed{\sin^2\alpha = \left(\frac{\gamma+1}{2}\right)^2\theta_0^2\left[\,1-\left\{\frac{1}{3}-\left(\frac{\gamma-1}{2}\right)^2\right\}\theta_0^2\cdots\right]}$$

$$\frac{1}{M_2^2} = \frac{1}{\dfrac{(\gamma+1)^2}{2\gamma(\gamma-1)}\dfrac{1}{\sin^2\alpha}-\dfrac{2}{\gamma-1}}$$

$$= \frac{\sin^2\alpha}{\dfrac{(\gamma+1)^2}{2\gamma(\gamma-1)}-\dfrac{2}{\gamma-1}\sin^2\alpha}$$

$$= \frac{\dfrac{2\gamma(\gamma-1)}{(\gamma+1)^2}\sin^2\alpha}{1-\dfrac{4\gamma}{(\gamma+1)^2}\sin^2\alpha}$$

$$\frac{1}{M_2^2} = \frac{\gamma(\gamma-1)}{2}\theta_0^2\left[1-\left\{\frac{1}{3}-\left(\frac{\gamma-1}{2}\right)^2\right\}\theta_0^2\cdots\right]\left[1+\gamma\theta_0^2\cdots\right]$$

$$\frac{1}{M_2^2} = \frac{\gamma(\gamma-1)}{2}\theta_0^2\left[1+\left\{\gamma+\left(\frac{\gamma-1}{2}\right)^2-\frac{1}{3}\right\}\theta_0^2\cdots\right]$$

$$\boxed{\frac{1}{M_2} = \sqrt{\frac{\gamma(\gamma-1)}{2}}\,\theta_0\left[1+\frac{1}{2}\left\{\gamma+\left(\frac{\gamma-1}{2}\right)^2-\frac{1}{3}\right\}\theta_0^2\cdots\right]}$$

Thus

$$\Theta_0 - \Theta = \sqrt{\frac{2\gamma}{\gamma-1}}\,\Theta_0 \left[1 + \frac{1}{2}\left\{ \gamma + \left(\frac{\gamma-1}{2}\right)^2 - \frac{1}{3} \right\} \Theta_0^2 - - - \right]$$

$$\left[\left\{ 1 - \left(\frac{p}{p_2}\right)^{\frac{\gamma-1}{2\gamma}} \right\} + \frac{\gamma}{4} \left\{ -\frac{\gamma+3}{3} + 2\left(\frac{p}{p_2}\right)^{\frac{\gamma-1}{2\gamma}} - \frac{3-\gamma}{3}\left(\frac{p}{p_2}\right)^{\frac{3(\gamma-1)}{2\gamma}} \right\} \Theta_0^2 - - - \right]$$

Hence

$$\Theta_0 - \Theta = \sqrt{\frac{2\gamma}{\gamma-1}}\,\Theta_0 \left[\left\{ 1 - \left(\frac{p}{p_2}\right)^{\frac{\gamma-1}{2\gamma}} \right\} + \left\{ \frac{1}{2}\left[\gamma + \left(\frac{\gamma-1}{2}\right)^2 - \frac{1}{3} \right] \left[1 - \left(\frac{p}{p_2}\right)^{\frac{\gamma-1}{2\gamma}} \right] + \frac{\gamma}{4}\left[-\frac{\gamma+3}{3} + 2\left(\frac{p}{p_2}\right)^{\frac{\gamma-1}{2\gamma}} - \frac{3-\gamma}{3}\left(\frac{p}{p_2}\right)^{\frac{3(\gamma-1)}{2\gamma}} \right] \right\} \Theta_0^2 - - - \right]$$

If $p=0$, then

$$-\Theta = \sqrt{\frac{2\gamma}{\gamma-1}}\,\Theta_0 \left[1 + \left\{ \frac{1}{2}\left[\gamma + \left(\frac{\gamma-1}{2}\right)^2 - \frac{1}{3} \right] - \frac{\gamma(\gamma+3)}{12} \right\} \Theta_0^2 \cdots \right] - \Theta_0$$

$$\sim \left(\sqrt{\frac{2\gamma}{\gamma-1}} - 1 \right) \Theta_0$$

If $\gamma = 1.405$, $\sqrt{\frac{2\gamma}{\gamma-1}} - 1 = 1.632$

Two-Dimensional Flow

The general differential equation is

$$\left(1-\frac{u^2}{a^2}\right)\frac{\partial u}{\partial x}-2\frac{uv}{a^2}\frac{\partial u}{\partial y}+\left(1-\frac{v^2}{a^2}\right)\frac{\partial v}{\partial y}=0$$

$$u=U+\frac{\partial\varphi}{\partial x}$$

$$v=\frac{\partial\varphi}{\partial y}.$$

$$a^2=a_0^2-\frac{\gamma-1}{2}\left[U^2+2U\frac{\partial\varphi}{\partial x}+\left(\frac{\partial\varphi}{\partial x}\right)^2+\left(\frac{\partial\varphi}{\partial y}\right)^2\right]$$

$$a^{\circ 2}=a_0^2-\frac{\gamma-1}{2}U^2, \qquad a_0^2=a^{\circ 2}+\frac{\gamma-1}{2}U^2$$

$$a^2=a^{\circ 2}+\frac{\gamma-1}{2}U^2-\frac{\gamma-1}{2}\left[U^2+2U\frac{\partial\varphi}{\partial x}+\left(\frac{\partial\varphi}{\partial x}\right)^2+\left(\frac{\partial\varphi}{\partial y}\right)^2\right]$$

$$=a^{\circ 2}-\frac{\gamma-1}{2}\left[2U\frac{\partial\varphi}{\partial x}+\left(\frac{\partial\varphi}{\partial x}\right)^2+\left(\frac{\partial\varphi}{\partial y}\right)^2\right]$$

$$\frac{u^2}{a^2}=\frac{U^2+2U\frac{\partial\varphi}{\partial x}+\left(\frac{\partial\varphi}{\partial x}\right)^2}{a^{\circ 2}\left[1-\frac{\gamma-1}{2}\left\{2M^\circ\frac{1}{a^\circ}\frac{\partial\varphi}{\partial x}+\frac{1}{a^{\circ 2}}\left(\frac{\partial\varphi}{\partial x}\right)^2+\frac{1}{a^{\circ 2}}\left(\frac{\partial\varphi}{\partial y}\right)^2\right\}\right]}$$

$$\cong\frac{M^{\circ 2}+2M^\circ\frac{1}{a^\circ}\frac{\partial\varphi}{\partial x}}{1-(\gamma-1)M^\circ\frac{1}{a^\circ}\frac{\partial\varphi}{\partial x}-\frac{\gamma-1}{2}\frac{1}{a^{\circ 2}}\left(\frac{\partial\varphi}{\partial y}\right)^2}$$

$$\frac{uv}{a^2}\cong\frac{\left(U+\frac{\partial\varphi}{\partial x}\right)\frac{\partial\varphi}{\partial y}}{a^{\circ 2}\left[1-(\gamma-1)M^\circ\frac{1}{a^\circ}\frac{\partial\varphi}{\partial x}-\frac{\gamma-1}{2}\frac{1}{a^{\circ 2}}\left(\frac{\partial\varphi}{\partial y}\right)^2\right]}\cong\frac{M^\circ\frac{1}{a^\circ}\frac{\partial\varphi}{\partial y}}{1-(\gamma-1)M^\circ\frac{1}{a^\circ}\frac{\partial\varphi}{\partial x}-\frac{(\gamma-1)}{2}\frac{1}{a^{\circ 2}}\left(\frac{\partial\varphi}{\partial y}\right)^2}$$

Therefore the differential equation becomes

$$\left[1-(\gamma-1)M^0\frac{1}{a^0}\frac{\partial\varphi}{\partial x}-\frac{\gamma-1}{2}\frac{1}{a^{02}}\left(\frac{\partial\varphi}{\partial y}\right)^2-M^{02}-2M^0\frac{1}{a^0}\frac{\partial\varphi}{\partial x}\right]\frac{\partial^2\varphi}{\partial x^2}-2M^0\frac{1}{a^0}\frac{\partial\varphi}{\partial y}\frac{\partial^2\varphi}{\partial x\partial y}$$

$$+\left[1-(\gamma-1)M^0\frac{1}{a^0}\frac{\partial\varphi}{\partial x}-\frac{\gamma-1}{2}\frac{1}{a^{02}}\left(\frac{\partial\varphi}{\partial y}\right)^2-\frac{1}{a^{02}}\left(\frac{\partial\varphi}{\partial y}\right)^2\right]\frac{\partial^2\varphi}{\partial y^2}=0$$

$$\left[1-(\gamma+1)M^0\frac{1}{a^0}\frac{\partial\varphi}{\partial x}-\frac{\gamma-1}{2}\frac{1}{a^{02}}\left(\frac{\partial\varphi}{\partial y}\right)^2-M^{02}\right]\frac{\partial^2\varphi}{\partial x^2}-2M^0\frac{1}{a^0}\frac{\partial\varphi}{\partial y}\frac{\partial^2\varphi}{\partial x\partial y}$$

$$+\left[1-(\gamma-1)M^0\frac{1}{a^0}\frac{\partial\varphi}{\partial x}-\frac{\gamma+1}{2}\frac{1}{a^{02}}\left(\frac{\partial\varphi}{\partial y}\right)^2\right]\frac{\partial^2\varphi}{\partial y^2}=0$$

Let $\varphi = a^0 b\,\frac{1}{M^0}\,f(\xi,\eta)$

$x = b\xi$

$y = b\eta\left(\frac{\delta}{b}\right)^n$

Boundary conditions, at ∞, $\frac{\partial f}{\partial\xi}=\frac{\partial f}{\partial\eta}=0$

at $\eta=0$, $\left(\frac{\partial\varphi}{\partial y}\right)_{y=0}=a^0M^0\left(\frac{\delta}{b}\right)h(\xi)$

$$\left\{1-(\gamma-1)\frac{\partial f}{\partial\xi}-\frac{\gamma+1}{2}\frac{1}{\left[M^0\left(\frac{\delta}{b}\right)^n\right]^2}\left(\frac{\partial f}{\partial\eta}\right)^2\right\}\frac{\partial^2 f}{\partial\eta^2}=2\frac{\partial f}{\partial\eta}\frac{\partial^2 f}{\partial\xi\partial\eta}+\left[M^0\left(\frac{\delta}{b}\right)^n\right]^2\frac{\partial^2 f}{\partial\xi^2}$$

at $\eta=0$, $a^0 b\,\frac{1}{M^0}\left(\frac{\partial f}{\partial\eta}\right)_{\eta=0}\frac{1}{b}\frac{1}{\left(\frac{\delta}{b}\right)^n}=a^0\left(M^0\frac{\delta}{b}\right)h(\xi)$

Or $\left(\frac{\partial f}{\partial\eta}\right)_{\eta=0}=\left[M^0\left(\frac{\delta}{b}\right)\right]\left[M^0\left(\frac{\delta}{b}\right)^n\right]h(\xi)$

Thus if $M^0\left(\frac{\delta}{b}\right) = K$, then

$$\left\{1-(\gamma-1)\frac{\partial f}{\partial \xi} - \frac{\gamma+1}{2}\frac{1}{K^2}\left(\frac{\partial f}{\partial \eta}\right)^2\right\}\frac{\partial^2 f}{\partial \eta^2} = 2\frac{\partial f}{\partial \eta}\frac{\partial^2 f}{\partial \xi \partial \eta} + K^2\frac{\partial^2 f}{\partial \xi^2}$$

Boundary conditions, At ∞, $\frac{\partial f}{\partial \xi} = \frac{\partial f}{\partial \eta} = 0$

At $\eta = 0$, $\left(\frac{\partial f}{\partial \eta}\right)_{\eta=0} = K^2 h(\xi)$

$$p = p_0\left[1 + \frac{\gamma-1}{2}\frac{u^2 + 2u\frac{\partial\varphi}{\partial x} + \left(\frac{\partial\varphi}{\partial y}\right)^2}{a^{0^2}\left[1-(\gamma-1)M^0\frac{1}{a^0}\frac{\partial\varphi}{\partial x} - \frac{\gamma-1}{2}\frac{1}{a^{0^2}}\left(\frac{\partial\varphi}{\partial y}\right)^2\right]}\right]^{-\frac{\gamma}{\gamma-1}}$$

$$p^0 = p_0\left[1 + \frac{\gamma-1}{2}M^{0^2}\right]^{-\frac{\gamma}{\gamma-1}}$$

$$p = p^0\left[\frac{1 + \frac{\gamma-1}{2}M^{0^2}}{1 + \frac{\gamma-1}{2}\dfrac{M^{0^2} + 2M^0\frac{1}{a^0}\frac{\partial\varphi}{\partial x} + \frac{1}{a^{0^2}}\left(\frac{\partial\varphi}{\partial y}\right)^2}{1-(\gamma-1)M^0\frac{1}{a^0}\frac{\partial\varphi}{\partial x} - \frac{\gamma-1}{2}\frac{1}{a^{0^2}}\left(\frac{\partial\varphi}{\partial y}\right)^2}}\right]^{\frac{\gamma}{\gamma-1}}$$

$$p = p^0\left[1-(\gamma-1)\frac{\partial f}{\partial \xi} - \frac{\gamma-1}{2}\frac{1}{K^2}\left(\frac{\partial f}{\partial \eta}\right)^2\right]^{\frac{\gamma}{\gamma-1}}$$

$$\text{Drag} = D = \int_{-b}^{b} p \cdot h(\xi)\left(\frac{f}{b}\right) dx = b\, p^0 \left(\frac{f}{b}\right) \int_{-1}^{1} \left[1 - (\gamma-1)\frac{\partial f}{\partial \xi} - \frac{\gamma-1}{2}\frac{1}{K^2}\left(\frac{\partial f}{\partial \eta}\right)^2\right]^{\frac{\gamma}{\gamma-1}} h(\xi)\, d\xi$$

$$C_D = \frac{D}{\frac{\rho^0}{2}U^2(2b)} = \frac{D}{\rho^0 U^2 b} = \frac{\left(\frac{f}{b}\right)M^0}{M^{03}}\frac{1}{\gamma}\int_{-1}^{1}\left[1 - (\gamma-1)\frac{\partial f}{\partial \xi} - \frac{\gamma-1}{2}\frac{1}{K^2}\left(\frac{\partial f}{\partial \eta}\right)^2\right]^{\frac{\gamma}{\gamma-1}} h(\xi)\, d\xi$$

$$\boxed{C_D = \frac{1}{M^{03}}\mathcal{D}\left(M^0\frac{f}{b}\right) \qquad C_L = \frac{1}{M^{02}}\mathcal{L}\left(M^0\frac{f}{b}\right)}$$

Checks with the linear Ackeret theory!

M^0

$$C_D \sim \frac{\left(\frac{f}{b}\right)^2}{\sqrt{M^{02}-1}}$$

Axially symmetric flows

$$\left[1 - (\gamma+1)M^0\frac{1}{a^0}\frac{\partial \varphi}{\partial x} - \frac{\gamma-1}{2}\frac{1}{a^{02}}\left(\frac{\partial \varphi}{\partial y}\right)^2 - M^{02}\right]\frac{\partial^2 \varphi}{\partial x^2} - 2M^0\frac{1}{a^0}\frac{\partial \varphi}{\partial y}\frac{\partial^2 \varphi}{\partial x \partial y} + \left[1 - (\gamma-1)M^0\frac{1}{a^0}\frac{\partial \varphi}{\partial x} - \frac{\gamma+1}{2}\frac{1}{a^{02}}\left(\frac{\partial \varphi}{\partial y}\right)^2\right]\frac{\partial^2 \varphi}{\partial y^2}$$

$$+ \left[1 - (\gamma-1)M^0\frac{1}{a^0}\frac{\partial \varphi}{\partial x} - \frac{\gamma-1}{2}\frac{1}{a_0^{02}}\left(\frac{\partial \varphi}{\partial y}\right)^2\right]\frac{1}{y}\frac{\partial \varphi}{\partial y} = 0.$$

Boundary conditions, at ∞, $\frac{\partial \varphi}{\partial x} = \frac{\partial \varphi}{\partial y} = 0$

at $y=0$, $\left(y\frac{\partial \varphi}{\partial y}\right)_{y=0} = a^0 M^0 h(\xi)\left(\frac{f}{b}\right)^2 b$

$$\left[1 - (\gamma-1)\frac{\partial f}{\partial \xi} - \frac{\gamma+1}{2}\frac{1}{\left[M^0\left(\frac{f}{b}\right)\eta\right]^2}\left(\frac{\partial f}{\partial \eta}\right)^2\right]\frac{\partial^2 f}{\partial \eta^2} + \left[1 - (\gamma-1)\frac{\partial f}{\partial \xi} - \frac{\gamma-1}{2}\frac{1}{\left[M^0\left(\frac{f}{b}\right)\eta\right]^2}\left(\frac{\partial f}{\partial \eta}\right)^2\right]\frac{1}{\eta}\frac{\partial f}{\partial \eta}$$

$$= 2\frac{\partial f}{\partial \eta}\frac{\partial^2 f}{\partial \xi \partial \eta} + \left[M^0\left(\frac{f}{b}\right)\eta\right]^2\frac{\partial^2 f}{\partial \xi^2}$$

at $\eta = 0$, $\quad a^0 b \frac{1}{M^0}\left(\eta \frac{\partial f}{\partial \eta}\right)_{\eta=0} = a^0 M^0 \left(\frac{\delta}{b}\right)^2 b\, h(\xi)$

$$\left(\eta \frac{\partial f}{\partial \eta}\right)_{\eta=0} = \left[M^0\left(\frac{\delta}{b}\right)\right]^2 h(\xi)$$

So

$$M^0\left(\frac{\delta}{b}\right) = K,$$

$$\left\{1-(\gamma-1)\frac{\partial f}{\partial \xi} - \frac{\gamma+1}{2}\frac{1}{K^2}\left(\frac{\partial f}{\partial \eta}\right)^2\right\}\frac{\partial^2 f}{\partial \eta^2} + \left\{1-(\gamma-1)\frac{\partial f}{\partial \xi} - \frac{\gamma-1}{2}\frac{1}{K^2}\left(\frac{\partial f}{\partial \eta}\right)^2\right\}\frac{1}{\eta}\frac{\partial f}{\partial \eta}$$

$$= 2\frac{\partial f}{\partial \eta}\frac{\partial^2 f}{\partial \xi \partial \eta} + K^2 \frac{\partial^2 f}{\partial \xi^2}$$

at ∞, $\quad \frac{\partial f}{\partial \xi} = \frac{\partial f}{\partial \eta} = 0.$

$$\left(\eta \frac{\partial f}{\partial \eta}\right)_{\eta=0} = K^2 h(\xi)$$

$$C_D = \frac{1}{M^{0\,2}} \mathcal{D}\left(M^0 \frac{\delta}{b}\right)$$

$C_D \sim \left(\frac{\delta}{b}\right)^2$

Section 3

Application of Tschapligin's Transformation to Two Dimensional Subsonic Flow

PART (III)

Application of Tschapligins' Transformation to Two Dimensional Subsonic Flow

The equations of two dimensional irrotational motion of compressible fluids, assuming that the pressure is a single valued function of density only, can be reduced to a single non-linear equation of the velocity potential. In the supersonic case, the problem is solved by Prandtl, Meyer and Busemann by means of the powerful method of characteristics. The essential difficulty of this problem lies in the subsonic case especially when the velocity is near to the velocity of sound. The first logical step is to linearize the equation based on the argument that the disturbance due to the presence of a solid body super-imposed on the parallel rectlinear flow is sufficiently small compared with parallel flow. This makes the second and higher order terms of disturbance potential to be negligible. An example of this method is the well-known theory of thin airfoil due to Prandtl and Glauert. But the presence of stagnation point at the nose of the airfoil makes the application of the linearized theory questionable, at least near this region; because there the

disturbance due to the presence of the body is no (2)
longer small. On the same ground, the theory breaks
down in case of bodies whose dimension across
the stream is not small compared with the dimension
parallel to the stream. The next method is that
devised originally by Janzen and Rayleigh. They solved the
equation by successive approximations. However, the
process is very tedious and the method convergent very slowly if the velocity
approaches that of sound.

Molenbroek (Ref. 1) and Tschaplygin (Ref. 2) suggested the use of
the magnitude of velocity and inclination of velocity to the x-axis
as independent variables and were able thus
reduced the equation of velocity potential to a
linear equation. This equation was solved
by Tschaplygin (Ref. 2) and recently put in a more
convenient form by F. Clauser and M. Clauser (Ref. 3). The
solution is essentially a series each term
of which is a product of hypergeometric function +
circular function. The chief difficulty in practical
application of this solution is to obtain a proper
set of boundary conditions in the transformed plane,
or the hodograph plane.

Tschapligin (Ref. 2) shown that a great simplification of the equation in hodograph plane results if ~~a~~ the ratio of specific heats of the gas is equal to −1. Then the equation becomes the equation of minimal surface whose solution is well-known. However, at first, this hypothetical value of ratios of specific heats (all ~~a~~ real gas has ~~the~~ the value ~~of~~ for this ratio ranging from 1.00 to 2.00) makes the practical ~~not until~~ application of Tschapligin's theory questionable. ~~Only~~ It was ~~through~~ Demtschenko (Ref. 4) ~~(#)~~ and Busemann (Ref. 5) who made the meaning of this special ~~so~~ value of ratio ~~made~~ clear. They found that this ~~speef~~ special value of ratio of specific heats really corresponds to ~~the~~ take the tangent of P-V curve of gas instead P-V curve itself. However, they limit themself to ~~the case~~ ~~take~~ use the tangent at the state of rest of the gas. Thus their theory can only apply to velocities up to 0.5 times sound velocity. In this section, the theory is ~~extended~~ generalized to ~~the case~~ ~~that~~ use the tangent at the state of gas corresponding to the undisturbed ~~par~~ parallel flow. Therefore the range of usefulness of the theory is greatly ~~x~~ extended.

In the first section, the general theory of this method[4] will be developed. In the second section, the theory will be applied to the case of symmetrical Joukowsky airfoil at zero angle of attack.

Section (I)

If p is the pressure and v is the density of gas, the adiabatic process is expressed as a curve in the p-v plane as shown in Fig. 3.1. Now condition near to the point (p_1, v_1) can be approximated by the tangent at this point. The equation of the tangent at this point can be written as

$$p_1 - p = C(v_1 - v) = C(\rho_1^{-1} - \rho^{-1}) \qquad (3.1)$$

where ρ is the density of the gas. Now the slope C must be equal to the slope of the curve at the point (p_1, v_1).

$$C = \left(\frac{dp}{dv}\right)_1 = \left(\frac{dp}{d\rho}\cdot\frac{d\rho}{dv}\right)_1 = -\left(\frac{dp}{d\rho}\right)_1 \rho_1^2 = -a_1^2\rho_1^2$$

Therefore $C = -a_1^2\rho_1^2$

Hence the approximate p-ρ relation near (p_1, ρ_1) can be written as

$$p_1 - p = a_1^2\rho_1^2\left(\frac{1}{\rho} - \frac{1}{\rho_1}\right) \qquad (3.2)$$

5)

~~From the consideration of mechanical energy of the gas, the following relation~~

From the generalized Bernoulli's theorem, the following relation is obtained

$$\frac{1}{2}w_2^2 - \frac{1}{2}w_3^2 = \int^{\rho} \frac{dp}{\rho} \qquad (3.3)$$

where w is the velocity of gas, the subscripts 2 + 3 indicate two conditions. But from Eq. (3.2), p can be expressed as a function of ρ, thus

$$dp = \frac{a_1^2 \rho_1^2}{\rho^2} d\rho \qquad (3.4)$$

Substituting into the ~~right~~ integrand in Eq. (3.3) and integrate, the following relation is obtained

$$\frac{1}{2}w_2^2 - \frac{1}{2}w_3^2 = \frac{1}{2}a_1^2\rho_1^2 \left\{ \frac{1}{\rho_3^2} - \frac{1}{\rho_2^2} \right\}$$

Now if $w_3 = 0$, $w_2 = w$, $\rho_3 = \rho_0$ and $\rho_2 = \rho$, then

$$\frac{a_1^2 \rho_1^2}{\rho_0^2} + w^2 = \frac{\rho_1^2 a_1^2}{\rho^2} \qquad (3.5)$$

where the subscript 0 denotes the rest state of the gas.

If ~~we~~ the sound velocity a is defined as the ~~differen~~ derivative of p with respect to ρ, then Eq. (3.4) gives

$$\frac{dp}{d\rho} \rho^2 = a^2\rho^2 = a_1^2\rho_1^2 = \text{constant} \qquad (3.6)$$

Therefore Eq. (3.5) can be written as

$$\left(\frac{\rho}{\rho_0}\right)^2 = 1 - \frac{w^2}{a^2} \qquad (3.7)$$

(a)

It is interesting at this stage to notice that from Eq. (3.8), the density decreases as velocity w increases, as it is expected. Thus from Eq. (3.7), the velocity of sound of the gas will increase as the velocity is increased. This is just opposite to real gas, because in the case of an adiabatic flow, it is well-known that the temperature of gas decreases as the velocity of gas is increased and thus the sound velocity also decreases. However from Eq. (3.7), the ratio $\left(\frac{w}{a}\right)$ or Mach's number increases as the velocity w increases. But this ratio only reaches the value unity when $\rho = 0$, or from Eq. (3.8) when $w = \infty$. It is thus seen that the entire region of flow is subsonic and thus the equations of motion is always of elliptic type. This may be considered as the physical reason why the complex representation of velocity potential and stream function is possible in all cases, as will be shown in following pages. However, one should bear in mind that the portion of tangent that could be used as an approximation to the true adiabatic curve must lie within the first quadrant. Thus the upper limit of velocity for practical application of the theory is when $p = 0$. By using Eq. (3.2)

(4.3.7) and (4.3.8), this upper limit is found to be

$$\left(\frac{w}{w_1}\right)_{max.} = \frac{1}{\left(\frac{w_1}{a_1}\right)}\sqrt{\left(\frac{\gamma p_1}{\rho_1 a_1^2}\right)\left(\frac{p_1}{\rho_1 a_1^2}+1\right)^2 - \left[1-\left(\frac{w_1}{a_1}\right)^2\right]}$$

Or by putting $a_1^2 = \gamma \frac{p_1}{\rho_1}$, the above equation reduces to

$$\left(\frac{w}{w_1}\right)_{max.} = \frac{1}{\left(\frac{w_1}{a_1}\right)}\sqrt{(\gamma+1)^2 - \left\{1-\left(\frac{w_1}{a_1}\right)^2\right\}}$$

The values of $\left(\frac{w}{w_1}\right)_{max}$ for different values of $\left(\frac{w_1}{a_1}\right)$ are shown Table 3.1.

Table 3.1

$\left(\frac{w_1}{a_1}\right)$	$\left(\frac{w}{w_1}\right)_{max.}$	$\left(\frac{w}{a_1}\right)_{max}$
0	∞	2.186
0.2	10.91	2.195
0.4	5.56	2.225
0.6	3.78	2.265
0.8	2.92	2.335
1.0	2.405	2.405

It is thus seen that for most ~~practical~~ applications of this theory, p will remain positive, However due to large deviation from the true adiabatic process at higher values of $\left(\frac{w}{w_1}\right)$, one has probably limit the ratio $\left(\frac{w}{w_1}\right)$ to about 2.

or $$\left(\frac{\rho}{\rho_0}\right) = \sqrt{1 - \frac{w^2}{a^2}} \qquad (3.7)$$

Furthermore, from Eq. (3.6), $\rho_1^2 a_1^2 = \rho_1^2 a_0^2$, thus Eq. (3.7) can also be written as

Page a-b

$$\left(\frac{\rho_0}{\rho}\right) = \sqrt{1 + \left(\frac{w}{a_0}\right)^2} \qquad (3.8)$$

Now if the flow is irrotational, there exists a velocity potential Φ such that

$$\frac{\partial \Phi}{\partial x} = u, \qquad \frac{\partial \Phi}{\partial y} = v \qquad (3.9)$$

where u, v are the x + y components of the velocity w. To satisfy the equation of continuity, the stream function Ψ is introduced. It is defined by

$$\frac{\rho}{\rho_0} u = \frac{\partial \Psi}{\partial y}, \qquad \frac{\rho}{\rho_0} v = -\frac{\partial \Psi}{\partial x} \qquad (3.10)$$

Now if the angle of inclination of the velocity w to the x-axis is β, then from Eqs. (3.9) + (3.10), one has

$$\left.\begin{aligned} d\phi &= w \cdot \cos\beta \, dx + w \cdot \sin\beta \, dy \\ d\Psi &= -w \frac{\rho}{\rho_0} \sin\beta \, dx + w \frac{\rho}{\rho_0} \cos\beta \cdot dy \end{aligned}\right\} \qquad (3.11)$$

Solving for dx and dy,

$$\left.\begin{aligned} dx &= \frac{\cos\beta}{w} d\phi - \frac{\sin\beta}{w} \frac{\rho_0}{\rho} d\Psi \\ dy &= \frac{\sin\beta}{w} d\phi + \frac{\cos\beta}{w} \frac{\rho_0}{\rho} d\Psi \end{aligned}\right\} \qquad (3.12)$$

(7)

So long as the correspondence between the ~~space~~ physical plane and the hodoplane is one to one, or mathematically $\frac{\partial(x,y)}{\partial(u,v)} \neq 0$, one can express x & y as functions of w, β and ~~also~~ so also ϕ and ψ as functions of w & β. Thus

$$\left.\begin{aligned} d\phi &= \phi'_w \, dw + \phi'_\beta \, d\beta \\ d\psi &= \psi'_w \, dw + \psi'_\beta \, d\beta \end{aligned}\right\} \quad (3.13)$$

where primes indicate the derivative, and subscripts indicate the variables with respect to which the functions ~~is~~ are differentiated. Now substitute Eq. (3.13) into Eq. (3.12), the following relations are obtained

$$\left.\begin{aligned} dx &= \left(\frac{\cos\beta}{w}\phi'_w - \frac{\sin\beta}{w}\frac{\rho_0}{\rho}\psi'_w\right)dw + \left(\frac{\cos\beta}{w}\phi'_\beta - \frac{\sin\beta}{w}\frac{\rho_0}{\rho}\psi'_\beta\right)d\beta \\ dy &= \left(\frac{\sin\beta}{w}\phi'_w + \frac{\cos\beta}{w}\frac{\rho_0}{\rho}\psi'_w\right)dw + \left(\frac{\sin\beta}{w}\phi'_\beta + \frac{\cos\beta}{w}\frac{\rho_0}{\rho}\psi'_\beta\right)d\beta \end{aligned}\right\} \quad (3.14)$$

Since the left-hand side of Eq (3.14) are exact differential, ~~we~~ one can apply the reciprocity relation, and obtains

$$\left.\begin{aligned} \frac{\partial}{\partial\beta}\left(\frac{\cos\beta}{w}\phi'_w - \frac{\sin\beta}{w}\frac{\rho_0}{\rho}\psi'_w\right) &= \frac{\partial}{\partial w}\left(\frac{\cos\beta}{w}\phi'_\beta - \frac{\sin\beta}{w}\frac{\rho_0}{\rho}\psi'_\beta\right) \\ \frac{\partial}{\partial\beta}\left(\frac{\sin\beta}{w}\phi'_w + \frac{\cos\beta}{w}\frac{\rho_0}{\rho}\psi'_w\right) &= \frac{\partial}{\partial w}\left(\frac{\sin\beta}{w}\phi'_\beta + \frac{\cos\beta}{w}\frac{\rho_0}{\rho}\psi'_\beta\right) \end{aligned}\right\} \quad (3.15)$$

Carrying out the differentiation, and cancelling identical (8) terms in left-hand and right hand side,

$$-\frac{\sin\beta}{w}\phi'_w - \frac{\cos\beta}{w}\frac{\rho_0}{\rho}\psi'_w = -\frac{\cos\beta}{w^2}\phi'_\beta + \frac{\sin\beta}{w^2}\frac{\rho_0}{\rho}\left(1-\frac{w^2}{a^2}\right)\psi'_\beta$$

$$\frac{\cos\beta}{w}\phi'_w - \frac{\sin\beta}{w}\frac{\rho_0}{\rho}\psi'_w = -\frac{\sin\beta}{w^2}\phi'_\beta - \frac{\cos\beta}{w^2}\frac{\rho_0}{\rho}\left(1-\frac{w^2}{a^2}\right)\psi'_\beta$$

(3.16)

Using Eq. (3.7), Eqn. (3.16) becomes

$$-\frac{\sin\beta}{w}\phi'_w - \frac{\cos\beta}{w}\frac{\rho_0}{\rho}\psi'_w = -\frac{\cos\beta}{w^2}\phi'_\beta + \frac{\sin\beta}{w^2}\frac{\rho}{\rho_0}\psi'_\beta$$

$$\frac{\cos\beta}{w}\phi'_w - \frac{\sin\beta}{w}\frac{\rho_0}{\rho}\psi'_w = -\frac{\sin\beta}{w^2}\phi'_\beta - \frac{\cos\beta}{w^2}\frac{\rho}{\rho_0}\psi'_\beta \qquad (3.17)$$

As in both equation ϕ'_w & ψ'_β, and ϕ'_β and ψ'_β are connected with a proportional factor, one can solve for them, and

$$\left.\begin{aligned}\phi'_w &= -\frac{\rho}{\rho_0}\frac{1}{w}\psi'_\beta \\ \phi'_\beta &= \frac{\rho_0}{\rho}w\,\psi'_w\end{aligned}\right\} \qquad (3.18)$$

~~T~~ Now Eq. (3.18) can be further* reduced if a new variable ω ~~defined~~ is introduced. ω is defined as

$$d\omega = \frac{\rho}{\rho_0}\frac{dw}{w} \qquad (3.19)$$

~~On integrating~~

Then Eq. (3.18) becomes

$$\left.\begin{aligned}\phi'_{\omega} &= -\psi'_{\beta} \\ \phi'_{\beta} &= \psi'_{\omega}\end{aligned}\right\} \qquad (3.20)$$

This is the fundamental set of equations for the present theory. It can be easily recognized as the Cauchy-Riemann differential equation, and thus $\phi + i\psi$ must be a analytic function of $\beta + i\omega$. However, for the convenience of ~~practical~~ numerical calculation, ~~a~~ a new variable W is used instead of ω, such that

$$W = a_0 \cdot e^{\omega} \qquad (3.21_a)$$

Or by integrating Eq. (3.19),

$$W = \frac{2a_0 w}{\sqrt{a_0^2 + w^2} + a_0} \qquad (3.21)$$

Hence by inverting,

$$w = \frac{4a_0^2 W}{4a_0^2 - W^2} \qquad (3.22)$$

Thus by substituting into Eq. (3.8)

$$\frac{\rho_0}{\rho} = \frac{4a_0^2 + W^2}{4a_0^2 - W^2} \qquad (3.23)$$

If another set of new variables $U = W\cos\beta$ and $V = W\sin\beta$ are used as independent variables, one has (10)

$$\frac{\partial}{\partial w} = \frac{\partial U}{\partial w}\frac{\partial}{\partial U} + \frac{\partial V}{\partial w}\frac{\partial}{\partial V} = W\left\{\cos\beta\frac{\partial}{\partial U} + \sin\beta\frac{\partial}{\partial V}\right\}$$

$$\frac{\partial}{\partial \beta} = \frac{\partial U}{\partial \beta}\frac{\partial}{\partial U} + \frac{\partial V}{\partial \beta}\frac{\partial}{\partial V} = W\left\{-\sin\beta\frac{\partial}{\partial U} + \cos\beta\frac{\partial}{\partial V}\right\} \quad (3.24)$$

Using Eq. (3.24), Eq. (3.20) can be written as

$$\cos\beta\frac{\partial\phi}{\partial U} + \sin\beta\frac{\partial\phi}{\partial V} = \sin\beta\frac{\partial\psi}{\partial U} - \cos\beta\frac{\partial\psi}{\partial V}$$

$$-\sin\beta\frac{\partial\phi}{\partial U} + \cos\beta\frac{\partial\phi}{\partial V} = \cos\beta\frac{\partial\psi}{\partial U} + \sin\beta\frac{\partial\psi}{\partial V}$$

These equations are satisfied by

$$\frac{\partial\phi}{\partial U} = \frac{\partial\psi}{\partial(-V)} \quad ; \quad \frac{\partial\phi}{\partial(-V)} = -\frac{\partial\psi}{\partial U} \quad (3.25)$$

These are the Cauchy-Riemann differential equations, therefore the complex potential $F = \phi + i\psi$ is a function of $U - iV = \bar{W}$. Or

$$\left.\begin{aligned} \phi + i\psi &= F(U - iV) = F(\bar{W}) \\ \text{Hence} \quad \phi - i\psi &= \bar{F}(U + iV) = \bar{F}(W) \end{aligned}\right\} \quad (3.26)$$

To transform from hodograph plane back to physical plane, the expression of x & y in terms of U & V must be found. By using Eqs (3.22) and (3.23), Eq. (3.12) can be written as

$$dx = \frac{U \cdot d\phi}{W^2}\left\{1 - \frac{W^2}{4a_0^2}\right\} - \frac{V \cdot d\psi}{W^2}\left\{1 + \frac{W^2}{4a_0^2}\right\} \qquad (A)$$

$$dy = \frac{V \cdot d\phi}{W^2}\left\{1 - \frac{W^2}{4a_0^2}\right\} + \frac{U \cdot d\psi}{W^2}\left\{1 + \frac{W^2}{4a_0^2}\right\}$$

where $W^2 = U^2 + V^2$. These equations can be combined into one equation by means of Eq. (3.26). Thus

$$dz = dx + i\,dy = \frac{dF}{\overline{W}} - \frac{W \cdot d\overline{F}}{4a_0^2} \qquad (3.27)$$

For practical application of the theory to the flow over an obstacle, the computation proceeds as follows:

(I) Find the complex potential for the flow of incompressible fluid over the obstacle, say

$$w_1\, G(\xi + i\eta) = w_1\, G(\zeta)$$

where w_1 is the velocity of parallel rectilinear undisturbed flow, and ξ, η the space coördinate of the physical plane.

(II) Now let $F = W_1\, G(\zeta)$. Here W_1 is the transformed undisturbed velocity, to be interpreted as Eq. (3.21). But the complex variable ζ has no direct physical meaning. ~~$\overline{W} = \frac{dF}{d\zeta} = W_1 \frac{dG}{d\zeta}$, ... Eq. (3.22)~~

(III) Using the above value of F, Eq. (3.27) can be written as

$$dz = d\zeta - \frac{1}{4}\left(\frac{W_1}{a_0}\right)^2 \left(\frac{d\overline{F}}{d\overline{\zeta}}\right)^2 d\overline{\zeta} \qquad \text{~~(3.28)~~}$$

(12)

Integrating, $$z = \zeta - \frac{1}{4}\left(\frac{W_1}{a_0}\right)^2 \int \left(\frac{dF}{d\zeta}\right)^2 d\zeta \qquad (3.28)$$

Thus it is seen that the complex coördinate in the physical plane of compressible fluid is equal to the corresponding complex coördinate in the physical plane of incompressible fluid plus a correction term. ~~[illegible]~~ The factor ~~[illegible]~~ before the integral depends upon the Mach's number of the undisturbed flow only. By using Eqs. (3.7) ~~and~~ (3.8), and (3.21), one has

$$\frac{1}{4}\left(\frac{W_1}{a_0}\right)^2 = \frac{\left(\frac{w_1}{a_1}\right)^2}{\left\{1+\sqrt{1-\left(\frac{w_1}{a_1}\right)^2}\right\}^2} \qquad (3.29)$$

~~It is~~ The integration constant ~~of~~ the integral in Eq. (3.28) is not important, because it only means ~~involve a~~ a ~~rotation and~~ a translation of the whole z-plane. ~~which does not affect the result of the cal velocity and pressure~~

(IV) ~~Finally, we~~ The velocity w corresponds to z can be computed ~~as follo~~ by starting with

$$\overline{W} = \frac{dF}{d\zeta} = W_1 \frac{dG}{d\zeta} = u - iV.$$

By means of Eqs. (3.29)

$$\frac{w}{w_1} = \frac{\frac{|W|}{W_1}}{\frac{w_1}{W_1}\left[1 - \frac{1}{4}\left(\frac{W_1}{a_0}\right)^2 \left(\frac{|W|}{W_1}\right)^2\right]}$$

Thus by putting $w = w_1$, one obtains

$$\frac{w_1}{W_1} = \frac{1}{1-\frac{1}{4}\left(\frac{W_1}{a_0}\right)^2}$$

Thus

$$\frac{w}{w_1} = \left\{1-\frac{1}{4}\left(\frac{W_1}{a_0}\right)^2\right\} \frac{\frac{|W|}{W_1}}{1-\frac{1}{4}\left(\frac{W_1}{a_0}\right)^2\left(\frac{|W|}{W_1}\right)^2} \qquad (3.30)$$

Using Eqns. (3.30) and (3.29), the ratio $\frac{w}{w_1}$ can be calculated easily.

(V) To determine the pressure acting on the surface of the body one has to use Eq. (3.2). ~~Thus~~ With some manipulation, the following relation is obtained:

$$\frac{p-p_1}{\frac{1}{2}\rho_1 w_1^2} = \frac{2}{\left(\frac{w_1}{a_1}\right)^2}\left[1 - \frac{\rho_0}{\rho}\left(\frac{\rho_1}{\rho_0}\right)\right]$$

$$= \frac{2}{\left(\frac{w_1}{a_1}\right)^2}\left[1 - \sqrt{1-\left(\frac{w_1}{a_1}\right)^2}\,\frac{\rho_0}{\rho}\right] \qquad \text{~~(3.31)~~}$$

~~where~~ But

$$\frac{\rho_0}{\rho} = \sqrt{1+\left(\frac{w}{w_1}\right)^2\left(\frac{w_1}{a_0}\right)^2}$$

$$= \sqrt{1+\left(\frac{w}{w_1}\right)^2 \frac{\left(\frac{w_1}{a_1}\right)^2}{1-\left(\frac{w_1}{a_1}\right)^2}} \qquad (3.31)$$

Therefore

$$\frac{p-p_1}{\frac{1}{2}\rho_1 w_1^2} = \frac{2}{\left(\frac{w_1}{a_1}\right)^2}\left\{1 - \sqrt{1+\left\{\left(\frac{w}{w_1}\right)^2-1\right\}\left(\frac{w_1}{a_1}\right)^2}\right\} \qquad (3.32)$$

Section II

In this section, the general theory developed in Section (2) is applied to the simple case of flow over a symmetrical Joukowsky airfoil at zero angle of attack. The complex potential in the circle-plane (see Fig. 3.2) is known to be

$$w_1 \left\{ (\mu - b) + \frac{a^2}{\mu - b} \right\} \qquad (3.33)$$

where a = radius of the airfoil circle, b = eccentricity of the airfoil circle. The relation between the airfoil plane and circle-plane is the well-known Joukowsky transformation

$$\zeta = \mu + \frac{1}{\mu} \qquad (3.34)$$

if the radius of the transforming circle is unity.

Now the starting point of the calculation is the function to find $W d\bar{F}$.

$$W d\bar{F} = \frac{d\bar{F}}{d\bar{\zeta}} \frac{d\bar{F}}{d\bar{\mu}} d\bar{\mu} = \frac{\left(\frac{d\bar{F}}{d\bar{\mu}}\right)^2}{\frac{d\bar{\zeta}}{d\bar{\mu}}} d\bar{\mu}$$

Therefore $W d\bar{F} = W_1^2 \left\{ 1 - \frac{a^2}{(\bar{\mu} - b)^2} \right\}^2 \left\{ 1 + \frac{1}{2} \left(\frac{1}{\bar{\mu} - 1} - \frac{1}{\bar{\mu} + 1} \right) \right\}$

Thus the correction term in Eqn (3.28) is

$$\frac{1}{4a_0^2} \int W d\bar{F} = \frac{1}{4} \left(\frac{W_1}{a_0} \right)^2 \left\{ I_1 + I_2 - I_3 \right\} \qquad (3.35)$$

(15)

where $I_1 = \int \left\{1 - \frac{2a^2}{(\bar{\mu}-b)^2} + \frac{a^4}{(\bar{\mu}-b)^4}\right\} d\bar{\mu}$

$$I_2 = \frac{1}{2}\int \left\{1 - \frac{2a^2}{(\bar{\mu}-b)^2} + \frac{a^4}{(\bar{\mu}-b)^4}\right\} \frac{d\bar{\mu}}{(\bar{\mu}-1)}$$

$$I_3 = \frac{1}{2}\int \left\{1 - \frac{2a^2}{(\bar{\mu}-b)^2} + \frac{a^4}{(\bar{\mu}-b)^4}\right\} \frac{d\bar{\mu}}{(\bar{\mu}+1)}$$

These integrals can be easily computed & simplified, noting that $a - b = 1$, If $(\bar{\mu}-b) = a e^{i\theta}$, and $\lambda = \frac{a}{1+b}$

$$\left.\begin{aligned} I_1 &= a\left\{e^{i\theta} + 2e^{-i\theta} - \frac{1}{3}e^{-i3\theta}\right\} \\ I_2 &= \frac{1}{2}\left\{\frac{1}{b} - e^{-i\theta} + \frac{1}{2}e^{-2i\theta} + \frac{1}{3}e^{-3i\theta} + \log(ae^{i\theta})\right\} \\ I_3 &= \frac{1}{2}\left\{(1-\lambda^2)^2 \log(ae^{i\theta} + \frac{1}{\lambda}) + \lambda^2(2-\lambda^2)\log a e^{i\theta} \right. \\ &\left. + \lambda^4(1-\lambda^2)e^{-i\theta} + \frac{\lambda^2}{2}e^{-2i\theta} - \frac{\lambda}{3}e^{-3i\theta}\right\} \end{aligned}\right\} \quad (3.36)$$

Separating the real and imaginary parts, and adding,

$$\left.\begin{aligned} Re(I_1 + I_2 - I_3) &= a\left(3\cos\theta - \frac{1}{3}\cos 3\theta\right) \\ &+ \frac{1}{2}\left\{\frac{(1-\lambda^2)^2}{2}\log\left(1 + \frac{1}{\lambda^2} + 2\frac{\cos\theta}{\lambda}\right) + (\lambda^3 - 2\lambda - 1)\cos\theta \right. \\ &\left. + \frac{1}{2}(1-\lambda^2)\cos 2\theta + \frac{1}{3}(1+\lambda)\cos 3\theta\right\} \\ Im(I_1 + I_2 - I_3) &= a\left(-\sin\theta + \frac{1}{3}\sin 3\theta\right) \\ &+ \frac{1}{2}\left\{(1+2\lambda-\lambda^3)\sin\theta - \frac{1}{2}(1-\lambda^2)\sin 2\theta - \frac{1}{3}(1+\lambda)\sin 3\theta \right. \\ &\left. - (1-\lambda^2)^2\tan^{-1}\frac{\sin\theta}{\cos\theta + \frac{1}{\lambda}} + (1-\lambda^2)^2\theta\right\} \end{aligned}\right\} \quad (3.37)$$

These give the correction term to x & y co-ordinates. (16)

¶ The ~~velocity over the~~ transformed velocity W over the surface of the airfoil can be easily found ~~that~~ by means of graphical method (Ref. 6). Then the actual velocity and pressure can be computed by ~~me~~ using Eq. (3.22) and (3.32).

¶ Fig 3.3 shows the result of calculation for the case $a = 1.20$ and $\frac{w_1}{a_1} = 0.550$. The nose of the airfoil is ~~shortened~~ somewhat rounded by transforming into the case of compressible fluid. However, the pressure gradient is ~~very much~~ steeper, as would be expected. The main ~~d~~ defect of this type of calculation is that during the transformation from incompressible flow to compressible ~~flow~~ flow, the shape of the body is also changed. To isolate the effect of compressibility of the fluid, it is necessary to bring back the original shape of the body. ~~In case of flow over an airfoil, the theory developed by von Kármán & Trefftz (7) can be used.~~ This is done by first deform the ~~Jo~~ original Joukowsky airfoil, such that final profile after correction for compressibility is same as the original Joukowsky airfoil. The amount of deformation is obtained from the calculation assuming that the airfoil were a Joukowsky airfoil ~~a~~ at start. That is the effect of deformation on the correction term of Eq. (3.28)

is neglected. This is allowable, because the quantity neglected is a second order quantity. (17)

This deformation of Joukowsky airfoil can be carried out by using the method developed by von Kármán and Trefftz (Ref. 7). However, for some practical reasons, the Kármán-Trefftz method is somewhat modified:

Fig. 3.4a shows two airfoils, both having the same chord, one is Joukowsky airfoil desired and the other is the airfoil resulted from the ~~calculated~~ first step calculation. Now apply the Joukowsky transformation to this figure, then the Joukowsky airfoil will become a circle C, while the other airfoil a near-circular shape C_1, as shown in Fig. 3.4 b. The desired deformed ~~airfoil~~ Joukowski airfoil will appear like C_2 in this figure. The difference between C_2 and C_1 is just opposite & equal to that between C_1 & C. Now let ζ_2 be written as $\zeta_2 = r e^{i\theta}$. ~~obvious~~ obviously,

$$r = [1 + g(\theta)] \quad (3.38)$$

where $g(\theta)$ will be small compared with 1.

← The function which establishes the conformal transformation of the outside of this boundary C into outside of the circle C_1 may be denoted

(18)

$$\zeta_1 = \zeta_2\left[1 + f(\zeta_2)\right] \qquad (3.39)$$

where ζ_1 & ζ_2 have their origin at the center O and the absolute value of $f(\zeta_2)$ is again small compared with 1. Then it is shown (Ref. 7) that

$$g(\theta) + \text{Re.}\left[f(\zeta_2)\right] = 0. \qquad (3.40)$$

In order to calculate $f(\zeta_2)$ we develope the function $g(\theta)$ in a Fourier series:

$$g(\theta) = \sum_0^\infty a_n \cos n\theta \qquad (3.41)$$

Here only cosine terms appear because the airfoil is symmetrical about the chord. On the other hand, the complex function $f(\zeta_2)$ has the form, for $|\zeta_2| \geq 1$:

$$f(\zeta_2) = \sum_0^\infty \frac{c_n}{\zeta_2^{\,n}} \qquad (3.42)$$

Now put $\zeta_2 = e^{i\theta}$, then (3.40) is satisfied by

$$c_n = -a_n$$

Thus

$$f(\zeta_2) = -\sum_0^\infty \frac{a_n}{\zeta_2^{\,n}} \qquad (3.43)$$

It can be easily seen that the velocity around the deformed Joukowsky airfoil can be calculated as

$$w = w_J \left|\frac{d\zeta_1}{d\zeta_2}\right| \qquad (3.44)$$

where w_J = velocity around the Joukowsky airfoil

Now from Eqs. (3.39) and (3.43),

$$\frac{d\zeta_1}{d\zeta_2} = 1 - \sum_0^\infty{}' \frac{a_n}{\zeta_2^n} + \sum_0^\infty{}' \frac{n\,a_n}{\zeta_2^n} = 1 + \sum_0^\infty{}' \frac{(n-1)a_n}{\zeta_2^n}$$

$$= \left(1 + \sum_0^\infty{}' (n-1)a_n \cos n\theta\right) + i \sum_0^\infty{}' (n-1)\,a_n \sin n\theta$$

Neglecting small quantities of second order, & noting Eq. (3.41),

$$\left|\frac{d\zeta_1}{d\zeta_2}\right| = 1 + \sum_0^\infty{}' (n-1)\,a_n \cos n\theta$$

$$= 1 + \sum_0^\infty{}' n\,a_n \cos n\theta - \sum_0^\infty{}' a_n \cos n\theta$$

$$= 1 + \frac{d}{d\theta}\sum_1^\infty{}' a_n \sin n\theta - g(\theta) \qquad \text{Eq. (3.45)}$$

A trial calculation shows that the convergence of the coefficients a_n is not very good. Therefore, one must avoid manipulation on the Fourier series as required by Eq. (3.45). This is possible, because $-\sum_1^\infty{}' a_n \sin n\theta$ is known to mathematicians as the ~~associated~~ allied or conjugate series of $\sum_0^\infty{}' a_n \cos n\theta$. It is also known (Ref. ?) that if $g(\theta) = \sum_0^\infty{}' a_n \cos n\theta$

$$-\sum_1^\infty{}' a_n \sin n\theta = \frac{1}{2\pi}\int_0^\pi \frac{g(\theta+\xi) - g(\theta-\xi)}{\tan\frac{\xi}{2}}\, d\xi$$

~~Therefore Eq. (3.45) can be written as~~

~~$$\left|\frac{d\zeta_1}{d\zeta_2}\right| = 1 - \frac{1}{2\pi}\int_0^\pi \frac{g'(\theta+\xi) - g'(\theta-\xi)}{\tan\frac{\xi}{2}}\, d\xi - g(\theta) \qquad (3.46)$$~~

~~where $g(\alpha) = \frac{dg(\alpha)}{d\alpha}$~~.

Therefore $$\frac{d}{d\theta}\sum_1^\infty a_n \sin n\theta = -\frac{1}{2\pi}\int_0^\pi \frac{g'(\theta+\xi)-g'(\theta-\xi)}{\tan\frac{\xi}{2}}\,d\xi$$

Integrating by parts, ~~the integral~~

$$-\frac{1}{2\pi}\left\{\left[\frac{g(\theta+\xi)+g(\theta-\xi)}{\tan\frac{\xi}{2}}\right]_0^\pi + \frac{1}{2}\int_0^\pi \frac{g(\theta+\xi)+g(\theta-\xi)}{\sin^2\frac{\xi}{2}}\,d\xi\right\}$$

$$= -\frac{1}{2\pi}\int_0^\pi \frac{\{g(\theta+\xi)-g(\theta)\}+\{g(\theta-\xi)-g(\theta)\}}{(1-\cos\xi)}\,d\xi$$

~~Therefore~~ Hence Eq. (3.45) can be written as

$$\left|\frac{dS_1}{dS_2}\right| = 1 - \frac{1}{2\pi}\int_0^\pi \frac{\{g(\theta+\xi)-g(\theta)\}+\{g(\theta-\xi)-g(\theta)\}}{(1-\cos\xi)}\,d\xi - g(\theta) \tag{3.46}$$

The integral ~~can be~~ ~~is computed by numerically~~ is evidently convergent for any continuous regular function $g(\theta)$, because then the integrand is always finite ~~regular~~. Its evaluation can be done numerically.

¶ Fig 3.5 is the results of calculation for a Joukowsky airfoil with the thickness parameter ~~b = 1.10~~ $b = 0.20$, at two speeds, $\frac{w_1}{a_1} = 0.450$ and 0.550. The suction peaks are considerably higher with higher speeds. ~~and~~ Also the positions of pressure peaks tend to move backward with increasing speed. Both ~~phen~~ are in agreement with the experimental results ~~of~~

obtained by J. Stack (Ref. 3). The values of $\frac{p-p_1}{\frac{1}{2}\rho_1 w_1^2}$ for $\frac{w_1}{a_1} = 0.550$ (21) & $\frac{w_1}{a_1} = 0.4$ at which real air will attain a velocity equal to the local sound velocity are equal to -1.653 and -2.755 respectively. It is thus seen that the effect of compressibility on pressure distribution is appreciable, even when no where the local sound velocity is reached. One should, however, bear in mind that the effect on the force coefficient of the airfoil will probably not be so marked as with the pressure distribution, because the resultant force on the airfoil is the algebraic difference of pressure force acting on two sides of the section.

Appendix to PART (III)

Comparison with Other Methods.

In order to check the accuracy of the method developed in PART (III), the flow over a finite circular cylinder with its axis perpendicular to the direction of undisturbed flow is studied. Method exposed in Section (II) of PART (III) for correction of shape of body is used. The following is the result of calculation for velocity at the top of the circular section, compared with results by other methods. [collected by E. Pistolesi (Ref. 10)]

$\frac{w_1}{a_1} = 0.400$

Method	$\frac{w}{w_1}$ at top of Section
PART (III)	2.268
Rayleigh	2.206
Poggi	2.194
Tayler's Electric Analogy	2.188

$\frac{w}{w_1} = 2.000$ for incompressible fluid.

Thus the present method gives a slightly higher value. However, the flow over a cylinder is a rather extreme case, because the difference of velocity calculated to the undisturbed velocity is very large, and thus larger error of using the tangent of the PV curve than curve itself.

Thus the present method gives a ~~slightly~~ higher value. (23)
However, the flow over a cylinder is rather an extreme case. Because the difference between ~~of velocity~~ ~~a~~ the velocities to be calculated and the undisturbed velocity is large, and thus ~~this method~~ this approximate method ~~introduces~~ involves larger than usual error. ~~of using the tangent of PV~~

References on PART (II)

(1) P. Molenbroek: Über einige ~~Bewegung~~ Bewegungen eines Gases bei Annahme eines Geschwindigkeitspotentials
Arch. d. Mathem. u. Phys., Grunert Hoppe (1890), Reihe 2, Bd. 9. S. 157

(2) A. Tschapligin: Scientific Memoirs of the Univ. Moscow. (In Russian) (1902)

(3) F. Clauser, & M. Clauser: ~~A New Method for the Study of Motion of Compressible Fluid~~ New Methods of Solving the Equations for the Flow of a Compressible Fluid. Unpublished Ph.D. Thesis at C.I.T. (1937)

(4) B. Demtchenko: Sur les mouvements lents des fluides compressibles, Comptes Rendus Vol. 194, p. 1218 (1932)
Also Variation de la résistance aux faibles vitesses sous l'influence de la compressibilité Comptes Rendus Vol. 194, p. 1720 (1932)

(5) A. Busemann: Die Expansionsberichtigung der Kontraktionsziffer von Blenden Forschung Bd. 4, S. 186–187 (1933)
Also. Hodographenmethode der Gasdynamik Z.A.M.M. Bd 12, S. 73–79 (1937)

(6) W. F. Durand: Aerodynamic Theory Vol. 2, p. 71–74, 1st Edition, Julius Springer, Berlin (1935)

(7) Th. von Kármán, E. Trefftz: Potentialströmung um gegebene Tragflächenquerschnitte Z.F.M. Bd 9, S. 111, (1918)
Also W. F. Durand: Aerodynamic Theory. Vol. 2, p. 80–83. (1935)

(8) G. H. Hardy, J. E. Littlewood: The allied Series of a Fourier Series Proc. of London Math. Soc. (2) Vol. 24, pp. 211–246 (1925)

(9) J. Stack: The Compressibility Bubble NACA Technical Note No. 543 (1935)

[See back side]

(10) E. Pistolesi: La portanza alle alte velocità inferiori a quella del suono

Atti dei V Convegno "Volta", fasc. 300, (1936)
Reale Accademia d'Italia, Rome.

Section 4

Report on the Present State of Theory of Thin Plate and Cylindrical Shells in Compression

Report on the Present State of Theory of Thin Plates and Cylindrical Shells in Compression

H.S. Tsien

References

(I) General Theory

(1) R.V. Southwell: On the General Theory of Elastic Stability. Transc. of Roy. Soc. of London 213: 187-244 (1914)

(2) K. Marguerre: Über die Behandlung von Stabilitätsproblemen mit Hilfe der energetischen Methode. ZAMM 18: 57-73 (1938)

(II) Cylindrical Shell without Stiffening in Elastic Regime

(3) K. v. Sanden; F. Tölke: Über Stabilitätsprobleme dünner kreiszylindrischen Schalen. Ing.-Arch. 3: 24-66 (1932)

(4) W. Flügge: Die Stabilität der Kreiszylinderschale. Ing.-Arch. 3: 463-506 (1932)

(5) J. Sutton Pippard: Distortion of Thin Tubes under Flecture. RM 1465 (1932)

(6) T. E. Schwerk: Zur Knickfestigkeit schwach gekrümmter zylindrischen Schalen. Ing.-Arch. 4: 394-414 (1933)

(7) L. H. Donnell: A new Theory for the Buckling of Thin Cylinders Under Axial Compression & Bending
Trans ASME 56: 795-806 (1934)

2)

(III) Conical ~~total~~ Shell ~~used~~ without Stiffening in Elastic Regime

(8) A. Pflüger: Stabilität dünner Kegelschalen
Ing.-Arch.: 8: 151-172 (1937)

(IV) Stiffened Cylindrical Shell

(9) ~~O.S. Heck; H. Ebner~~
H. Wagner: Einiges über schalenförmiges Flugzeug Bauteiles Lff. 13: 281-292 (1936) TM 817

(10) J. L. Taylor: Stability of a Monocoque in Compression
RM 1679 (1936)

(11) H. Ebner; H Köller: Zur Berechnung des Kraftverlaufes in versteiften Zylinderschalen Lff. 14: 607-626 (1936)
TM 866

(12) E. Schapitz; G. Krümling: Belastungsversuche mit einer versteiften Kreiszylinderschale bei Krafteinleitung an einzelnen Punkten
Lff. 14: 593-606 (1937) TM 864

(13) N.J. Hoff: Instability of Monocoque Structures in Pure Bending
J. of Roy. Ae. Soc. 42: 291-345 (1938)

(V) Large Deflection Theory of Flat Plate

(14) K. Marguerre; E. Trefftz: Über die Tragfähigkeit eines Plattenstreifens nach Überschreiten der Beullast
ZAMM 17: 85 - 100 (1937)

(15) K. Marguerre: Die mittragende Breite der gedrückten Platte Lff. 14: 124 - (1937)

(16) A. Kromm; K. Marguerre: Verhalten eines von Schub- und Druckkräften beanspruchten Plattenstreifens oberhalb der Beulgrenze Lff. 14: 627 - 639 (1937)

(VI) Plate with Stiffener

(10) J. L. Taylor:

(17) R. Barbré: Stabilität gleichmäßig gedrückter Rechteckplatten mit Längs oder Quersteifen
Ing.-Arch. 8: 117 - 150 (1937) [Galcit Trans.]

(VII) Plastic Buckling

(18) ~~W. Kaufmann~~
J. W. Geckeler: Plastisches Knicken der Wandung von Hohlzylindern und einige andere Faltungserscheinungen an Schalen und Blechen
ZAMM 8: 341 - 352 (1928)

(19) W. Kaufmann: Platisches Knicken dünnwandiger Hohlzylindern infolge axialer Belastung. Ing-Arch 6: 334 – 337 (1935)

(20) W. Kaufmann: Bemerkungen zur Stabilität dünnwandiger kreiszylindrischen Schalen oberhalb der Proportionalitätsgrenze Ing-Arch. 6: 419-430 (1935)

(21) W. Kaufmann: Über unelastisches Knicken rechteckiger Platten Ing-Arch. 7: 156-165 (1936)

(22) W. A. Weyck: Die mittragende Breite nach dem Ausknicken bei krummen Blechen Lff. 15: 340-344 (1938)

(23) Th. Pöschl: Zur Theorie der platischen Knickung gerader Stäbe Der Bauingeneur 19: 499-505 (1938)

4)

(I)

General Consideration

From the point of view of method of design analysis, there are two types of monocoque construction: One which occurs in rather small aircraft, has strong rings, & weak skin covering; and one which appears more recently due to the increase in size of aircraft has weak rings. For the first type of structures, the buckling always occurs between the rings and the stiffened sheet can be considered as simply supported between the rings. The current American practice, assumes the validity of Navier beam hypothesis and determine the effective moment of inertia of the section by means of effective width of the sheet. H. Wagner (9) and H. Ebner and H. Köller (11) suggested the method of taking the system of stiffeners & rings as an statically indeterminate truss with sheet which is assumed only taking shear replacing the diagonal bracing. Thus the problem is reduced to that of rigid airship structure. However, from the experience of Wagner tension field beam theory, this

method of analysis tends to give very conservative & heavy structure.

The second type of structure which has weak rings, ~~usually buckles with rings~~ with two or three rings, usually buckle with the ~~skin~~ sheet. Due to its recent occurence, this type of structures is never been satisfactorily studied, & a method of analysis is still to be developed. J.L. Taylor (40) & N.J. Hoff (13) made some calculation in this direction but there are a number of their assumptions which seems ~~are~~ doubtful. ~~to the present reporter~~

~~However, before the discussion such complicated structure, it seems essential to understand the fundamental physical principle of the buckling phenomenon, and to study of the elementary components of the structure. The following is such an attempt.~~

However, before the discussion of such complicated structure, it is useful to have a clear understanding of the buckling & related phenomena. In the literature of thin shell structure, it is frequent that the writers do not emphases the difference between buckling ~~stress~~ load and maximum load. It is ~~the opinion of~~ evident that the ordinary small deflection theory can

at most give the elastic buckling load of the structure. The condition beyond the buckling load is very complicated. If the buckling load is low [i.e., the load is not far above buckling load] and the waves rather shallow, then it can be expected that there is no place in the sheet where the elastic limit is exceeded. Then we can calculate the relation between load and deflection by using large deflection theory and Hook's Law. The assumption of large deflection and consequently the resulting non-linear differential equation is necessary for the reason that even in case of rather shallow wave, the maximum deflection in normal direction may amounts to 100 times the sheet thickness.

But if the deflection involves very small radius of curvature or the initial buckling load is high [as is the case for curved sheet], then there must be some place in the sheet where the yielding point is exceeded. Hence not only that we have to take into acount the large deflection, but also the plastic flow of the material. But here Karman's well-known theory of

plastic buckling with two elastic modulus is not sufficient. Because not only the plastic regions are ~~entirely~~ localized, but the bending stress usually ~~usually~~ far exceeds the direct ~~compressive~~ stress & so the correct diagram of stress distribution is that of Fig. 1a instead of Fig. 1b.]]



]] T. Pöschl (23) recently has ~~extended~~ developed the theory of column for stress distribution like that shown in Fig. 1c. Therefore for the investigation of plastic failure of plates & shells ~~use~~, a further extention to the case shown in Fig. 1a is necessary.

Fig. 1a

Fig. b:

~~All~~ The theory of plastic buckling for rather thick plates & shells with two elastic modulus is developed by J. W. Geckeler (18) & W. Kaufmann (19)(20)(21). However, in their calculation, ~~as~~ the Navier's hypothesis is

1) $\beta = \frac{2.5^\circ}{57.3} = 0.0436$, $\geq$ 0.0384

$3.46 \sqrt{\left(\frac{h}{l a}\right)} = 3.46 \sqrt{8/120} = \underline{0.0384}$

retained. But due to the fact that for all ordinary material(9) only thick plates & shells fails by plastic buckling, it seems necessary to combine it with R. V. Southwell's more general theory (1) to give a satisfactory solution.

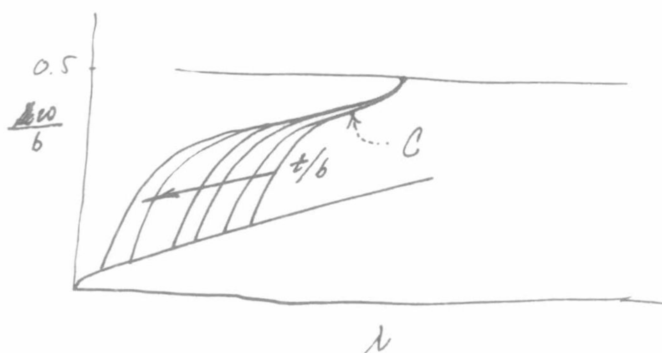
From the above consideration, it is quite evident that the load after buckling is a complicated matter. The question whether the load will increase or decrease depends upon the buckling load and characteristics of the shell. If the load still increases after buckling, then the maximum load will be higher than the buckling load. But if the load do not increase then the buckling load is the maximum load. In first case, the specimen fails by yielding. In the second case the specimens fails by instability. This shows the importance of differentiation of buckling load and maximum load.

(II) Plate

The failing of a flat plate of ordinary dimension is clearly of the first kind, i.e., plastic yielding. The plate buckles at load near to the theoretical buckling load calculated from the theory of small deflection. & The load increases with the deflection & the wave pattern becomes more & more complicated

with appearance of small waves at the supported edges. (10)

K. Marguerre, E. Trefftz and A. Kromm (14), (15), (16) applied the theory of large deflection to investigate the load & deflection relation after buckling. And they were the first to obtain ~~the~~ a ~~theoretical~~ calculated result which agrees with ~~the voluminous~~ numerous experiments. However, they ~~all~~ assumed the Hooke's stress-strain relation, & so the theory can only expected to work at load few times the buckling load when no plastic region appears. There is another difficulty which is due to the ~~method~~ energy used by them, i.e., the necessity of assuming different wave pattern for different loading & t/b ratios. This is inferred from the experimental results of ~~Mr~~ Dunn, as show in Fig. 2.



K. Marguerre, only gives one curve C independent (11)
of t/b, probably because he assumed only one type of wave form.

(III)

Cylindrical Shell

The failing of cylindrical shell is of the second type, i.e., fails by instability, and the buckling load & maximum load coincides.][The notable results of experiments are [see Fig. 3]

(1) The large scatter of experimental points

(2) The very low value of buckling stress as compared to the theoretical results.

(3) The tendency towards lower stress at larger R/t ratios.

][The theoretical study of instability of thin cylinder assuming the small deflection was carried out by a number of writers and was very well summaried by K. v. Sanden, F. Tölke (3) and W. Flügge (4). W. Flügge in the later part of his paper tried to explain the discrepancy by considering the end conditions more carefully. That is, consider the end to be supported in grooves which does not allow displacement but is free to change of slope. But by so doing he obtained a set of inhomogeneous boundary conditions, and therefore like an eccentrically load column, it

gives no instability problem. (2)

Instead, the waves gradually grows deeper and deeper & fail by yielding. But the experiments shows that most of the cylinders fail by sudden buckling accompanied by the emission of noise. This is typically an instability phenomena. W. Flügge and later L. H Donnel (7) also introduced the idea of initial imperfection of the specimen. But in a series of tests made by W. L. Holland, it is impossible to detect any initial imperfection by naked eye.

L. H. Donnel (7) also extended the theory to large deflection and set up the failing criterion by yielding. This is also questionable because for at least the test mad W. L. Holland on very thin steel cylinders, the buckling wave can be removed completely by unloading just after buckling occurs.

It seem at present, a critical examination of the theory of thin shells, originally developed by A.E.H. Love is necessary. Although the Navier's assumption could be retained, it is probably necessary to use theory of finite deflection & examine the instability under finite deflection. [See Fig 4] This is suggested

by the rather meager experimental results of W. A. Wenzek (22). [Fig. 5] (14)
~~It is evident that~~

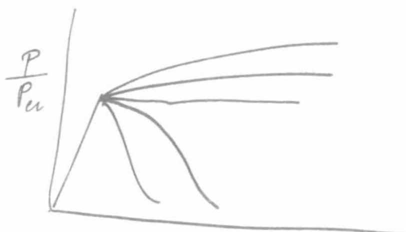


Fig. 5.

~~Though~~ Due to this difference in the character of failing, the well-known method developed by ~~Dr.~~ E. E. Sechler, although an excellent first approximation, needs improvement especially for large curvatures. However, a more satisfactory treatment of this problem probably ~~Furthermore,~~ have to await the solution of apparent mystery of thin cylindrical shell.

It is interesting to notice that the ratio of experimental & theoretical ~~results~~ buckling loads is higher for smaller b/R and lower for larger R/b.

(V)

Stiffened Plates & Shells.

The usual practice in the calculation of stiffened plates & shells is to distribute the stiffeners uniformly over the shell, and take the ~~~~ sheet as having different elastic properties in direction ⊥ to stiffeners & parallel to stiffeners, the so-called orthotropic shell & plate. But this practice is only good for ~~corrugated~~ shells or plates stiffened by corrugation. In case of stiffeners placed not very

close together, this is only a first approximation. (15)
J. L. Taylor (10) even went so far as to assume the rings also uniformly distributed, this is very doubtful from the point of view of actual construction.

R. Barbré (17) made a very elaborate calculation of the buckling load of the stiffened plate using the exact theory of small deflection. His results agree with that of the well-known work of S. Timoshenko who used the much simpler energy method. However, the calculation of load beyond buckling, or the maximum load remains to be done.

N. J. Hoff (13) applied the energy method to solve the problem of buckling of stiffened cylinders with rings buckle with the sheet. His work can be said as pioneering in this field, but it suffers the defects of a rather arbitrary wave pattern, neglection of effect of sheet and small deflection theory.

(VI)

Mathematical Methods

The methods used in the study of thin plates & shells fall into two general headings:

(1) Method of Equilibrium — This is to find a deformed shape of the shell or plate other than straight compression, such that it will be in equilibrium with the external load. When the boundary conditions are homogeneous, ~~then~~ the problem is reduced to find the characteristic values of the differential equations of deflection. ~~The~~

(2) Method of Lowest Energy, or Energy method of Elasticity. In this method, the difference between the strain energy and the potential energy of applied load is made to be a minimum. The problem is essentially a variation problem. The most popular method to solve it, is that due to Rayleigh & Ritz.

For ~~most cases~~ almost all cases, the second method involves less thought. ~~and~~ In the case of non-linear equations, like that obtained by means of finite deflection theory, or ~~stiffened shell, the calculation~~ the energy method is almost the only means ~~to~~ solve ~~the equations~~. The uniqueness of solution by

using energy method for large deflection is studied by K. Marguerre (2) (17). The reason why this is necessary is this: the energy expression in case of small deflection theory is a positive definite quadratic form, so that condition of a extremum is a linear equation. Therefore there is only one solution. The solution is also a minimum, because the quadratic form is positive definite. This is the well-known Kirchhoff's principle of uniqueness of solution. But the energy expression in case of large deflection theory involves third, and higher order terms, the extremum condition is not linear. Therefore there are more than one solution, for each load condition. To decide which is the true minimum, one has to use the second variation. This is done for the case of column by K. Marguerre (2) using Ritz' method.

Another difficulty of using energy method for large deflection theory is to assume proper deflection forms, especially the tangential components. The normal component is fairly easily obtained from experiments. Both L. H. Donnell (7) & K. Marguerre (14) (15) (16) used the equilibrium differential equations

combined with the assumed wave form of normal component (18)
to obtain proper wave form of tangential components.
Then the tangent components are then expressed in
terms of parameters & functions of assumed normal
component. These values are then put into
the energy integral and minized to determine
the parameters.

The equilibrium differential equations
used by K. Marguerre (15) and L.H. Donnel (7) have
to be critically examined too. The reason is that they
used the equilibrium differential equation for
small deflection which is no longer true in the
theory of large deflection, the point is that certain second order
terms of deflection are neglected. This is
evidently incorrect, because the inclusion of second
order terms in the calculation is the main feature
of large deflection theory.

Note: The reviewer has no wish of claiming all
the opinions expresed in this report to be his own.
Some of them are really first suggested by Mr. W.L.
Holland and Dr. E.E. Sechler.

Section 5

The Buckling of Thin Cylindrical Shells under Axial Compression

First Draft

THE BUCKLING OF thin CYLINDRICAL SHELLS UNDER AXIAL COMPRESSION

Th. von Karman and Hsue-shen Tsien
California Institute of Technology

In two previous papers (Ref.1 and Ref.2), the authors have discussed in detail the inadequacy of the classical theory of thin shells in explaining the buckling phenomenon of ~~both the~~ cylindrical ~~shells~~ and ~~the~~ spherical shells. It was shown that not only the calculated buckling load is 4 to 5 times higher than that experimentally observed, but the buckling wave pattern found is also different from that predicted. It was pointed out, furthermore, that the different explainations for this discrepancy advanced by L.H. Donnell (Ref.3) and W.Flügge (Ref.4) are untenable when certain conclusions drawn from these explainations are compared with the experimental facts. The authors are then led by ~~both the~~ a theoretical investigation on spherical shells (Ref.1) ~~and~~ a model experiment (Ref.2) on thin columns ~~supported by~~ with non-linear elastic support to the belief that the buckling phenomenon of curved shells can only be explained by means of ~~the~~ non-linear large deflection theory. This point of view is fundamentally substantiated by ~~The~~ It is evident ~~found~~ from the two cases investigated that ~~crucial point seems to be~~ the ~~rapid drop in~~ load necessary to keep the shell in equilibrium drops very rapidly with increase in wave amplitude ~~once the shell started to buckle~~. This characteristic of dropping load shows, first of all, that there is a release of the elastic energy stored in the shell once the buckling has started, and thus explains the observed rapidity

of the buckling process. Furthermore, this characteristic also brings in the possibility of a decrease in the buckling load when there are slight imperfections in the test specimen and when there are vibrations during the testing process.

In this paper, the authors will show by means of an approximate calculation the dropping load characteristic of a uniform, thin cylindrical shell under axial compression. Consequently, they hope that they have thus offered an aceptable explaination of the observed facts.

Stresses in the Median Surface and the Expression for the Total Energy of the System

If u, v, and w (Fig. 1) are the displacement of a point on the median surface of the shell in the axial, x, direction, the circumferential, y, direction, and the radial direction, then the unit strains in the x and y directions, ε_x, ε_y and the unit shear γ_{xy} at a point in the median surface can be expressed in the following form, including terms up to second order:

$$\left.\begin{aligned}\varepsilon_x &= \frac{\partial u}{\partial x} + \frac{1}{2}\left(\frac{\partial w}{\partial x}\right)^2 \\ \varepsilon_y &= \frac{\partial v}{\partial y} + \frac{1}{2}\left(\frac{\partial w}{\partial y}\right)^2 - \frac{w}{R} \\ \gamma_{xy} &= \frac{\partial u}{\partial y} + \frac{\partial v}{\partial x} + \left(\frac{\partial w}{\partial x}\right)\left(\frac{\partial w}{\partial y}\right)\end{aligned}\right\} \quad (1)$$

where R is the radius of the undeformed median surface of the shell. The stresses and the strains in the median surface of the shell are, however, related to each other by the following expressions:

$$\sigma_x = \frac{E}{1-\nu^2}(\varepsilon_x + \nu \varepsilon_y)$$
$$\sigma_y = \frac{E}{1-\nu^2}(\varepsilon_y + \nu \varepsilon_x) \qquad (2)$$
$$\tau_{xy} = \frac{E}{2(1+\nu)} \gamma_{xy}$$

where E is the Young's modulus of elasticity and ν is Poisson's ratio.
Therefore by substituting Eq.s(1) into Equs.(2) the following connections between the stress components of the median surface and the components of displacement of the median surface are obtained:

$$\sigma_x = \frac{E}{1-\nu^2}\left\{\frac{\partial u}{\partial x} + \frac{1}{2}\left(\frac{\partial w}{\partial x}\right)^2 + \nu\left[\frac{\partial v}{\partial y} + \frac{1}{2}\left(\frac{\partial w}{\partial y}\right)^2 - \frac{w}{R}\right]\right\}$$
$$\sigma_y = \frac{E}{1-\nu^2}\left\{\frac{\partial v}{\partial y} + \frac{1}{2}\left(\frac{\partial w}{\partial y}\right)^2 - \frac{w}{R} + \nu\left[\frac{\partial u}{\partial x} + \frac{1}{2}\left(\frac{\partial w}{\partial x}\right)^2\right]\right\} \qquad (3)$$
$$\tau_{xy} = \frac{E}{2(1+\nu)}\left\{\frac{\partial u}{\partial y} + \frac{\partial v}{\partial x} + \frac{\partial w}{\partial x}\frac{\partial w}{\partial y}\right\}$$

It is generally accepted that the equilibrium conditions of the stresses in the median surface can be ~~satisfactorily~~ approximately expressed by the following equations in case of thin shells:

$$\frac{\partial \sigma_x}{\partial x} + \frac{\partial \tau_{xy}}{\partial y} = 0$$
$$\frac{\partial \tau_{xy}}{\partial x} + \frac{\partial \sigma_y}{\partial y} = 0 \qquad (4)$$

This pair of equations can be ~~automatically~~ satisfied by introducing the well-known Airy stress function, F, defined by the relations

$$\sigma_x = \frac{\partial^2 F}{\partial y^2}, \quad \tau_{xy} = -\frac{\partial^2 F}{\partial x \partial y}, \quad \sigma_y = \frac{\partial^2 F}{\partial x^2} \qquad (5)$$

Eliminating the variables u and v between Eqs. (3) and (5) a relation between the Airy stress function, F and the radial component w of a point in the median surface of displacement ~~w~~ is obtained;

$$\frac{\partial^4 F}{\partial x^4} + 2\frac{\partial^4 F}{\partial x^2 \partial y^2} + \frac{\partial^4 F}{\partial y^4} = E\left[\left(\frac{\partial^2 w}{\partial x \partial y}\right)^2 - \frac{\partial^2 w}{\partial x^2}\frac{\partial^2 w}{\partial y^2} - \frac{1}{R}\frac{\partial^2 w}{\partial x^2}\right] \qquad (6)$$

This equation is very similar to the large deflection equation for flat plate derived by the senior author. (Ref. 5) L.H.Donnell (Ref; 3) first obtained this equation in its present form. With a given form of the radial component w of the displacement ~~deflection, w,~~ Eq. (6) gives the induced stresses in the median surface of the shell. ~~These stresses will represent an~~ The extensional elastic energy W_1 for one complete wave panel corresponding to these stresses can be written as ~~calculated by the following equation~~:

$$W_1 = \frac{t}{2E} 4\int_0^a\int_0^b \left\{(\sigma_x+\sigma_y)^2 - 2(1+\nu)\left(\sigma_x\sigma_y + \tau_{xy}^2\right)\right\} dx\,dy \qquad (7)$$

where a and b are the half wave lengths in the axial and the circumferential direction respectively.

To calculate the bending elastic energy, it is necessary first to find the expressions for the change of ~~radii~~ of curvatures and the unit twist of the median surface. In this paper, the following simplified expressions ~~are~~ will be used:

$$\chi_x = \frac{\partial^2 w}{\partial x^2}, \qquad \chi_y = \frac{\partial^2 w}{\partial y^2}, \qquad \chi_{xy} = \frac{\partial^2 w}{\partial x \partial y} \qquad (8)$$

In Eq. (8), certain additional terms in χ_y and χ_{xy} involving v are neglected. It was shown by L.H.Donnell (Ref. 6) that those neglected terms ~~have a factor~~ differ from the terms retained in Eq. (8) by a factor $1/n^2$, where n is the number of waves in the circumferential direction. For thin cylindrical shells, the value of n is ~~usually~~ around 10; therefore the neglection is jusitfied. With these expressions for the change of the curvatures and the unit twist of the median surface, the bending

W_2 for one complete wave panel energy can be obtained as

$$W_2 = \frac{t^3}{24(1-\nu^2)} E \, 4\int_0^b\int_0^a \left\{\left(\frac{\partial^2 w}{\partial x^2}+\frac{\partial^2 w}{\partial y^2}\right)^2 - 2(1-\nu)\left(\frac{\partial^2 w}{\partial x^2}\frac{\partial^2 w}{\partial y^2} - \left(\frac{\partial^2 w}{\partial x \partial y}\right)^2\right)\right\} dx\,dy \qquad (9)$$

The lowering of the potential, W_3, of the applied force on the end of the cylindrical shell can be calculated as the product of the change in length of the shell and the applied force. ~~This can be expressed as~~ Therefore the following expression is obtained:

$$W_3 = - \; t \, 4\int_0^b \sigma_x \, dy \int_0^a \frac{\partial u}{\partial x} \cdot dx \qquad (10)$$

The equilibrium condition of the shell is obtained by equating the first variation of the sum of energies, W_1, W_2 and W_3 to zero. In the following calculation, the Rayleigh-Ritz method or the energy method will be used by assuming a plausible form for the function w.

Calculation of the Total Energy

To obtain a plausible form for w , one has to resort to the experimental results ~~from~~. It is observed that, for large values of the wave amplitude, the waves are so-called diamond shaped. This particular wave shape can be approximately expressed by

$$\cos^2\frac{(m'x+ny)}{2R}\cos^2\frac{(m'x-ny)}{2R} \qquad (11)$$

where the squares are introduced to account for the fact that the shell has a definite preference to buckle inward. Eq. (11)

can be rewritten as

$$\frac{1}{4} + \frac{1}{2}\left[\cos\frac{mx}{R}\cos\frac{ny}{R} + \frac{1}{4}\cos\frac{2mx}{R} + \frac{1}{4}\cos\frac{2ny}{R}\right] \quad (12)$$

On the other hand, the classical theory which is correct for infinitesimal values of the wave amplitude, requires the waves to be of the form

$$\cos\frac{mx}{R}\cos\frac{ny}{R} \quad (13)$$

In order to satisfy this requirement, the wave form assumed in the following calculations is of the

$$\frac{w}{R} = \left(f_0 + \frac{1}{4}f_1\right) + \frac{1}{4}f_1\left[\cos\frac{mx}{R}\cos\frac{ny}{R} + \frac{1}{4}\cos\frac{2mx}{R} + \frac{1}{4}\cos\frac{2ny}{R}\right] + \frac{1}{4}f_2\left[\cos\frac{2mx}{R} + \cos\frac{2ny}{R}\right] \quad (14)$$

where f_0, f_1, and f_2 are unknowns to be determined by conditions of minimum total energy of the system.

f_0 is introduced in order to allow the shell to expand radially. It is evident that no end effect can be take into account by this form of radial displacement, and therefore the following calculation really corresponds to an cylindrical shell of very large length. This simplifies is justified by the experimental findings of N. Nojima and B. K... as reported in a previous paper (Ref. 4). It is found that there is no appreciable length effect when the length of the cylindrical shell is greater than 1.5 times the radius.

Substituting Eq.(14) into Eq.(6), the differential equation for the Airy stress function F is obtained:

$$\Delta\Delta F = -E\mu^2\left(\frac{m}{R}\right)^2\left\{A\cos\frac{2mx}{R} + B\cos\frac{2ny}{R} + D\cos\frac{3mx}{R}\cos\frac{ny}{R} + E\cos\frac{mx}{R}\cos\frac{3ny}{R} + C\cos\frac{mx}{R}\cos\frac{ny}{R} + F\cos\frac{2mx}{R}\cos\frac{2ny}{R}\right\} \quad (15)$$

where $\mu = \frac{m}{n}$, = the aspect ratio of the waves,

$$A = \frac{1}{8} f_1^2 n^2 - \left(\frac{1}{2} f_1 + f_2\right)$$

$$B = \frac{1}{8} f_1^2 n^2$$

$$D = \frac{1}{4} f_1 \left(\frac{1}{2} f_1 + f_2\right) n^2$$

$$E = \frac{1}{4} f_1 \left(\frac{1}{2} f_1 + f_2\right) n^2 \qquad (16)$$

$$C = \frac{1}{2} f_1 \left(\frac{1}{2} f_1 + f_2\right) n^2 - \frac{1}{2} f_1$$

and $F = \left(\frac{1}{2} f_1 + f_2\right)^2 n^2$

The solution of this differential equation can be easily obtained as

$$F = -E\mu^2\left(\frac{R}{n}\right)^2 \left\{ \frac{A}{16\mu^4} \cos\frac{2mx}{R} + \frac{B}{16} \cos\frac{2ny}{R} + \frac{C}{(\mu^2+1)^2} \cos\frac{mx}{R} \cos\frac{ny}{R} + \frac{D}{(9\mu^2+1)^2} \cos\frac{3mx}{R} \cos\frac{ny}{R} + \frac{E}{(9+\mu^2)} \cos\frac{mx}{R} \cos\frac{3ny}{R} + \frac{F}{16(\mu^2+1)^2} \cos\frac{2mx}{R} \cos\frac{2ny}{R} \right\} + \frac{\alpha}{2} x^2 + \frac{\beta}{2} y^2 \qquad (17)$$

Using Eq. (5), the stress components in the median surface ~~is obtained~~ can be written as

$$\sigma_x = E\mu^2 \left\{ \frac{B}{4} \cos\frac{2ny}{R} + \frac{C}{(\mu^2+1)^2} \cos\frac{mx}{R} \cos\frac{ny}{R} + \frac{D}{(9\mu^2+1)^2} \cos\frac{3mx}{R} \cos\frac{ny}{R} + \frac{9E}{(\mu^2+9)^2} \cos\frac{mx}{R} \cos\frac{3ny}{R} + \frac{F}{4(\mu^2+1)^2} \cos\frac{2mx}{R} \cos\frac{2ny}{R} \right\} + \beta$$

$$\sigma_y = E\mu^2 \left\{ \frac{A}{4\mu^2} \cos\frac{2mx}{R} + \frac{\mu^2 C}{(1+\mu^2)^2} \cos\frac{mx}{R} \cos\frac{ny}{R} + \frac{9\mu^2 D}{(9\mu^2+1)} \cos\frac{3mx}{R} \cos\frac{ny}{R} + \frac{\mu^2 E}{(\mu^2+9)^2} \cos\frac{mx}{R} \cos\frac{3ny}{R} + \frac{\mu^2 F}{4(\mu^2+1)^2} \cos\frac{2mx}{R} \cos\frac{2ny}{R} \right\} + \alpha \qquad (18)$$

$$\tau_{xy} = -E\mu^2 \left\{ \right\}$$

In all experimental results, the data is usually expressed in term of the average compression stress σ in the axial direction. It can be easily seen from Eq.(18) that

$$\beta = -\sigma \tag{19}$$

Using Eq.(3), for the following expressions for $\frac{\partial u}{\partial x}$ and $\frac{\partial v}{\partial y}$ can be obtained:

$$\frac{\partial u}{\partial x} = \frac{1}{E}\left(\sigma_x - \nu\sigma_y\right) - \frac{1}{2}\left(\frac{\partial w}{\partial x}\right)^2$$
$$\frac{\partial v}{\partial y} = \frac{1}{E}\left(\sigma_y - \nu\sigma_x\right) - \frac{1}{2}\left(\frac{\partial w}{\partial x}\right)^2 + \frac{w}{R} \tag{20}$$

By substituting Eqs.(14) and (18) into Eq.(20), it is found that

$$\frac{\partial u}{\partial x} = -\left[\left(\frac{\sigma}{E} + \nu\frac{\alpha}{E}\right) + \frac{1}{2}n^2\mu^2\left\{\frac{3}{32}f_1^2 + \frac{1}{8}f_1f_2 + \frac{1}{8}f_2^2\right\}\right] + \text{cosine Terms}$$
$$\frac{\partial v}{\partial y} = \frac{\alpha}{E} + \nu\frac{\sigma}{E} - \frac{1}{2}n^2\left\{\frac{3}{32}f_1^2 + \frac{1}{8}f_1f_2 + \frac{1}{8}f_2^2\right\} + \left(f_0 + \frac{1}{4}f_1\right) + \text{cosine Terms} \tag{21}$$

Since y is measured the circumferential direction, v must be a periodic function; therefore the constant term in $\frac{\partial v}{\partial y}$ must be equal to zero. Or

$$\frac{\alpha}{E} + \nu\frac{\sigma}{E} - \frac{1}{2}\left\{\frac{3}{32}f_1^2 + \frac{1}{8}f_1f_2 + \frac{1}{8}f_2^2\right\} + \left(f_0 + \frac{1}{4}f_1\right) = 0 \tag{22}$$

This is the condition for the determination of α.

Using Eqs. (7) (18) and (22), the externsional energy of the shell is obtained as

$$\frac{W_1}{\frac{1}{2}Et\cdot ab} = 4\Big[(1-\nu^2)\left(\frac{\sigma}{E}\right)^2 + n^4\left\{\frac{3}{64}f_1^2 + \frac{1}{16}f_1f_2 + \frac{1}{16}f_2^2\right\}^2$$

$$+ \left(f_0 + \frac{1}{4}f_1\right)^2 - 2n^2\left\{\frac{3}{64}f_1^2 + \frac{1}{16}f_1f_2 + \frac{1}{16}f_2^2\right\}\left(f_0 + \frac{1}{4}f_1\right)\Big]$$

$$+ \Big\{\frac{A^2}{8} + \frac{B^2\mu^4}{8} + \frac{\mu^4}{(1+\mu^2)}C^2 + \frac{\mu^4}{(9\mu^2+1)^2}D^2 + \frac{\mu^4}{(\mu^2+9)^2}E^2$$

$$+ \frac{\mu^4}{16(1+\mu^2)^2}F\Big\} \tag{23}$$

Using Eqs. (9) and (14), the bending energy of the shell can be calculated as

$$\frac{W_2}{\frac{1}{2}Et\,ab} = \frac{1}{6(1-\nu^2)}\left(\frac{t}{R}\right)^2 n^2\Big\{f_1^2\Big[\frac{1}{8}(1+\mu^2)^2 + \frac{1}{4}(1+\mu^4)\Big] + (1+\mu^4)f_1f_2 + (1+\mu^4)f_2^2\Big\} \tag{24}$$

The lowering in potential of the applied force can be obtained by means of Eqs.(10), (18), (21) and (22). The result is

$$\frac{W_3}{\frac{1}{2}Et\,ab} = -\Big[2(1-\nu^2)\left(\frac{\sigma}{E}\right)^2 + n^2\Big\{\frac{3}{32}(\mu^2+\nu)f_1^2 \tag{25}$$

$$+ \frac{1}{8}(\mu^2+\nu)f_1f_2 + \frac{1}{8}(\mu^2+\nu)f_2^2\Big\}\frac{\sigma}{E} - 2\nu\left(f_0 + \frac{1}{4}f_1\right)\frac{\sigma}{E}\Big]$$

Relation between the Compression Stress and the Amplitude of Waves

To find the relation between the compression stress and the amplitude of the waves, the conditions which will make the sum of the energies W_1, W_2, and W_3 a minimum have to be obtained. It was found that the calculations can be simplified to a certain extend by first using the condition that

$$\frac{\partial}{\partial f_0}\left(W_1 + W_2 + W_3\right) = 0 \tag{26}$$

This condition will determine a relation between f_0 and f_1 and f_2, which can be written as:

$$f_0 + \frac{1}{4} f_1 = n^2\left\{\frac{3}{64} f_1^2 + \frac{1}{16} f_1 f_2 + \frac{1}{16} f_2^2\right\} - 4\frac{\sigma}{E} \tag{27}$$

Substituting Eq. (27) into the expressions for W_1, W_2 and W_3 as given by Eqs. (23), (24) and (25) and using Eq. (16), the total energy of the system is expressed finally in the following form:

$$\frac{(W_1 + W_2 + W_3)}{\frac{1}{2} E t a b} = -4\left(\frac{\sigma}{E}\right)^2 - \frac{\sigma}{E} n^2 \mu^2 \left[\frac{3}{8} f_1^2 + \frac{1}{2} f_1 f_2 + \frac{1}{2} f_2^2\right]$$

$$+ \frac{1}{4}\left[n^4\left\{\left(\frac{1+\mu^4}{128} + \frac{17}{64}\frac{\mu^4}{(\mu^2+1)^2} + \frac{1}{16}\frac{\mu^4}{(9\mu^2+1)^2} + \frac{1}{16}\frac{\mu^4}{(\mu^2+9)^2}\right) f_1^4\right.\right.$$

$$+ \left(\frac{9}{8}\frac{\mu^4}{(\mu^2+1)^2} + \frac{\mu^4}{4(9\mu^2+1)^2} + \frac{\mu^4}{4(\mu^2+9)^2}\right) f_1^3 f_2 + \left(\frac{11}{8}\frac{\mu^4}{(\mu^2+1)^2} + \frac{\mu^4}{4(9\mu^2+1)^2} + \frac{\mu^4}{4(\mu^2+9)^2}\right) f_1^2 f_2^2 \tag{28}$$

$$\left.\left. + \frac{\mu^4}{2(\mu^2+1)^2} f_1 f_2^3 + \frac{\mu^4}{4(\mu^2+1)^2} f_2^4\right\} + \cdots\right]$$

The equilibrium conditions are then obtained by differentiating the expression for total energy, Eq.(28), with respect to f_1 and f_2 , and then set these expressions equal to zero. The results can be written in a simpler form by introducing the following parameters

$$\rho = f_2/f_1$$
$$\gamma = n^2 \frac{t}{R} \tag{29}$$
$$\xi = f_1 \frac{R}{t} = \frac{\delta}{t}$$

where δ is the wave amplitude of the buckled shape of the cylindrical shell.

Then the equilibrium conditions are

$$\frac{\sigma R}{Et} \gamma \mu^2 (\rho + \frac{3}{2}) = (\gamma\xi)^2 \Big\{ \frac{\mu^4}{4(\mu^2+1)^2} \rho^3 + \Big[\frac{11}{8} \frac{\mu^4}{(\mu^2+1)^2} + \frac{\mu^4}{4(9\mu^2+1)^2}$$

(30)

Eliminating $\frac{\sigma R}{Et}$ from the above equations, the following equation for ρ is obtained

$$A_3\rho^3 + A_2\rho^2 + A_1\rho + A_0 = 0 \qquad (31)$$

where the coefficients are

$$A_3 = (\gamma\xi)^2 \left[\frac{3\mu^4}{(\mu^2+1)^2} + \frac{\mu^4}{(9\mu^2+1)^2} + \cdots \right]$$

A_2

A_1

A_0

(32)

Thus with a given value of μ and γ, the coefficients for various values of the wave amplitude ξ can be first calculated by using the Eq.(32). Then Eq.(31) can be solved for different values of ρ corresponding to this particular value of μ and γ at various wave amplitude ξ. When the value of ρ is known, Eq.(30) can be used to calculate the corresponding value of the compression stress $\frac{\sigma R}{Et}$. It is found, however, that the following expression for the compression stress which is obtained from Eq. (30) by

eliminating the third powers of ρ ,is more suitable for numerical computation:

(33)

These calculation was carried out for two values of the parameter μ , ~~the aspect ratio of the waves, or more definitely,~~ the ratio of the wave lengths in circumferential direction and in axial direction. These values of μ are 1 and 0.5. The former value was chosen because the experiments indicates that at large wave amplitudes, the diamond waves have almost equal sides. The latter value of μ was chosen because the experiments made by N. Nojima and S.Kanemitsu (Ref.2) shown the occurance of this type of waves. The results of these computations are shown in Fig.2 and Fig.3 where the compression stress is plotted against the wave amplitudes.

The parameter in the figures is μ. The values written in the parenthesis is the actual number of waves n in circumferential direction for $R/t = 1000$. The dropping load characteristic is immediately evident. It should be noticed that for large values of the amplitude of the waves, the shell will finally buckle into a smaller number of waves in the circumferential direction. For the case $R/t = 1000$, the shell starts to buckle with a value of $n = 26$ for $\mu = 1$, but the value of n decreases to 10 when the wave amplitude is 16 times that of the shell thickness. The lower number of waves in circumf. direction agrees very well with the experimentally observed values at large wave amplitude. The gradual increase of the size of waves as the wave amplitude is increased is also found in the experimental study made by N. Nojima (Ref. 2).

The Relation between the Compression Stress and the Shortening in the Axial Direction

Although the dropping load characteristic of the cylindrical shell is shown very clearly by Figs. 2 and 3, the actual load taken by the specimen under a testing machine can not be predicted from these figures. In a testing machine, the only factor under the control of the operator is the distance between the end plates and this is the one which determine geometrical restraining the specimen must conform. Therefore, it is clear that the compression stress on the shell is not determined by the wave amplitude, but by the end shortening. The unit end shortening ε, i.e., the total shortening in a wave length of the shell in axial direction divided by the wave length, can be easily calculated from Eq.(21). It is found that

$$\frac{\varepsilon R}{t} = \frac{\sigma R}{Et} + \frac{\mu^2}{16}\xi(1+\xi)\left(\rho^2+\rho+\frac{3}{4}\right) \qquad (33)$$

Thus the approximate calculation presented does reproduce the main features of the buckling phenomena shown in laboratory, which the classical theory is unable to do.

Thus the unit end shortening canbe easily calculated by using the already found values of ρ and $\frac{\sigma R}{Et}$. In Fig. 4 and 5, the compression stress is plotted against the unit end shortenings, for $\mu = 1$ and $\mu = 0.5$. It is immediately clear from this two figures that if the buckling process follows the curves drawn, once the shell starts to buckle the end shortening has to decrease. This means that the end plates has to move apart. This is mechanically impossible, because the end plates in a testing machine is held at a certain position by the loading mechanism. Therefore, the shell must first jump to the point P (Fig4 or 5) which has the same end shortening as the starting point of buckling process, but has a much lower compression stress . This jump definitely involves a release of elastic energy and thus explains the rapidity of buckling process observed in laboratory with its accompanied vibration.

However, it is still difficult to say the shell will jump to a state with narrow waves, as shown by Fig.5, or to a state with almost square waves, as shown by Fig.4. Superficially, one might conclude that narrow waves are more probable because it gives a much compression stress, as can be seen by comparing Fig.4 with Fig.5. But at a given end shortening, the true criterion offered by the fundamental concept of mechanics for the most probable equilibrium position is that the elastic energy stored in

shell should be the lowest. An approximate calculation of the elastic energy of the shells shows that for values of $\gamma < 0.0121$, the occurance of narrow waves is improbable, because the elastic energy is higher than that for square waves at same value of end shortening. However, for $\frac{\varepsilon R}{t}$ near 0.6, the elastic energy stored in the shell for narrow waves is comparable to that for the square waves at same values of the end shortening. This indicates the possibility of the appearance of narrow waves during the initial stages of the buckling process. This is in agreement with the experimental findings of N.Nojima and S.Kanemitsu as reported in a previous paper by the present authors (Ref.2).

In any case it is certain that there are equilibrium positions of a buckled cylindrical shell which involve much lower average compression stress σ than that predicted in case of the beginning of buckling. Take for instance, the square wave pattern, the lowest compression stress is given by

$$\frac{\sigma}{E} = 0.194 \left(\frac{t}{R}\right) \tag{35}$$

This value corresponds closely to most of the experimental results obtained by E.E.Lundquist (Ref.7) and L.H. Donnell. (Ref.3) In the two previous papers (Ref.1 and Ref.2) the authors have pointed out that due to imperfections present in test specimen and vibrations in the surroundings, the test buckling load will probably nearer to

the minimum load necessary to keep the shell in buckled shape rather than the initail buckling load given by the classical theory. ~~Hence, although due to the approximation used in the present calculation, the authors are not able to give a complete solution of the problem, they do believe that they have given a satisfactory explaination for the experimental results.~~ It thus seems that the experimental results are satisfactorily explained by the present approximate calculation, although the details of the whole buckling phenomenon of cylindrical shells under axial compression is still lacking.

The Effect of the Elastic Characteristic of the Testing Machine on the Buckling Behavior

In the previous paragraphs, it is stated that the compression on the specimen is determined by the distance between the end plates which is in turn determined by the loading mechanism. However, in actual cases, there is always a certain amount of elasticity in the testing machine and thus the distance between the end plates is not only determined by the loading mechanism but also by the compression force ~~which~~ on the specimen. With the loading mechanism ~~locked~~ held at a certain position, a compression force on the specimen will force the end plates apart and thus reduce ~~the~~ the amount of end shortening which ~~of~~ the specimen must has, in order to conform with the geometrical restraining. Assuming that the testing machine has a linear elastic behavior, the compression load is related to the end shortening by parallel straight lines, say, for constant values of ~~any~~ number of turns of the loading crank of the testing machine. If the loading crank is held at a fixed position, then the compression load of the specimen must follow the straight line corresponding to this crank position.

In Fig.6, the load-end shortening curves of different character are superimposed on a system of straight lines representing the characteristics of the testing machine. It is evident that after the maximum, or initial buckling load is reached, the shell will jump to a new equilibrium state involving much lower compression load. The new equilibrium state is determined by two factors: ~~First,~~ the first factor is the shape of the load-end shortening curve. The curve A (Fig.6) will give higher load than the curve B (Fig.6). ~~Secondly,~~ the second factor is the elastic character of the testing machine. A more elastic machine will give a set of characteristic straight lines having smaller slopes. Therefore, in case of Curve A, a more elastic machine will result in a higher load, while in case of curve B, a more elastic machine will result in a lower load. Therefore, the buckling behavior of a cylindrical shell is not only determined by the elastic characteristics of the shell itself, but also influenced by the elastic characteristics of the testing machine. This fact is first discussed by the senior author ~~in his~~ in connection with the ~~early paper~~ plastic buckling of short columns (Ref. 8).

~~If there is a slight imperfection in the testing specimen, then~~

Concluding Remarks

In the previous paragraphs, the authors have shown that there are equilibrium positions in the buckled shape involving much lower load than the buckling load predicted by classical thoery, and thus if the specimen is slightly imperfect, it is reasonable to expect much lower buckle loads

of the order observed in the laboratory. They have also pointed out that the elastic behavior of the testing machine has a profound influence on the buckling phenomenon and this might be another cause of the large scattering of experimental data obtained by different experimenters. However, due to complexity of the problem, the results given in this paper can be only considered as a rough approximation and most of the discussion made is qualitative rather than quantitative. To put the new theory on a solid footing, a more accurate solution of the differential equations of equilibrium is necessary. Particular attention must be given to the calculation of the elastic energy stored in the shell, because it is found that final factor which determines the most probable equilibrium positions is neither the compression stress on the specimen nor the wave amplitude of the buckled cylindrical shell, but rather the elastic energy stored.

Perhaps, a more inquisitive investigator would be pleased by a rigorous proof of the validity of all the large deflection equations. All the equations used are established by intuitive arguments rather by systematic reasoning. For instance, it is not certain whether the curvature of the shell has to be calculated more accurately by taking into account the second order terms, or the extensions of median surface should be more accurately determined. It is the belief of the present authors that an investigation of these problems

by starting from the general non-linear elasticity theory developed by E. Cosserat (Ref.9) and others is very desirable. The senior author has already expressed this opinion in his 1940 Gibbs Lecture of the American Mathematical Society

THE BUCKLING OF THIN CYLINDRICAL SHELLS

UNDER AXIAL COMPRESSION

Theodore von Kármán and Hsue-shen Tsien
California Institute of Technology

In two previous papers (Ref. 1 and Ref. 2), the authors have discussed in detail the inadequacy of the classical theory of thin shells in explaining the buckling phenomenon of cylindrical and spherical shells. It was shown that not only the calculated buckling load is 3 to 5 times higher than that found by experiments, but the observed wave pattern of the buckled shell is also different from that predicted. Furthermore, it was pointed out that the different explanations for this discrepancy advanced by L. H. Donnell (Ref. 3) and W. Flügge (Ref. 4) are untenable when certain conclusions drawn from these explanations are compared with the experimental facts. ~~The authors are then led~~ By a theoretical investigation on spherical shells (Ref. 1) the authors were led to ~~the belief~~ believe that in general the buckling phenomenon of curved shells can only be explained by means of a non-linear large deflection theory. This point of view ~~is further~~ was substantiated by ~~a~~ model experiments on ~~thin~~ slender columns with non-linear elastic support (Ref. 2). The non linear characteristics ~~It is evident from these two investigations that~~ the load necessary to keep the shell in equilibrium drops very rapidly with increase in wave amplitude once the shell started to buckle. This characteristic shows, first of all, that there is a release of the elastic energy stored in the shell once the buckling has started, and thus explains the observed rapidity of the buckling process. Furthermore, it also brings in the possibility of a decrease in the buckling load when there are slight imperfections in the test specimen and when there are vibrations during the testing process.

In this paper, the authors will show by means of an approximate

calculation that in case of a thin uniform cylindrical shell under axial compression, the load sustained by the shell drops with increasing deflection. Consequently, they hope that they have thus offered an acceptable explanation of the observed facts.

Stresses in the Median Surface and the Expression for the Total Energy of the System

Let x and y be measured in the axial and the circumferential direction in the median surface of the undeformed cylindrical shell and u, v, and w be the components of displacement of a point on the median surface of the shell in the x-direction, the y-direction, and the radial direction. Then the unit strains in the x and y-directions, ε_x, ε_y and the unit shear γ_{xy} at a point in the median surface can be expressed in the following forms, including terms up to second order:

$$\begin{aligned} \varepsilon_x &= \frac{\partial u}{\partial x} + \frac{1}{2}\left(\frac{\partial w}{\partial x}\right)^2 \\ \varepsilon_y &= \frac{\partial v}{\partial y} + \frac{1}{2}\left(\frac{\partial w}{\partial y}\right)^2 - \frac{w}{R} \\ \gamma_{xy} &= \frac{\partial u}{\partial y} + \frac{\partial v}{\partial x} + \frac{\partial w}{\partial x}\frac{\partial w}{\partial y} \end{aligned} \tag{1}$$

where R is the radius of the undeformed median surface of the shell. The stresses and the strains in the median surface of the shell are, however, related to each other by the following equations:

$$\begin{aligned} \sigma_x &= \frac{E}{1-\nu^2}\left(\varepsilon_x + \nu\varepsilon_y\right) \\ \sigma_y &= \frac{E}{1-\nu^2}\left(\varepsilon_y + \nu\varepsilon_x\right) \\ \tau_{xy} &= \frac{E}{2(1+\nu)}\gamma_{xy} \end{aligned} \tag{2}$$

where E is Young's modulus of elasticity and ν is Poisson's ratio. Therefore by substituting Eq. (1) into Eq. (2), the following connections between the components of stress in the median surface and the components of displacement of the median surface are obtained:

$$\sigma_x = \frac{E}{1-\nu^2}\left[\frac{\partial u}{\partial x} + \frac{1}{2}\left(\frac{\partial w}{\partial x}\right)^2 + \nu\left\{\frac{\partial v}{\partial y} + \frac{1}{2}\left(\frac{\partial w}{\partial y}\right)^2 - \frac{w}{R}\right\}\right]$$

$$\sigma_y = \frac{E}{1-\nu^2}\left[\frac{\partial v}{\partial y} + \frac{1}{2}\left(\frac{\partial w}{\partial y}\right)^2 - \frac{w}{R} + \nu\left\{\frac{\partial u}{\partial x} + \frac{1}{2}\left(\frac{\partial w}{\partial x}\right)^2\right\}\right] \quad (3)$$

$$\tau_{xy} = \frac{E}{2(1+\nu)}\left[\frac{\partial u}{\partial y} + \frac{\partial v}{\partial x} + \frac{\partial w}{\partial x}\frac{\partial w}{\partial y}\right]$$

It is generally accepted that the equilibrium conditions of the stresses in the median surface of a thin shell can be approximately expressed by the following equations:

$$\frac{\partial \sigma_x}{\partial x} + \frac{\partial \tau_{xy}}{\partial y} = 0$$

$$\frac{\partial \tau_{xy}}{\partial x} + \frac{\partial \sigma_y}{\partial y} = 0 \quad (4)$$

This pair of equations can be satisfied by introducing the well-known Airy's stress function, $F(x,y)$ defined by the relations

$$\sigma_x = \frac{\partial^2 F}{\partial y^2}, \quad \tau_{xy} = -\frac{\partial^2 F}{\partial x \partial y}, \quad \sigma_y = \frac{\partial^2 F}{\partial x^2} \quad (5)$$

Eliminating the variables u and v in Eqs. (3) and (5) a relation between Airy's stress function $F(x,y)$ and the radial component of the displacement, w is obtained:

$$\frac{\partial^4 F}{\partial x^4} + 2\frac{\partial^4 F}{\partial x^2 \partial y^2} + \frac{\partial^4 F}{\partial y^4} = E\left[\left(\frac{\partial^2 w}{\partial x \partial y}\right)^2 - \frac{\partial^2 w}{\partial x^2}\frac{\partial^2 w}{\partial y^2} - \frac{1}{R}\frac{\partial^2 w}{\partial x^2}\right] \quad (6)$$

This equation expresses the condition of compatibility between stress and strain. When $R \to \infty$, it reduces to the corresponding equation for a flat plate derived by the senior author (Ref. 5). L. H. Donnell (Ref. 3) first obtained this equation in its present form. With a given form of the radial component of the displacement, w, Eq. (6) gives the induced stresses in the median surface of the shell.

For one complete wave panel, the extensional elastic energy W_1 corresponding to these stresses can be written as

$$W_1 = \frac{t}{2E}\,4\int_0^a\int_0^b\left[(\sigma_x + \sigma_y)^2 - 2(1+\nu)(\sigma_x\sigma_y - \tau_{xy}^2)\right]dx\,dy \quad (7)$$

where a and b are the half wave lengths in the axial and the circumferential directions respectively.

To calculate the bending elastic energy, it is necessary to find the expressions for the change of curvatures and the unit twist of the median surface. In this paper, the following simplified expressions will be used:

$$\chi_x = \frac{\partial^2 w}{\partial x^2}, \quad \chi_{xy} = \frac{\partial^2 w}{\partial x \partial y}, \quad \chi_y = \frac{\partial^2 w}{\partial y^2} \tag{8}$$

In Eq. (8), certain additional terms in χ_y and χ_{xy} involving v are neglected. It was shown by L. H. Donnell (Ref. 6) that those neglected terms differ from the terms retained in Eq. (8) by a factor $\frac{1}{n^2}$, where n is the number of waves in the circumferential direction. For thin cylindrical shells, the value of n is around 10; therefore the neglection is justified. With these expressions for the change of curvatures and the unit twist of the median surface, the bending energy W_2 for one complete wave panel can be written as

$$W_2 = \frac{t^3 E}{24(1-\nu^2)} 4 \int_0^a \int_0^b \left[\left\{ \frac{\partial^2 w}{\partial x^2} + \frac{\partial^2 w}{\partial y^2} \right\}^2 - 2(1-\nu) \left\{ \frac{\partial^2 w}{\partial x^2} \frac{\partial^2 w}{\partial y^2} - \left(\frac{\partial^2 w}{\partial x \partial y} \right)^2 \right\} \right] dx\, dy \tag{9}$$

The lowering of the potential W_3 of the applied force on the end of the cylindrical shell can be calculated as the product of the change in length of the shell and the applied force. Therefore the following expression is obtained for one complete wave panel:

$$W_3 = -t\, 4 \int_0^b (\sigma_x)_{x=a}\, dy \int_0^a \frac{\partial u}{\partial x} dx \tag{10}$$

The equilibrium condition of the shell can be obtained either by equating the first variation of the sum of the energies W_1, W_2 and W_3 to zero, or by actually analyzing the moments and the stresses in the median surface of the shell. Using the approximations stated previously, Donnell (Ref. 6) derived the equilibrium equation as

$$\frac{Et^3}{12(1-\nu^2)}\left(\frac{\partial^2}{\partial x^2}+\frac{\partial^2}{\partial y^2}\right)^4 w+\frac{Et}{R^2}\frac{\partial^4 w}{\partial x^4}=\left(\frac{\partial^2}{\partial x^2}+\frac{\partial^2}{\partial y^2}\right)^2\left\{p+t\left(\sigma_x\frac{\partial^2 w}{\partial x^2}+2\tau_{xy}\frac{\partial^2 w}{\partial x\partial y}+\sigma_y\frac{\partial^2 w}{\partial y^2}\right)\right\} \quad (11)$$

where p is the external radial pressure on the surface of the shell. In the case concerned, $p=0$, then using Eq. (5), the second equation connecting Airy's stress function $F(x,y)$ and the radial component of displacement, w is obtained as

$$\frac{Et^2}{12(1-\nu^2)}\left(\frac{\partial^2}{\partial x^2}+\frac{\partial^2}{\partial y^2}\right)^4 w+\frac{E}{R^2}\frac{\partial^4 w}{\partial x^4}=\left(\frac{\partial^2}{\partial x^2}+\frac{\partial^2}{\partial y^2}\right)^2\left[\frac{\partial^2 F}{\partial y^2}\frac{\partial^2 w}{\partial x^2}-2\frac{\partial^2 F}{\partial x\partial y}\frac{\partial^2 w}{\partial x\partial y}+\frac{\partial^2 F}{\partial x^2}\frac{\partial^2 w}{\partial y^2}\right] \quad (12)$$

When $R\rightarrow\infty$, Eq. (12) reduces to the corresponding equation for a flat plate.

There are two different ways to solve the problem of the buckling of a thin uniform cylindrical shell under axial compression. The more exact method is to solve Eqs. (6) and (12) simultaneously, using appropriate boundary conditions. The approximate method is to first assume a plausible function for w , with undetermined parameters and then use Eq. (6) to determine the stresses in the median surface of the shell. The energies W_1 , W_2 and W_3 can then be calculated by means of Eqs. (7), (9), and (10). The undetermined parameters can be ascertained by the condition that the sum of energies W_1 , W_2, and W_3 must be a minimum. This approximate method will be used in the following calculations.

Calculation of the Total Energy

To obtain a plausible form for w , one has to resort to the experimental results. It is observed that, for large values of the wave amplitude, the waves show a so-called diamond shaped pattern. This particular wave shape can be approximately expressed by

$$\frac{w_1}{R} = \cos^2\frac{(mx+ny)}{2R}\cos^2\frac{(mx-ny)}{2R} \quad (13)$$

where the squares are introduced to account for the fact that the shell has a definite preference to buckle inward. Eq. (13) can be re-written as

$$\frac{w_1}{R} = \frac{1}{4} + \frac{1}{2}\left[\cos\frac{mx}{R}\cos\frac{ny}{R} + \frac{1}{4}\cos\frac{2mx}{R} + \frac{1}{4}\cos\frac{2ny}{R}\right] \tag{14}$$

On the other hand, the classical theory which is correct for infinitesimal values of the wave amplitude, requires the wave to be of the form

$$\frac{w_2}{R} = \cos\frac{mx}{R}\cos\frac{ny}{R} \tag{15}$$

In order to satisfy this requirement, the wave form assumed in the following calculation is

$$\frac{w}{R} = \left(f_0 + \frac{f_1}{4}\right) + \frac{f_1}{2}\left(\cos\frac{mx}{R}\cos\frac{ny}{R} + \frac{1}{4}\cos\frac{2mx}{R} + \frac{1}{4}\cos\frac{2ny}{R}\right) + \frac{f_2}{4}\left(\cos\frac{2mx}{R} + \cos\frac{2ny}{R}\right) \tag{16}$$

where f_0 , f_1 , f_2 are unknowns to be determined by conditions of minimum total energy of the system. f_0 is introduced in order to allow the shell to expand radially. The amplitude of the wave pattern defined as the maximum difference in the radial deflection, w is evidently given by f_1 . The wave lengths in the axial and the circumferential direction are $\frac{2\pi R}{m}$ and $\frac{2\pi R}{n}$ respectively. Hence the number of waves along the circumference of the shell is equal to n . It is evident that no end effect can be accounted for by this form of wave pattern, and therefore the following calculation really corresponds to the case of a very long cylindrical shell. This simplification is justified by the experimental findings of N. Nojima and S. Kanemitsu as reported in a previous paper (Ref. 2). It was found that there is no appreciable length effect when the length of the cylindrical is greater than 1.5 times the radius of the shell. Furthermore, it is seen that by setting $f_0 = f_2 = 0$, Eq. (16) is reduced to Eq. (14); while by setting $\frac{f_1}{4} + \frac{f_2}{2} = 0$ and $f_0 + \frac{f_1}{4} = 0$, Eq.

(16) is reduced to Eq. (15). With other values of these parameters, wave patterns intermediate between these two limits can be obtained.

Substituting Eq. (16) into Eq. (6), the differential equation for Airy's stress function $F(x,y)$ is obtained:

$$\left(\frac{\partial^2}{\partial x^2}+\frac{\partial^2}{\partial y^2}\right)^2 F = -E\mu^2\left(\frac{n}{R}\right)^2\Big[A\cos\frac{2mx}{R}+B\cos\frac{2ny}{R}+C\cos\frac{mx}{R}\cos\frac{ny}{R}$$
$$+D\cos\frac{3mx}{R}\cos\frac{ny}{R}+G\cos\frac{mx}{R}\cos\frac{3ny}{R}+H\cos\frac{2mx}{R}\cos\frac{2ny}{R}\Big] \quad (17)$$

where $\mu=\frac{m}{n}$, the aspect ratio of the waves. If $\mu>1$ the waves are longer in the circumferential direction; if $\mu<1$, the waves are longer in the axial direction. The coefficients in Eq. (17) are given by the following relations:

$$\begin{aligned}
A &= \frac{1}{8}f_1^2n^2-\left(\frac{1}{2}f_1+f_2\right)\\
B &= \frac{1}{8}f_1^2n^2\\
C &= \frac{1}{2}f_1n^2\left(\frac{1}{2}f_1+f_2\right)-\frac{1}{2}f_1\\
D &= \frac{1}{4}f_1n^2\left(\frac{1}{2}f_1+f_2\right)\\
G &= \frac{1}{4}f_1n^2\left(\frac{1}{2}f_1+f_2\right)
\end{aligned} \quad (18)$$

and $H = n^2\left(\frac{1}{2}f_1+f_2\right)^2$

The solution of this differential equation can be easily obtained as

$$F=-E\mu^2\left(\frac{R}{n}\right)^2\Big[\frac{A}{16\mu^4}\cos\frac{2mx}{R}+\frac{B}{16}\cos\frac{2ny}{R}+\frac{C}{(1+\mu^2)^2}\cos\frac{mx}{R}\cos\frac{ny}{R}$$
$$+\frac{D}{(1+9\mu^2)^2}\cos\frac{3mx}{R}\cos\frac{ny}{R}+\frac{G}{(9+\mu^2)^2}\cos\frac{mx}{R}\cos\frac{3ny}{R}+\frac{H}{16(1+\mu^2)^2}\cos\frac{2mx}{R}\cos\frac{2ny}{R}\Big] \quad (19)$$
$$+\frac{\alpha}{2}x^2+\frac{\beta}{2}y^2$$

Using Eq. (5), the stress components in the median surface can be written as

$$\sigma_x=E\mu^2\Big[\frac{B}{4}\cos\frac{2ny}{R}+\frac{C}{(1+\mu^2)^2}\cos\frac{mx}{R}\cos\frac{ny}{R}+\frac{D}{(1+9\mu^2)^2}\cos\frac{3mx}{R}\cos\frac{ny}{R}$$
$$+\frac{9G}{(9+\mu^2)^2}\cos\frac{mx}{R}\cos\frac{3ny}{R}+\frac{H}{4(1+\mu^2)^2}\cos\frac{2mx}{R}\cos\frac{2ny}{R}\Big]+\beta \quad (20)$$

$$\sigma_y = E\mu^2\Big[\frac{A}{4\mu^2}\cos\frac{2mx}{R} + \frac{\mu^2 C}{(1+\mu^2)^2}\cos\frac{mx}{R}\cos\frac{ny}{R} + \frac{9\mu^2}{(1+9\mu^2)^2}\cos\frac{3mx}{R}\cos\frac{ny}{R}$$
$$+ \frac{\mu^2 G}{(9+\mu^2)^2}\cos\frac{mx}{R}\cos\frac{3ny}{R} + \frac{\mu^2 H}{4(1+\mu^2)^2}\cos\frac{2mx}{R}\cos\frac{2ny}{R}\Big] + \alpha$$

$$\tau_{xy} = E\mu^2\Big[\frac{\mu C}{(1+\mu^2)^2}\sin\frac{mx}{R}\sin\frac{ny}{R} + \frac{3\mu D}{(1+9\mu^2)^2}\sin\frac{3mx}{R}\sin\frac{ny}{R}$$
$$+ \frac{3\mu G}{(9+\mu^2)^2}\sin\frac{mx}{R}\sin\frac{3ny}{R} + \frac{\mu H}{4(1+\mu^2)^2}\sin\frac{2mx}{R}\sin\frac{2ny}{R}\Big]$$

In all experimental work, the data is usually expressed in terms of the average compression stress σ in the axial direction. It can be easily seen from Eq. (20) that

$$\beta = -\sigma \tag{21}$$

Using Eq. (3), the following expressions for $\frac{\partial u}{\partial x}$ and $\frac{\partial v}{\partial y}$ can be obtained:

$$\frac{\partial u}{\partial x} = \frac{1}{E}(\sigma_x - \nu\sigma_y) - \frac{1}{2}\left(\frac{\partial w}{\partial x}\right)^2$$
$$\frac{\partial v}{\partial y} = \frac{1}{E}(\sigma_y - \nu\sigma_x) - \frac{1}{2}\left(\frac{\partial w}{\partial y}\right)^2 + \frac{w}{R} \tag{22}$$

By substituting Eqs. (16) and (20) into Eq. (22), it is found that

$$\frac{\partial u}{\partial x} = -\Big[\Big(\frac{\sigma}{E} + \nu\frac{\alpha}{E}\Big) + \frac{1}{2}n^2\mu^2\Big(\frac{3}{32}f_1^2 + \frac{1}{8}f_1f_2 + \frac{1}{8}f_2^2\Big)\Big] + \text{Terms of periodic functions}$$

$$\frac{\partial v}{\partial y} = \frac{\alpha}{E} + \nu\frac{\sigma}{E} - \frac{1}{2}n^2\Big(\frac{3}{32}f_1^2 + \frac{1}{8}f_1f_2 + \frac{1}{8}f_2^2\Big) + \Big(f_0 + \frac{f_1}{4}\Big) + \text{Terms of periodic functions} \tag{23}$$

Since y is measured along the circumference of the shell, v must be a periodic function of y; therefore, the constant term in $\frac{\partial v}{\partial y}$ must be equal to zero. Or

$$\frac{\alpha}{E} + \nu\frac{\sigma}{E} - \frac{1}{2}n^2\Big(\frac{3}{32}f_1^2 + \frac{1}{8}f_1f_2 + \frac{1}{8}f_2^2\Big) + \Big(f_0 + \frac{f_1}{4}\Big) = 0 \tag{24}$$

This is the condition for the determination of α.

Using Eqs. (7), (20) and (24), the extensional energy W_1 of the shell is obtained as

$$\frac{W_1}{\frac{1}{2}Et\cdot ab} = 4\Big[(1-\nu^2)\left(\frac{\sigma}{E}\right)^2 + n^4\left(\frac{3}{64}f_1^2 + \frac{1}{16}f_1f_2 + \frac{1}{16}f_2^2\right)^2 + \left(f_0 + \frac{1}{4}f_1\right)^2 -$$

$$-2n^2\left(\frac{3}{64}f_1^2 + \frac{1}{16}f_1f_2 + \frac{1}{16}f_2^2\right)\left(f_0 + \frac{1}{4}f_1\right)\Big] + \Big[\frac{A^2}{8} + \frac{B^2\mu^4}{8} + \frac{\mu^4}{(1+\mu^2)^2}C^2 \tag{25}$$

$$+ \frac{\mu^4}{(1+9\mu^2)^2}D^2 + \frac{\mu^4}{(9+\mu^2)^2}G^2 + \frac{\mu^4}{16(1+\mu^2)^2}H^2\Big]$$

Using Eqs. (9) and (16), the bending energy W_2 of the shell can be calculated as

$$\frac{W_2}{\frac{1}{2}Etab} = \frac{1}{6(1-\nu^2)}\left(\frac{t}{R}\right)^2 n^4\Big[f_1^2\Big\{\frac{1}{8}(1+\mu^2)^2 + \frac{1}{4}(1+\mu^4)\Big\} + (1+\mu^4)f_1f_2 + (1+\mu^4)f_2^2\Big] \tag{26}$$

The ~~lowering of the potential~~ virtual work of the applied force can be obtained by means of Eqs. (10), (20), (23) and (24). The result is

$$\frac{W_3}{\frac{1}{2}Etab} = +\Big[2(1-\nu^2)\left(\frac{\sigma}{E}\right)^2 + n^2\frac{\sigma}{E}\Big\{\frac{3}{32}(\mu^2+\nu)f_1^2 + \frac{1}{8}(\mu^2+\nu)f_1f_2 + \frac{1}{8}(\mu^2+\nu)f_2^2\Big\} \tag{27}$$

$$- 2\nu\frac{\sigma}{E}\left(f_0 + \frac{1}{4}f_1\right)\Big]$$

Relation between the Compression Stress and the Amplitude of Waves

To find the relation between the compression stress and the amplitude of the waves, the conditions which will make the sum of the energies W_1, W_2, and W_3 a minimum have to be obtained. It was found that the calculations can be simplified to a certain extent by first using the condition that the sum of energies must be minimum with respect to f_0. Or

$$\frac{\partial}{\partial f_0}\left(W_1 + W_2 + W_3\right) = 0 \tag{28}$$

This condition determines a relation between f_0 and f_1 and f_2, which can be written as:

$$f_0 + \frac{1}{4}f_1 = n^2\left(\frac{3}{64}f_1^2 + \frac{1}{16}f_1f_2 + \frac{1}{16}f_2^2\right) - \nu\frac{\sigma}{E} \tag{29}$$

Using this relation and Eq. (24), it is easily seen that $\alpha=0$. In other words, the shell will expand radially to such an extent that the average of the circumferential stress σ_y is equal to zero. Substituting Eq. (29) into the expressions for W_1, W_2 and W_3 as given by Eqs. (25), (26) and (27) and using Eq. (18), the total energy of the system is expressed finally in the following form:

$$
\begin{aligned}
\frac{W_1+W_2+W_3}{\frac{1}{2}Etab} = & -4\left(\frac{\sigma}{E}\right)^2 - \frac{\sigma}{E}n^2\mu^2\left(\frac{3}{8}f_1^2+\frac{1}{2}f_1f_2+\frac{1}{2}f_2^2\right) + n^4\Bigg[\Bigg\{\frac{1+\mu^6}{512}+\frac{17}{256}\frac{\mu^4}{(1+\mu^2)^2} \\
& + \frac{1}{64}\frac{\mu^4}{(1+9\mu^2)^2}+\frac{1}{64}\frac{\mu^4}{(9+\mu^2)^2}\Bigg\}f_1^4 + \Bigg\{\frac{9}{32}\frac{\mu^4}{(1+\mu^2)^2}+\frac{1}{16}\frac{\mu^4}{(1+9\mu^2)^2}+\frac{1}{16}\frac{\mu^4}{(9+\mu^2)^2}\Bigg\}f_1^3f_2 + \\
& + \Bigg\{\frac{11}{32}\frac{\mu^4}{(1+\mu^2)^2}+\frac{1}{16}\frac{\mu^4}{(1+9\mu^2)^2}+\frac{1}{16}\frac{\mu^4}{(9+\mu^2)^2}\Bigg\}f_1^2f_2^2 + \frac{1}{8}\frac{\mu^4}{(1+\mu^2)^2}f_1f_2^3 + \frac{1}{16}\frac{\mu^4}{(1+\mu^2)^2}f_2^4\Bigg] \\
& - n^2\Bigg[\Bigg\{\frac{1}{64}+\frac{1}{4}\frac{\mu^4}{(1+\mu^2)^2}\Bigg\}f_1^3 + \Bigg\{\frac{1}{32}+\frac{1}{2}\frac{\mu^4}{(1+\mu^2)^2}\Bigg\}f_1^2f_2\Bigg] + \\
& + \Bigg[\Bigg\{\frac{1}{32}+\frac{1}{4}\frac{\mu^4}{(1+\mu^2)^2}\Bigg\}f_1^2+\frac{1}{8}f_1f_2+\frac{1}{8}f_2^2\Bigg] + \qquad (30) \\
& + \frac{1}{6(1-\nu^2)}\left(\frac{t}{R}\right)^2 n^4\Bigg[\Bigg\{\frac{1}{8}(1+\mu^2)^2+\frac{1}{4}(1+\mu^4)\Bigg\}f_1^2+(1+\mu^4)f_1f_2+(1+\mu^4)f_2^2\Bigg]
\end{aligned}
$$

The equilibrium conditions are then obtained by differentiating the expression for total energy, Eq. (30), with respect to f_1 and f_2, and then set these expressions equal to zero. The results can be written in a simpler form by introducing the following parameters:

$$
\rho = \frac{f_2}{f_1}, \quad \eta = n^2\frac{t}{R}, \quad \xi = f_1\frac{R}{t} = \frac{\delta}{t} \qquad (31)
$$

where δ is the wave amplitude of the buckled shape of the cylindrical shell. Then the equilibrium conditions are

$$\frac{\sigma R}{Et}\eta\mu^2\left(\rho+\frac{3}{2}\right) = (\eta\xi)^2\Big[\frac{\mu^4}{4(1+\mu^2)^2}\rho^3 + \Big\{\frac{11}{8}\frac{\mu^4}{(1+\mu^2)^2}+\frac{1}{4}\frac{\mu^4}{(1+9\mu^2)^2}+\frac{1}{4}\frac{\mu^4}{(9+\mu^2)^2}\Big\}\rho^2$$

$$+\Big\{\frac{27}{16}\frac{\mu^4}{(1+\mu^2)^2}+\frac{3}{8}\frac{\mu^4}{(1+9\mu^2)^2}+\frac{3}{8}\frac{\mu^4}{(9+\mu^2)^2}\Big\}\rho+\Big\{\frac{1+\mu^4}{64}+\frac{17}{32}\frac{\mu^4}{(1+\mu^2)^2}+\frac{1}{8}\frac{\mu^4}{(1+9\mu^2)^2}+\frac{1}{8}\frac{\mu^4}{(9+\mu^2)^2}\Big\}\Big]$$

$$-(\eta\xi)\Big[\Big\{\frac{1}{8}+2\frac{\mu^4}{(1+\mu^2)^2}\Big\}\rho+\Big\{\frac{3}{32}+\frac{3}{2}\frac{\mu^4}{(1+\mu^2)^2}\Big\}\Big]+\Big[\frac{1}{4}\rho+\Big\{\frac{1}{8}+\frac{\mu^4}{(1+\mu^2)^2}\Big\}\Big]$$

$$+\frac{1}{3(1-\nu^2)}\eta^2\Big[(1+\mu^4)\rho+\Big\{\frac{1}{4}(1+\mu^2)^2+\frac{1}{2}(1+\mu^4)\Big\}\Big] \tag{32}$$

$$\frac{\sigma R}{Et}\eta\mu^2\left(\rho+\frac{1}{2}\right) = (\eta\xi)^2\Big[\frac{1}{4}\frac{\mu^4}{(1+\mu^2)^2}\rho^3+\frac{3}{8}\frac{\mu^4}{(1+\mu^2)^2}\rho^2+\Big\{\frac{11}{16}\frac{\mu^4}{(1+\mu^2)^2}+\frac{1}{8}\frac{\mu^4}{(1+9\mu^2)^2}+\frac{1}{8}\frac{\mu^4}{(9+\mu^2)^2}\Big\}\rho$$

$$+\Big\{\frac{9}{32}\frac{\mu^4}{(1+\mu^2)^2}+\frac{1}{16}\frac{\mu^4}{(1+9\mu^2)^2}+\frac{1}{16}\frac{\mu^4}{(9+\mu^2)^2}\Big\}\Big]-(\eta\xi)\Big[\frac{1}{32}+\frac{1}{2}\frac{\mu^4}{(1+\mu^2)^2}\Big]$$

$$+\Big[\frac{1}{4}\rho+\frac{1}{8}\Big]+\frac{1}{3(1-\nu^2)}\eta^2\Big[(1+\mu^4)\rho+\frac{1}{2}(1+\mu^4)\Big]$$

Eliminating $\frac{\sigma R}{Et}$ from the above equations, the following equation for ρ is obtained

$$A_3\rho^3+A_2\rho^2+A_1\rho+A_0=0 \tag{33}$$

where the coefficients are

$$A_3 = (\eta\xi)^2\Big\{\frac{3\mu^4}{(1+\mu^2)^2}+\frac{\mu^4}{(1+9\mu^2)^2}+\frac{\mu^4}{(9+\mu^2)^2}\Big\}$$

$$A_2 = (\eta\xi)^2\Big\{\frac{9}{2}\frac{\mu^4}{(1+\mu^2)^2}+\frac{3}{2}\frac{\mu^4}{(1+9\mu^2)^2}+\frac{3}{2}\frac{\mu^4}{(9+\mu^2)^2}\Big\}-(\eta\xi)\Big\{\frac{1}{2}+\frac{8\mu^4}{(1+\mu^2)^2}\Big\}$$

$$A_1 = (\eta\xi)^2\Big\{\frac{1+\mu^4}{16}+\frac{1}{4}\frac{\mu^4}{(1+\mu^2)^2}+\frac{1}{4}\frac{\mu^4}{(1+9\mu^2)^2}+\frac{1}{4}\frac{\mu^4}{(9+\mu^2)^2}\Big\}-(\eta\xi)\Big\{\frac{1}{2}+\frac{8\mu^4}{(1+\mu^2)^2}\Big\}+\Big\{\frac{4\mu^4}{(1+\mu^2)^2}-1\Big\}-\frac{2}{3(1-\nu^2)}\eta^2\Big\{2(1+\mu^4)-\frac{(1+\mu^2)^2}{2}\Big\} \tag{34}$$

$$A_0 = (\eta\xi)^2\Big\{\frac{1+\mu^4}{32}-\frac{5}{8}\frac{\mu^4}{(1+\mu^2)^2}-\frac{1}{8}\frac{\mu^4}{(1+9\mu^2)^2}-\frac{1}{8}\frac{\mu^4}{(9+\mu^2)^2}\Big\}+\Big\{\frac{2\mu^4}{(1+\mu^2)^2}-\frac{1}{2}\Big\}$$

$$-\frac{2}{3(1-\nu^2)}\eta^2\Big\{(1+\mu^4)-\frac{1}{4}(1+\mu^2)^2\Big\}$$

Therefore, when $\xi=0$, i.e., when the wave amplitude approaches zero Eq. (32) gives $A_3=A_2=0$; and

$$A_1 = -\frac{2}{3(1-\nu^2)}\eta^2\left\{2(1+\mu^4) - \frac{1}{2}(1+\mu^2)^2\right\}$$

$$A_0 = -\frac{2}{3(1-\nu^2)}\eta^2\left\{(1+\mu^4) - \frac{1}{4}(1+\mu^2)^2\right\} = \frac{A_1}{2}$$

Substituting into Eq. (31) it is seen that $\rho = -\frac{1}{2}$, or $f_2 = -\frac{1}{2}f_1$. Putting this relation between f_1 and f_2 into Eq. (14), the wave pattern is reduced to that represented by Eq. (13), i.e., the classical wave pattern for infinitesimal wave amplitude.

With a given value of μ and η, the coefficients for various values of the wave amplitude ξ can be first calculated by using the Eq. (34). Then Eq. (33) can be solved for ρ corresponding to this particular set of values of μ and η at various wave amplitude ξ. When the value of is known, Eq. (32) can be used to calculate the corresponding value of the compression stress $\frac{\sigma R}{Et}$. It is found, however, that the following expression for the compression stress $\frac{\sigma R}{Et}$ which is obtained from Eq. (30) by eliminating the third powers of ρ is more suitable for numerical computations:

$$\begin{aligned}
\frac{\sigma R}{Et} = & \left\{\frac{1}{\eta}\frac{\mu^2}{(1+\mu^2)^2} + \frac{1}{12(1-\nu^2)}\frac{\eta(1+\mu^2)^2}{\mu^2}\right\} \\
& + \frac{1}{\eta\mu^2}\Big[(\eta\xi)^2\left\{\frac{\mu^4}{(1+\mu^2)^2} + \frac{\mu^4}{4(1+9\mu^2)^2} + \frac{\mu^4}{4(9+\mu^2)^2}\right\}\rho^2 + \\
& + \left\{(\eta\xi)^2\left(\frac{\mu^4}{(1+\mu^2)^2} + \frac{1}{4}\frac{\mu^4}{(1+9\mu^2)^2} + \frac{1}{4}\frac{\mu^4}{(9+\mu^2)^2}\right) - (\eta\xi)\left(\frac{1}{8} + \frac{2\mu^4}{(1+\mu^2)^2}\right)\right\}\rho \\
& + \left\{(\eta\xi)^2\left(\frac{1+\mu^4}{64} + \frac{1}{4}\frac{\mu^4}{(1+\mu^2)^2} + \frac{1}{16}\frac{\mu^4}{(1+9\mu^2)^2} + \frac{1}{16}\frac{\mu^4}{(9+\mu^2)^2}\right) - \right. \\
& \left. - (\eta\xi)\left(\frac{1}{16} + \frac{\mu^4}{(1+\mu^2)^2}\right)\right\}\Big]
\end{aligned} \tag{35}$$

Therefore, when $\xi \to 0$, i.e., when the wave amplitude becomes very small, Eq. (35) reduces to

$$\left(\frac{\sigma R}{Et}\right)_{\xi \to 0} = \frac{1}{\eta}\frac{\mu^2}{(1+\mu^2)^2} + \frac{1}{12(1-\nu^2)}\frac{1}{\frac{1}{\eta}\frac{\mu^2}{(1+\mu^2)^2}} \tag{36}$$

The minimum value of the average compression stress is given by

$$Min\left(\frac{\sigma R}{Et}\right)_{\xi \to 0} = \frac{1}{\sqrt{3(1-\nu^2)}} \tag{37}$$

which is the well-known result from the classical theory of infinitesimal deflections. This minimum value is obtained when

$$\eta\frac{(1+\mu^2)^2}{\mu^2} = 2\sqrt{3(1-\nu^2)} \tag{38}$$

It is interesting to notice that for infinitesimal wave amplitude, the minimum value of average compression stress is not determined by separate parameters η and μ, but by a combined parameter shown in Eq. (38).

These calculations were carried out for two values of the parameter μ , the ratio of the wave lengths in circumferential direction and in axial direction. These values of μ are 1 and 0.5 . The value 1 was chosen because the experiments indicate that at large values of wave amplitude, the diamond waves have almost equal sides. The value 0.5 was chosen to investigate the possibility of occurrence of narrow waves. The results of these computations are shown in Fig. 2 and Fig. 3, where the compression stress $\frac{\sigma R}{Et}$ is plotted against the wave amplitudes ξ . The parameter in the figures is η . The values written in the parenthesis after η is the actual number of waves n in circumferential direction for R/t = 1000. For a given value of η and μ, i.e., a fixed size of the wave, the load sustained by the shell, $\frac{\sigma R}{Et}$ first decreases as the wave amplitude, ξ , is increased. After a minimum is reached, the load will rise with increase in wave amplitude. When the waves are larger, the initial buckling

load, i.e., the value of $\frac{\sigma R}{Et}$ at $\xi = 0$, is higher. However, the minimum load reached tends to a lower value, except for $\eta < 0.169$ and $\mu = 1.0$. For $\mu = 0.5$, the lowest value of the minimum load is not yet reached at $\eta = 0.081$.

The Relation between the Compression Stress and the Shortening in the Axial Direction

Although the load characteristic of the cylindrical shell shown in the Figs. 2 and 3 give the possible equilibrium relations between load and amplitude of the deflection wave, the actual behaviour of a specimen in a testing machine cannot be directly seen from these figures. In a testing machine, the only factor under the control of the operator is the distance between the end plates; this is the geometrical restraint the specimen must conform. Therefore, in order to determine the behaviour of the specimen the compression stress will have to be plotted as function of the end shortening. The unit end shortening, ε, i.e., the total shortening in one wave length of the shell in axial direction divided by the wave length, can be easily calculated from Eq. (23). It is found that

$$\frac{\varepsilon R}{t} = \frac{\sigma R}{Et} + \frac{\mu^2}{16}\xi(\eta\xi)\left(\rho^2 + \rho + \frac{3}{4}\right) \tag{39}$$

This equation for the unit end shortening contains only quantities already found such as the values of ρ and $\frac{\sigma R}{Et}$. In Figs. 4 and 5, the compression stress $\frac{\sigma R}{Et}$ is plotted against the unit end shortening $\frac{\varepsilon R}{t}$ for $\mu = 1$ and $\mu = 0.5$, respectively. It is immediately clear from this two figures that if the buckling process follows the curves drawn, after the shell starts to buckle the end shortening has to decrease. In other words, the end plates of the testing machine have to move apart. Therefore, the process of buckling in this region is highly unstable, since before the operator has

times to separate the end plates, the shell will jump to the point P (Figs. 4 or 5) which has the same end shortening as the starting point of the buckling process, but has a much lower compression stress. This jump in equilibrium positions involves a release of elastic energy and thus explains the rapidity of the buckling process observed and the accompanied vibration.

However, it is still difficult to say whether the shell will jump to a state with almost square waves, as shown in Fig. 4, or to a state with narrow waves, as shown in Fig. 5. Superficially, one might conclude that the narrow waves are the more probable shape because it gives a much lower compression stress, as can be seen by comparing Figs. 4 and 5. But, according to the fundamental concept of mechanics, the true criterion for the most probable equilibrium position compatible with a given value of the end shortening is that the elastic energy stored in the shell should be the lowest. An approximate calculation of the elastic energy of the shells shows that for values of $\eta < 0.121$, the occurrence of the narrow waves is improbable, because the elastic energy stored is higher than that for the square waves at same value of the end shortening. However, for $\frac{\varepsilon R}{t}$ near 0.6, and $\eta \geqq 0.121$ the elastic energy stored in the shell for the narrow waves is comparable to that for the square waves at the same value of the end shortening. This indicates the possibility of the appearance of narrow waves during the very initial stages of the buckling process.

In any case, it is certain that there are equilibrium positions of a buckled cylindrical shell which involve much lower average compression stress $\frac{\sigma R}{Et}$ than that at the beginning of buckling. For instance, in the case of square wave pattern, the lowest compression stress is given by

$$\frac{\sigma}{E} = 0.194 \frac{t}{R} \tag{40}$$

Incidentally, this value corresponds closely to most of the experimental results obtained by L. H. Donnell (Ref. 3) and E. E. Lundquist (Ref. 7).

The corresponding value of the parameter η which determines the number of waves is equal to 0.225. In case of R/t = 1000, the number of waves, n, will be 15 which also agrees well with the experimental evidence. For this particular value of the radius to thickness ratio, the number of waves along the circumference decreases from the n = 26 at the beginning of the buckling to n = 15 at the calculated minimum buckling stress. This gradual increase in the size of waves with the unit shortening is also observed by the experiments reported in an earlier paper (Ref. 2).

It is particularly interesting, however, to trace the gradual change in the wave pattern during the buckling process. Figs. 6 and 7 show the lines of equal deflection of the wave surfaces corresponding to different equilibrium states for two values of the aspect ratio of the wave pattern, $\mu=1.0$ and $\mu=0.5$. These particular equilibrium states are denoted in Figs. 2, 3, 4 and 5 by a small circle in order to indicate their relative position during the buckling process. It is seen that there is a rapid shift from the rectangular waves bounded by lines, x = const., and y = const., as predicted by the classical theory for infinitesimal wave amplitudes, to staggered rows of circular or elliptical waves. Whereas, the rectangular waves are directed alternatively inward and outward, the circular or elliptical waves are all directed inwards. The transition is practically completed for $\xi=4$ or 6, i.e., when the wave amplitude is only 4 or 6 times the thickness of the shell. The occurrence of such inwardly directed circular and elliptical waves at this stage of the buckling process is in good agreement with the experimental observations (Ref. 2). If the experiment ($\xi\sim30$) is continued to larger deflections, these staggered waves

obtain characteristic diamond shapes. The present approximate theory fails to give these sharp diamond shaped waves. It is obviously not sufficiently exact for such large deflections. Furthermore, when these diamond shaped waves occur, the load on the specimen actually falls to a very low value such as $\frac{\sigma R}{Et} \approx 0.06$, whereas the theory shows a slight increase of the stress at least for the case $\mu = 1.0$. Therefore, the present calculation can be only considered as a good approximation to the earlier stages of buckling when the wave amplitude is only a few times the thickness of the shell. Nevertheless, it reproduces the characteristic features of the buckling process observed in the laboratory.

The Effect of the Elastic Characteristic of the Testing Machine on the Buckling Phenomenon

It was stated in the previous paragraph that the state of the specimen is determined by the distance between the end plate and that this distance is the independent parameter controlled by the experimenter. This statement is correct only insofar the elasticity in the mechanism of the testing machine is neglected. Since there is always a certain amount of elastic deflection in the loading mechanism and this deflection is a function of the load. Hence, if, for example, the loading crank is held at a certain position, the compression force acting on the specimen will force the end plates apart and thus reduce the amount of end shortening of the specimen. The actual shortening is determined by the load-deflection characteristics of the specimen and the testing machine. Assuming that the testing machine has a linear elastic characteristic, the compression load is related to the end shortening by parallel straight lines, each line corresponding to, say, a constant number of turns of the loading crank. If the loading crank of

the machine is held at a fixed position, corresponding values of the compression load and end shortening of the specimen must lie on the straight line for this crank position. If the load-end shortening characteristics of the specimen itself are given, it is evident that the equilibrium positions of the entire system are determined by intersections of the curves representing the characteristics of the specimen with the straight lines representing the characteristics of the machine.

Fig. 8 shows representative curves for the characteristics of the specimen and two families of straight lines representing the characteristics of two different testing machines. It is evident that after the maximum or initial buckling load is reached, the shell will jump to a new equilibrium position involving much lower compression load. But this new equilibrium position is determined not only by the load-end shortening relationship and also by the elastic characteristic of the testing machine. A more elastic machine will give a set of characteristic straight lines with smaller slopes. Therefore, in case of curve A (Fig. 8), a more elastic machine will make the shell to jump to a higher load, while in case of curve B, a more elastic machine will make the shell to jump to a lower load. This influence of the elasticity of the testing machine has been discussed by the senior author in connection with the plastic buckling of columns (Ref. 8).

Concluding Remarks

In the previous paragraphs, the authors have shown that there are equilibrium positions in the buckled shape involving much lower load than the buckling load predicted by the classical theory, and thus if the specimen is slightly imperfect, it is reasonable to expect much lower buckling loads. They have also pointed out that the elastic characteristic

of the testing machine might have quite a large influence on the buckling process and this might be another cause of the large scattering of the data obtained by different experimenters. However, due to the complexity of the problem, the results given in this paper can be only considered as a rough approximation and most of the statements made are qualitative rather than quantitative. To put the new theory on a solid footing, a more accurate solution of the differential equations of equilibrium is necessary. Particular attention must be given to the calculation of the elastic energy stored in the shell, because it is found that the most probable equilibrium depends on the magnitude of the elastic energy stored in the various equilibrium positions compatible with the constraint exerted by the loading process.

Furthermore, an inquisitive mind will, perhaps, be pleased by a rigorous proof of the validity of all the large deflection equations. These equations are established by intuitive arguments, not by systematic reasoning. For instance, due to the appearance of sharp curvatures in the diamond shaped wave surfaces at large deflections, it is not certain whether the curvature of the shell has to be calculated more accurately by taking into account the second order terms, or the extensions of the median surface should be more accurately determined. It is the belief of the authors that an investigation of these problems by starting from the general non-linear theory of elasticity developed by G. Kirchhoff, J. Boussinesq and others is very desirable. The recent work by R. Kappus (Ref. 9) is a noteworthy contribution in this field of investigation. The senior author has already expressed this opinion in his 1939 Gibbs Lecture (Ref. 10) given before the American Mathematical Society.

Section 6

Take-off from Satellite Orbit

Rough draft, one copy! 1

Take-Off from Satellite Orbit

H. S. Tsien

Summary

The mass ratio or the characteristic velocity for the take-off of a space ship from the satellite orbit is computed for two cases: the radial thrust and the circumferential thrust. The circumferential thrust is much more efficient in that the required mass ratio is much less than for the radial thrust. Both cases show, however, an increase of the required mass ratio and the characteristic velocity with a reduction in acceleration. With circumferential thrust, the characteristic velocity increases by a factor of two when the acceleration is reduced from $\frac{1}{2} g$ to $1/3000\ g$.

For take-off of a rocket from the earth surface, it is convenient to have the initial trajectory in the vertical direction and then the thrust should be considerably larger than the initial weight of the rocket. Depending upon the relative magnitudes of the aerodynamic drag and the weight, the initial ratio of the thrust and the weight should be between 2 and 3 for minimum expenditure of the propellant. The situation is quite different for a space ship taking off from the satellite orbit: In a satellite orbit, the gravitational attraction is completely balanced by the centrifugal force, and the vehicle is effectively in a weightless state. This fact has led many fanciers of interplanetary travel to conclude that take-off from satellite orbit requires only a very minute thrust. For instance, L. Spitzer (Ref. 1) proposed a nuclear power plant for his space ship to be accelerated at only at 1/3000 g. Another example is the extensive discussion of interorbital transport techniques by H. Preston-Thomas (Ref. 2) based upon the assumption of equally small acceleration. On the other hand, W. von Braun (Ref. 3) seems to prefer a very much larger acceleration of approximately 1/2 g for take-off from the satellite orbit. ¶ The magnitude of the acceleration has a strong bearing on the optimum type of power plant to be used: The ion-beam rocket is only possible for very small acceleration, while for moderate acceleration, chemical rocket is required. Therefore the question of the magnitude of acceleration is an important one for interplanetary flight. The purpose of this note is to demonstrate clearly the relation between the acceleration and the mass ratio required for escape from the earth's gravitational field starting from the satellite orbit. It is hoped that the present investigation will give the future generation of astronautical engineers a more rational basis for designing space ships.

Basic Equations

The problem considered is the motion of a space ship under the influence of the rocket thrust and the gravitational attraction of ~~the~~ , say the earth ~~alone, or~~ a single ~~massive~~ body. Then if the rocket thrust is in the plane of trajectory, the trajectory of the space ship will remain in a plane. Let the position of the ship at any time instant t be given by the polar coordinates r and θ: r the distance from the center of attraction, and θ the angular position. If the components of the rocket thrust per unit mass of the vehicle are R in the radial direction and Θ in the circumferential direction, and if g is the magnitude of gravitational attraction at the starting satellite orbit $r = r_0$ (Fig. 1), then the equations of motion of the space ship are

$$\frac{d^2r}{dt^2} = R + r\left(\frac{d\theta}{dt}\right)^2 - g\left(\frac{r_0}{r}\right)^2 \qquad (1)$$

and

$$\frac{d}{dt}\left(r^2\frac{d\theta}{dt}\right) = r\Theta \qquad (2)$$

By using the subscript 0 to indicate quantities at the starting instant $t = 0$, the equilibrium condition of the satellite orbit is given by

$$r_0\left(\frac{d\theta}{dt}\right)_0^2 = g \qquad (3)$$

Initially, the radial velocity is zero, i.e.,

$$\left(\frac{dr}{dt}\right)_0 = 0 \qquad (4)$$

These are the initial conditions. For the space ship to have sufficient energy to escape the earth gravitational field at the end of the powered flight, the sum of the kinetic energy and the potential energy must vanish at the end of the accelerating period. Let that instant be denoted by the subscript 1. Thus at $t = t_1$

$$\frac{1}{2}\left[\left(\frac{dr}{dt}\right)_1^2+\left(r\frac{d\theta}{dt}\right)_1^2\right]-g\frac{r_0^2}{r_1}=0 \qquad (5)$$

With any specified variation of the thrust forces R and Θ as functions of time, the above system of equations determine completely the take-off trajectory of the space ship. In the following sections, two special cases of practical significance will be discussed in detail: the case $R=$ constant, $\Theta=0$, purely radial thrust; and the case $R=0$, $\Theta=$ constant, purely circumferential thrust.

Radial Thrust

If the thrust is always radial and is proportional to the instantaneous mass of the vehicle, a non-dimensional thrust factor μ can be introduced as

$$R=\mu g \qquad (5)$$

Furthermore, let

$$\rho=r/r_0, \qquad \tau=\sqrt{\frac{g}{r_0}}\,t \qquad (6)$$

Then Eqs. (1) and (2) can be written in the nondimensional form as

$$\frac{d^2\rho}{d\tau^2}=\mu+\rho\left(\frac{d\theta}{d\tau}\right)^2-\frac{1}{\rho^2} \qquad (7)$$

and

$$\frac{d}{d\tau}\left(\rho^2\frac{d\theta}{d\tau}\right)=0 \qquad (8)$$

Eq. (8) can be immediately integrated and by using the initial condition of Eq. (3), the result of integration is

$$\frac{d\theta}{d\tau}=\frac{1}{\rho^2} \qquad (9)$$

By substituting this equation into Eq. (7), the final equation for ρ is

$$\frac{d^2\rho}{d\tau^2}=\mu+\frac{1}{\rho^3}-\frac{1}{\rho^2} \qquad (10)$$

The non-dimensional radial velocity is $d\rho/d\tau$. This is related to the physical radial velocity dr/dt as follows

$$\frac{dr}{dt} = \sqrt{g r_0}\,\frac{d\rho}{d\tau} \qquad (11)$$

Eq. (10) can be rewritten as

$$\frac{1}{2}\frac{d}{d\rho}\left(\frac{d\rho}{d\tau}\right)^2 = \mu + \frac{1}{\rho^3} - \frac{1}{\rho^2}$$

Since $d\rho/d\tau = 0$ when $\tau = 0$ and $\rho = 1$ according to Eq. (4), the result of integrating the above equation is

$$\left(\frac{d\rho}{d\tau}\right)^2 = 2\mu(\rho-1) + \left(1-\frac{1}{\rho^2}\right) - 2\left(1-\frac{1}{\rho}\right) \qquad (12)$$

Therefore the non-dimensional time τ can be calculated as a function of the radius ρ as follows

$$\tau = \int_1^{\rho} \frac{\rho\, d\rho}{\sqrt{(\rho-1)(2\mu\rho^2-\rho+1)}} \qquad (13)$$

With Eqs. (9) and (12), the end condition of Eq. 15) can be written as

$$\frac{1}{2}\left[\left\{2\mu(\rho_1-1) + \left(1-\frac{1}{\rho_1^2}\right) - 2\left(1-\frac{1}{\rho_1}\right)\right\} + \frac{1}{\rho_1^2}\right] - \frac{1}{\rho_1} = 0$$

Or simply

$$\rho_1 = 1 + \frac{1}{2\mu} \qquad (14)$$

Then the velocities at the end of acceleration period are

$$\left.\begin{aligned} \left(\frac{dr}{dt}\right)_1 &= \sqrt{g r_0}\,\frac{\sqrt{1+\frac{1}{\mu}}}{1+\frac{1}{2\mu}} \\ \text{and} \quad \left(r\frac{d\theta}{dt}\right)_1 &= \sqrt{g r_0}\,\frac{1}{1+\frac{1}{2\mu}} \end{aligned}\right\} \qquad (15)$$

The time τ_1 for the powered flight can be obtained from Eq. (13) by setting the upper limit of integration to ρ_1. Thus

$$\tau_1 = \sqrt{\frac{2}{\mu}}\left[\frac{\sqrt{2(\mu+1)}}{2\mu+1} + F\left(\frac{1}{\sqrt{8\mu}},\ \cos^{-1}\frac{2\mu-1}{3\mu+1}\right) + E\left(\frac{1}{\sqrt{8\mu}},\ \cos^{-1}\frac{2\mu-1}{3\mu+1}\right)\right] \quad (16)$$

where F and E are the elliptical integrals of first kind and second kind respectively.*

If $M(t)$ is the instantaneous mass of the space ship, and c the effective exhaust velocity of the rocket, then

$$RM = \mu g M = -c\frac{dM}{dt} = -c\sqrt{\frac{g}{r_0}}\frac{dM}{d\tau}$$

Therefore the mass ratio M_0/M_1 can be calculated as follows:

$$\log(M_0/M_1) = \frac{\sqrt{g r_0}}{c}\mu\tau_1$$

By using the result of Eq. (16),

$$\frac{c}{\sqrt{g r_0}}\log(M_0/M_1) = \frac{2\sqrt{\mu(\mu+1)}}{2\mu+1} + \sqrt{2\mu}\left\{F\left(\frac{1}{\sqrt{8\mu}},\ \cos^{-1}\frac{2\mu-1}{3\mu+1}\right) + E\left(\frac{1}{\sqrt{8\mu}},\ \cos^{-1}\frac{2\mu-1}{3\mu+1}\right)\right\} \quad (17)$$

When the acceleration is very large, $\mu \gg 1$, the integrand in Eq. (13) can be expanded in terms of this parameter. Then the mass ratio is

$$\frac{c}{\sqrt{g r_0}}\log(M_0/M_1) = 1 + \frac{1}{24\mu^2} - \frac{1}{40\mu^3} + \cdots \quad (18)$$

The relation of Eqs. (17) and (18) is plotted in Fig. 2. For $\mu = \frac{1}{8}$, the mass ratio becomes infinite. The reason is that at this value

---

*The author is indebted to Dr. Y. T. Wu who kindly supplied the relation of Eq. (16)

of) acceleration, there is a radial position where the thrust force is equal to the gravitational attraction and no further increase in the energy of the vehicle can occur. Therefore the radial thrust per unit mass, if maintained constant throughout the powered flight, should be larger than 1/8 g. With increasing thrust, the required mass ratio for escape from the earth's gravitational field decreases. The asymptotic value of $\log(M_0/M_1)$ is $\sqrt{g r_0}/c$. However there is no appreciable improvement in going to higher thrust than 1 g. This strong dependence of the mass ratio upon the acceleration factor is contrary to opinion that for take-off from satellite orbit only very small thrust is required.

Circumferential Thrust

If the thrust is always circumferential and proportional to the mass of the vehicle, then

$$\Theta = \nu g \tag{19}$$

By using the same non-dimensional variables as defined in Eq. (16), the equations of motion are

$$\frac{d^2\rho}{d\tau^2} = \rho\left(\frac{d\theta}{d\tau}\right)^2 - \frac{1}{\rho^2} \tag{20}$$

$$\frac{d}{d\tau}\left(\rho^2\frac{d\theta}{d\tau}\right) = \nu\rho \tag{21}$$

The initial conditions of Eqs (3) and (4) are

$$\left(\frac{d\theta}{d\tau}\right)_0 = 1\ ,\quad \left(\frac{d\rho}{d\tau}\right)_0 = 0\ ,\quad \text{at } \rho=1,\ \tau=0 \tag{22}$$

Therefore Eq. (20) gives another initial condition that

$$\left(\frac{d^2\rho}{d\tau^2}\right)_0 = 0 \tag{23}$$

By eliminating θ from Eqs. (20) and (21),

$$\frac{d}{d\tau}\left(\rho^3\frac{d^2\rho}{d\tau^2}+\rho\right)^{\frac{1}{2}} = \nu\rho \qquad (24)$$

This is a third order differential equation with three initial conditions specified by Eqs. (22) and (23). No simple general solution can, however, be obtained. The following discussion is thus centered around approximations that are valid for large values of ν or small values of ν.

For very large values of ν, the acceleration period is expected to be short and the change of the radial position to be small. Then the value of ρ must be very close to the initial value of unity. By taking ρ to be unity, Eq. (24) becomes

$$\frac{d}{d\tau}\left(\frac{d^2\rho}{d\tau^2}+1\right)^{\frac{1}{2}} = \nu$$

Then

$$\frac{d^2\rho}{d\tau^2}+1 = C^2 + 2C\nu\tau + \nu^2\tau^2$$

where C is the integration constant. C, however, must be 1 because of the initial condition of Eq. (23). The appropriate approximate solution for ρ for very large ν is thus

$$\rho \cong 1 + \frac{1}{3}\nu\tau^3 + \frac{1}{12}\nu^2\tau^4 \qquad (25)$$

To obtain higher terms in this power series, the usual series substitution method may be used. The calculation is somewhat lengthy and therefore will not be reproduced here. The result is

$$\rho = 1 + \frac{1}{3}\nu\tau^3 + \frac{1}{12}\nu^2\tau^4 - \frac{\nu}{60}\tau^5 - \frac{23\nu^2}{360}\tau^6 + \cdots \qquad (26)$$

By using the result of Eq. (26), the radial velocity is obtained by differentiation. Then Eq. (20) gives the circumferential velocity. The end condition of Eq. (15) can be modified into the following more convenient form by multiplying it by r^2:

$$0 = \left[\left(\rho\frac{d\rho}{d\tau}\right)^2 + \left(\rho^2\frac{d\theta}{d\tau}\right)^2 - 2\rho\right]_1$$

By substituting the solution of Eq. (26) into this condition, an equation for determining τ_1 is obtained:

$$0 = -1 + 2\nu\tau_1 + \nu^2\tau_1^2 - \frac{2}{3}\nu\tau_1^3 + \nu^2\tau_1^4 + \frac{\nu}{30}(1+26\nu^2)\tau_1^5 - \frac{\nu^2}{90}(4-13\nu^2)\tau_1^6 + \cdots \quad (27)$$

The mass ratio M_0/M_1 can be calculated in the same way as in the previous section and can be determined through the new parameter x defined as follows:

$$\frac{c}{\sqrt{g r_0}} \log(M_0/M_1) = \nu\tau_1 = x \quad (28)$$

Eq. (27) then can be written as

$$0 = -1 + 2x + x^2 - \frac{2}{3}\frac{x^3}{\nu^2} + \frac{x^4}{\nu^2} + \frac{x^5}{30\nu^4} + \frac{13}{15}\frac{x^5}{\nu^2} - \frac{2}{45}\frac{x^6}{\nu^4} + \frac{13}{90}\frac{x^6}{\nu^2} \quad (29)$$

Since the calculation is designed for large values of ν, the appropriate expansion of x should be a series in inverse powers of ν. Eq. (29) suggests specifically

$$x(\nu) = x^{(0)} + \frac{x^{(1)}}{\nu^2} + \frac{x^{(2)}}{\nu^4} + \cdots \quad (30)$$

---

where $x^{(0)}$, $x^{(1)}$ and $x^{(2)}$ are constants independent of ν. By substituting Eq. (30) into Eq. (29) and equating equal powers of ν, the following set of equations results:

$$x^{(0)2} + 2x^{(0)} - 1 = 0 \quad (31)$$

$$x^{(1)} = \frac{1}{2(1+x^{(0)})}\left[\frac{2}{3}x^{(0)3} - x^{(0)4} - \frac{13}{15}x^{(0)5} - \frac{13}{90}x^{(0)6}\right] \quad (32)$$

$$x^{(2)} = \frac{1}{2(1+x^{(0)})}\left[-x^{(1)2} + 2x^{(0)2}x^{(1)} - 4x^{(0)3}x^{(1)} - \frac{1}{30}x^{(0)6} - \frac{13}{3}x^{(0)4}x^{(1)} + \frac{2}{45}x^{(0)6} - \frac{13}{15}x^{(0)5}x^{(1)}\right] \quad (33)$$

The explicit numerical solutions are then

(the acceleration will be very small and) 10

$$x^{(0)} = \sqrt{2} - 1 = 0.41421$$
$$x^{(1)} = 0.002349$$
$$x^{(2)} = -0.0004791 \quad (34)$$

This completes the calculation of mass ratio for large values of the acceleration factor ν.

For the other extreme case of very small values of ν, it is to be expected that in Eq. (24), the term $\rho^3 \frac{d^2\rho}{d\tau^2}$ will be very much smaller than ρ. Therefore a good approximation of Eq. (24) at small ν is

$$\frac{d}{d\tau}(\rho)^{\frac{1}{2}} = \nu\rho \qquad \text{or} \qquad \frac{1}{2}\frac{d\rho}{\rho^{3/2}} = \nu\, d\tau$$

The solution of this equation with the initial condition of $\rho = 1$ at $\tau = 0$ is

$$\rho = \frac{1}{(1-\nu\tau)^2} \quad (35)$$

Therefore

$$\frac{d\rho}{d\tau} = \frac{2\nu}{(1-\nu\tau)^3}, \quad \frac{d^2\rho}{d\tau^2} = \frac{6\nu^2}{(1-\nu\tau)^4} \quad (36)$$

At $\tau = 0$, the radial velocity and the radial acceleration are thus not zero as required by the initial conditions of Eqs. (22) and (23). They are however very small, because ν is very small. Therefore the solution of Eq. (35) is a good approximation to the exact solution.

To the same approximation, Eq. (20) becomes

$$\rho\frac{d\theta}{d\tau} = \frac{1}{\rho^{1/2}} = (1-\nu\tau) \quad (37)$$

This means that because of the extremely slow acceleration, the centrifugal force per unit mass $r\left(\frac{d\theta}{dt}\right)^2$ practically balances the gravitational attraction at every instant. The end condition of Eq. 15) can then

be written as

$$\frac{4\nu^2}{(1-x)^6} - (1-x)^2 = 0 \tag{38}$$

where x is $\nu\tau_1$. The appropriate solution for x is then

$$x = 1 - (2\nu)^{1/4} \tag{39}$$

Since the mass ratio M_0/M_1 is related to x by Eq. (28), Eq. (39) actually gives the mass ratio for escaping the gravitational field with very small acceleration.

The parameter x is plotted against ν in Fig. 3, using both Eq. (30) with Eq. (34) and Eq. (39). When ν approaches zero, x approaches 1. When ν is very large, x approaches $\sqrt{2}-1$. As ν increases, x and hence the mass ratio M_0/M_1 decrease monotonically. Therefore, same as the result for purely radial thrust, there is a strong influence of the magnitude of acceleration on the required mass ratio. However as far as decreasing the mass ratio is concerned, there is no appreciable advantage in using ν greater than ½.

Discussion

By comparing Fig. 2 with Fig. 3, it is apparent that the radial thrust is much less efficient than the circumferential thrust for take-off from the satellite orbit. For large thrusts, the value of $\log(M_0/M_1)$ for radial thrust is more than twice that for circumferential thrust. Furthermore, in case of radial thrust, the ratio of thrust to the instantaneous mass, if maintained constant, must be larger than 1/8. In case of circumferential thrust, no such limit exist. Therefore circumferential thrust is definitely preferred.

The quantity $c \log(M_0/M_1)$ is a measure of the performance or the

capability of the vehicle. It has the dimension of a velocity and is actually the increase of velocity which the vehicle is capable of in space without gravitation. This quantity is conveniently called the <u>characteristic velocity</u> of the vehicle. Let this be denoted by V, Then for the case of circumferential thrust, Eq. (28) gives

$$V = c \log(M_0/M_1) = \sqrt{g r_0}\, x = \frac{S}{\sqrt{2\lambda}}\, x \qquad (40)$$

where S is the "escape velocity" from the surface of the earth and λ is the ratio of the radii of the satellite orbit and of the earth. S is equal to 11.2 km/sec. Fig. 3 then shows that by decreasing the acceleration from $1/2\, g$ to $1/3000\, g$, x, hence the required characteristic velocity V, will increase by a factor of two. This is a very important point for the designers of space ships.

References

1. "Interplanetary Travel between Satellite Orbits" by L. Spitzer, Jr. Journal of the American Rocket Society, Vol. 22, pp. 92-96 (1952)

2. "Interorbital Transport Techniques" by H. Preston-Thomas. Journal of the British Interplanetary Society, Vol. 11, pp. 173-193 (1952)

3. "Man on the Moon, the Journey" by W. von Braun. Collier's, Oct. 18, 1952 p. 52

Our cartoon!

Take-Off From Satellite Orbit

H. S. Tsien*

Daniel and Florence Guggenheim Jet Propulsion Center, California Institute of Technology

Summary

The mass ratio or the characteristic velocity for the take-off of a space ship from the satellite orbit is computed for two cases: the radial thrust and the circumferential thrust. The circumferential thrust is much more efficient in that the required mass ratio is much less than for the radial thrust. Both cases show, however, an increase of the required mass ratio and the characteristic velocity with a reduction in acceleration. With circumferential thrust, the characteristic velocity increases by a factor of two when the acceleration is reduced from 1/2 g to 1/3000 g.

* Robert H. Goddard Professor of Jet Propulsion

For take-off of a rocket from the earth surface, it is convenient to have the initial trajectory in the vertical direction and then the thrust should be considerably larger than the initial weight of the rocket (to overcome the gravity and to give an appropriate acceleration). Depending upon the relative magnitudes of the aerodynamic drag and the weight, the initial ratio of the thrust and the weight should be between 2 and 3 for minimum expenditure of the propellant. The situation is quite different for a space ship taking off from the satellite orbit: In a satellite orbit, the gravitational attraction is completely balanced by the centrifugal force, and the vehicle is effectively in a weightless state. This fact has led many fanciers of interplanetary travel to conclude that take-off from satellite orbit requires only a very minute thrust. For instance, L. Spitzer (Ref. 1) proposed a nuclear power plant for ~~his~~ a space ship to be accelerated at only 1/3000 g. Another example is the extensive discussion of interorbital transport techniques by H. Preston-Thomas (Ref. 2) based upon the assumption of equally small acceleration. On the other hand, W. von Braun (Ref. 3) seems to prefer a very much larger acceleration of approximately 1/2 g for take-off from the satellite orbit.

The magnitude of the acceleration has a strong bearing on the optimum type of power plant to be used: The ion-beam rocket is only possible for very small acceleration, while for moderate acceleration, chemical rocket is required. Therefore the question of the magnitude of acceleration is an important one for interplanetary flight. The purpose of this note is to ~~demonstrate clearly~~ compute the relation between the acceleration and the mass ratio required for escape from the earth's gravitational field, starting from the satellite orbit. It is hoped that the present investigation will give the future generation of astronautical engineers a ~~more~~ rational basis for designing space ships.

Basic Equations

The problem considered is the motion of a space ship under the influence of the rocket thrust and the gravitational attraction of a single massive body, say the earth. Then if the rocket thrust is in the plane of trajectory, the trajectory of the space ship will remain in a plane. Let the position of the ship at any time instant t be given by the polar coordinates r and θ : r the distance from the center of attraction, and θ the angular position. If the components of the rocket thrust per unit mass of the vehicle are R in the radial direction and Θ in the circumferential direction, and if g is the magnitude of gravitational attraction at the starting satellite orbit $r = r_0$ (Fig. 1), then the equations of motion of the space ship are

$$\frac{d^2r}{dt^2} = R + r\left(\frac{d\theta}{dt}\right)^2 - g\left(\frac{r_0}{r}\right)^2 \tag{1}$$

and

$$\frac{d}{dt}\left(r^2\frac{d\theta}{dt}\right) = r\Theta \tag{2}$$

By using the subscript o to indicate quantities at the starting instant t = 0, the equilibrium condition of the satellite orbit is given by

$$r_0\left(\frac{d\theta}{dt}\right)_0^2 = g \tag{3}$$

Initially, the radial velocity is zero, i.e.,

$$\left(\frac{dr}{dt}\right)_0 = 0 \tag{4}$$

These are the initial conditions. ¶ For the space ship to have sufficient energy to escape the earth gravitational field at the end of the powered flight, the sum of the kinetic energy and potential energy must vanish at the end of the

end of the accelerating period. Let that instant be denoted by the subscript 1. Thus at $t = t_1$

$$\frac{1}{2}\left[\left(\frac{dr}{dt}\right)_1^2 + \left(r\frac{d\theta}{dt}\right)_1^2\right] - g\frac{r_0^2}{r_1} = 0 \tag{5}$$

With any specified variation of the thrust forces R and Θ as functions of time, the above system of equations determine completely the take-off trajectory of the space ship. In the following sections, two special cases of practical significance will be discussed in detail: the case R = constant, $\Theta \equiv 0$, purely radial thrust; and the case R = 0, Θ = constant, purely circumferential thrust.

Radial Thrust

If the thrust is always radial and is proportional to the instantaneous mass of the vehicle, a non-dimensional thrust factor μ can be introduced as

$$R = \mu g \tag{6}$$

Furthermore, let

$$\rho = \frac{r}{r_0}, \qquad \tau = \sqrt{\frac{g}{r_0}}\, t \tag{7}$$

ρ is then the nondimensional radial distance and τ is the nondimensional time. Then Eqs. (1) and (2) can be written in the nondimensional form as

$$\frac{d^2\rho}{d\tau^2} = \mu + \rho\left(\frac{d\theta}{d\tau}\right)^2 - \frac{1}{\rho^2} \tag{8}$$

and

$$\frac{d}{d\tau}\left(\rho^2\frac{d\theta}{d\tau}\right) = 0 \tag{9}$$

Eq. (9) can be immediately integrated and by using the initial condition of Eq. (3), the result of integration is

$$\frac{d\theta}{d\tau} = \frac{1}{\rho^2} \tag{10}$$

By substituting this equation into Eq. (4), the final equation for ρ is

$$\frac{d^2\rho}{d\tau^2} = \mu + \frac{1}{\rho^3} - \frac{1}{\rho^2} \tag{11}$$

The nondimensional radial velocity is $d\rho/dt$. This is related to the physical radial velocity dr/dt as follows

$$\frac{dr}{dt} = \sqrt{g r_0}\,\frac{d\rho}{d\tau} \tag{12}$$

Eq. (11) can be rewritten as

$$\frac{1}{2}\frac{d}{d\rho}\left(\frac{d\rho}{d\tau}\right)^2 = \mu + \frac{1}{\rho^3} - \frac{1}{\rho^2}$$

Since $d\rho/dt = 0$ when $t = 0$ and $\rho = 1$ according to Eq. (4), the result of integrating the above equation is

$$\left(\frac{d\rho}{d\tau}\right)^2 = 2\mu(\rho - 1) + \left(1 - \frac{1}{\rho^2}\right) - 2\left(1 - \frac{1}{\rho}\right) \tag{13}$$

Therefore the non-dimensional time τ can be calculated as a function of the radius ρ as follows

$$\tau = \int_1^{\rho} \frac{\rho\, d\rho}{\sqrt{(\rho - 1)(2\mu\rho^2 - \rho + 1)}} \tag{14}$$

With Eqs. (10) and (13), the end condition of Eq. (5) can be written as

$$\frac{1}{2}\left[\left\{2\mu(\rho_1 - 1) + \left(1 - \frac{1}{\rho_1^2}\right) - 2\left(1 - \frac{1}{\rho_1}\right)\right\} + \frac{1}{\rho_1^2}\right] - \frac{1}{\rho_1} = 0$$

Or simply

$$\rho_1 = 1 + \frac{1}{2\mu} \tag{15}$$

Then the velocities at the end of acceleration period are

$$\left.\begin{aligned} \left(\frac{dr}{dt}\right)_1 &= \sqrt{g r_0}\,\frac{\sqrt{1 + \frac{1}{\mu}}}{1 + \frac{1}{2\mu}} \\ \text{and} \quad \left(r\frac{d\theta}{dt}\right)_1 &= \sqrt{g r_0}\,\frac{1}{1 + \frac{1}{2\mu}} \end{aligned}\right\} \tag{16}$$

Don't type!

The time τ_1 for the powered flight can be obtained from Eq. (14) by setting the upper limit of integration to ρ_1. The result of this integration is*

$$\tau_1 = \sqrt{\frac{2}{\mu}}\left[\frac{\sqrt{2(\mu+1)}}{2\mu+1} + F\left(\frac{1}{\sqrt{8\mu}}, \cos^{-1}\frac{2\mu-1}{2\mu+1}\right) + E\left(\frac{1}{\sqrt{8\mu}}, \cos^{-1}\frac{2\mu-1}{2\mu+1}\right)\right] \qquad (17)$$

where F and E are the elliptical integrals of first kind and second kind respectively.

If M(t) is the instantaneous mass of the space ship, and c the effective exhaust velocity of the rocket, then

$$RM = \mu g M = -c\frac{dM}{dt} = -c\sqrt{\frac{g}{r_0}}\frac{dM}{d\tau}$$

Therefore the mass ratio M_o/M_1 can be calculated as follows:

$$\log(M_0/M_1) = \frac{\sqrt{g r_0}}{c}\mu\tau_1$$

By using the result of Eq. (16),

$$\frac{c}{\sqrt{g r_0}}\log(M_0/M_1) = \frac{2\sqrt{\mu(\mu+1)}}{2\mu+1} + \sqrt{2\mu}\left\{F\left(\frac{1}{\sqrt{8\mu}}, \cos^{-1}\frac{2\mu-1}{2\mu+1}\right) + E\left(\frac{1}{\sqrt{8\mu}}, \cos^{-1}\frac{2\mu-1}{2\mu+1}\right)\right\} \qquad (18)$$

When the acceleration is very large, $\mu \gg 1$, the integrand in Eq. (14) can be expanded in terms of this parameter. Then the mass ratio is calculated as

$$\frac{c}{\sqrt{g r_0}}\log(M_0/M_1) = 1 + \frac{1}{24\mu^2} - \frac{1}{40\mu^3} + \cdots \qquad (19)$$

The relation of Eqs. (18) and (19) is plotted in Fig. 2. For $\mu = \frac{1}{8}$, the mass ratio becomes infinite. The reason is that at this value of

---

* The author is indebted to Dr. Y. T. Wu who kindly supplied the relation of Eq. (17).

Insert for p. 6

A!

Eq. (175) shows that at very large values of the acceleration factor μ, the acceleration is accomplished in so short an interval that the circumferential velocity at the end of the acceleration remains at the initial value of $\sqrt{g r_0}$. The radial velocity increases from nothing at the initial instant to the final value of $\sqrt{g r_0}$. The total kinetic energy is thus $g r_0$ at the end of acceleration and this is equal to the negative of potential energy at that instant, since the radial position r must be practically the initial value r_0 under very large thrust. The work of the rocket is to produce the radial velocity $\sqrt{g r_0}$. Thus it is evident that the value of $c \log (M_0/M_1)$ must be $\sqrt{g r_0}$, as the calculation shows.

acceleration, there is a radial position where the thrust force is equal to the gravitational attraction and ~~one~~ no further increase in the energy of the vehicle can occur. Therefore the radial thrust per unit mass, if maintained constant throughout the powered flight, should be larger than 1/8 g. With increasing thrust, the required mass ratio for escape from the earth's gravitational field decreases. The asymptotic value of $\log(M_0/M_1)$ is $\sqrt{g r_0}/c$. However there is no appreciable improvement in going to higher thrust than 1 g. This strong dependence of the mass ratio upon the acceleration factor is contrary to opinion that for take-off from satellite orbit only very small thrust is required.

insert!

Circumferential Thrust

If the thrust is always circumferential and proportional to the mass of the vehicle, then a new thrust factor ν can be introduced such that

$$\Theta = \nu g \qquad (20)$$

By using the same non-dimensional variables as defined in Eq. (6), the equations of motion are

$$\frac{d^2\rho}{d\tau^2} = \rho\left(\frac{d\theta}{d\tau}\right)^2 - \frac{1}{\rho^2} \qquad (21)$$

$$\frac{d}{d\tau}\left(\rho^2 \frac{d\theta}{d\tau}\right) = \nu\rho \qquad (22)$$

The initial conditions of Eqs. (3) and (4) are

$$\left(\frac{d\theta}{d\tau}\right)_0 = 1, \quad \left(\frac{d\rho}{d\tau}\right)_0 = 0, \quad \text{at} \quad \rho = 1, \quad \tau = 0 \qquad (23)$$

Therefore Eq. (21) gives another initial condition that

$$\left(\frac{d^2\rho}{d\tau^2}\right)_0 = 0 \qquad (24)$$

By eliminating β from Eqs. (1) and (2),

$$\frac{d}{d\tau}\left(\rho^3 \frac{d^2\rho}{d\tau^2} + \rho\right)^{\frac{1}{2}} = \nu\rho \qquad (25)$$

This is a third order differential equation with three initial conditions specified by Eqs. (3) and (4). No simple general solution can, however, be obtained. The following discussion will be concerned with the approximations that are valid for large values of ν or for small values of ν .

For very large values of ν , the acceleration period is expected to be short and the change of the radial position to be small. Then the value of ρ must be very close to the initial value of unity. By taking ρ to be unity, Eq. (25) becomes

$$\frac{d}{d\tau}\left(\frac{d^2\rho}{d\tau^2} + 1\right)^{\frac{1}{2}} = \nu$$

Then

$$\frac{d^2\rho}{d\tau^2} + 1 = C^2 + 2C\nu\tau + \nu^2\tau^2$$

where C is the integration constant. C, however, must be 1 because of the initial condition of Eq. (4). The appropriate approximate solution for ρ for very large ν is thus

$$\rho \cong 1 + \frac{1}{3}\nu\tau^3 + \frac{1}{12}\nu^2\tau^4 \qquad (26)$$

To obtain higher terms in this power series, the usual series substitution method may be used. The calculation is somewhat lengthy and therefore will not be reproduced here. The result is

$$\rho = 1 + \frac{1}{3}\nu\tau^3 + \frac{1}{12}\nu^2\tau^4 - \frac{\nu}{60}\tau^5 - \frac{23\nu^2}{360}\tau^6 + \cdots \qquad (27)$$

By using the result of Eq. (26) [21], the radial velocity is obtained by differentiation. Then Eq. (20) [21] gives the circumferential velocity. The end condition of Eq. (5) can be modified into the following more convenient form by multiplying it by $2r^2$:

$$0 = \left[\left(\rho \frac{d\rho}{d\tau}\right)^2 + \left(\rho^2 \frac{d\theta}{d\tau}\right)^2 - 2\rho \right]_1$$

By substituting the solution of Eq. (26) [27] into this condition, an equation for determining τ_1 is obtained:

$$0 = -1 + 2\nu\tau_1 + \nu^2\tau_1^2 - \frac{2}{3}\nu\tau_1^3 + \nu^2\tau_1^4 + \frac{\nu}{30}(1+26\nu^2)\tau_1^5 - \frac{\nu^2}{90}(4-13\nu^2)\tau_1^6 + \cdots \qquad (27)\ [28]$$

The mass ratio M_0/M_1 can be calculated in the same way as in the previous section and can be determined through the new parameter x defined as follows:

$$\frac{c}{\sqrt{g r_0}} \log (M_0/M_1) = \nu\tau_1 = x \qquad (28)\ [29]$$

Eq. (27) [28] then can be written as

$$0 = -1 + 2x + x^2 - \frac{2}{3}\frac{x^3}{\nu^2} + \frac{x^4}{\nu^2} + \frac{x^5}{30\nu^4} + \frac{13}{15}\frac{x^5}{\nu^2} - \frac{2}{45}\frac{x^6}{\nu^4} + \frac{13}{90}\frac{x^6}{\nu^2} + \cdots \qquad (29)\ [30]$$

Since the calculation is designed for large values of ν , the appropriate expansion of x should be a series in inverse powers of ν . Eq. (29) [30] suggests specifically

$$x(\nu) = x^{(0)} + \frac{x^{(1)}}{\nu^2} + \frac{x^{(2)}}{\nu^4} + \cdots \qquad (30)\ [31]$$

where $x^{(0)}$, $x^{(1)}$ and $x^{(2)}$ are constants independent of γ. By substituting Eq. (31) into Eq. (30) and equating equal powers of γ, the following set of equations results:

$$x^{(0)2} + 2x^{(0)} - 1 = 0 \tag{32}$$

$$x^{(1)} = \frac{1}{2(1+x^{(0)})}\left[\frac{2}{3}x^{(0)3} - x^{(0)4} - \frac{13}{15}x^{(0)5} - \frac{13}{90}x^{(0)6}\right] \tag{33}$$

$$x^{(2)} = \frac{1}{2(1+x^{(0)})}\left[-x^{(1)2} + 2x^{(0)2}x^{(1)} - 4x^{(0)3}x^{(1)} - \frac{1}{30}x^{(0)6} - \frac{13}{3}x^{(0)4}x^{(1)} + \frac{2}{45}x^{(0)6} - \frac{13}{15}x^{(0)5}x^{(1)}\right] \tag{34}$$

The explicit numerical solutions are then

$$x^{(0)} = \sqrt{2} - 1 = 0.41421 \tag{35}$$

$$x^{(1)} = 0.002349$$

$$x^{(2)} = -0.00004791$$

This completes the calculation of mass ratio for large values of the acceleration factor γ.

For the other extreme case of very small values of γ, it is to be expected that in Eq. (25), the acceleration will be very small, and the term $\rho^3 \frac{d^2\rho}{d\tau^2}$, will be very much smaller than ρ. Therefore a good approximation of Eq. (24) at small γ is

$$\frac{d}{d\tau}\rho^{\frac{1}{2}} = \gamma\rho \qquad \text{or} \qquad \frac{1}{2}\frac{d\rho}{\rho^{3/2}} = \gamma\, d\tau$$

The solution of this equation with the initial condition of $\rho = 1$ at $\tau = 0$ is

$$\rho = \frac{1}{(1-\gamma\tau)^2} \tag{36}$$

Therefore

$$\frac{d\rho}{d\tau} = \frac{2\nu}{(1-\nu\tau)^3}\,, \quad \frac{d^2\rho}{d\tau^2} = \frac{6\nu^2}{(1-\nu\tau)^4} \tag{37}$$

At $\tau = 0$, the radial velocity and the radial acceleration are thus not zero as required by the initial conditions of Eqs. (23) and (24). They are however very small, because ν is very small. Therefore the solution of Eq. (36) is a good approximation to the exact solution.

To the same approximation, Eq. (20) becomes

$$\rho \frac{d\theta}{d\tau} = \frac{1}{\rho^{1/2}} = (1-\nu\tau) \tag{38}$$

This means that, because of the extremely small acceleration, the centrifugal force per unit mass $r\left(\frac{d\theta}{dt}\right)^2$ practically balances the gravitational attraction at every instant. The end condition of Eq. (5) can then be written as

$$\frac{4\nu^2}{(1-x)^6} - (1-x)^2 = 0 \tag{39}$$

where x is again $\nu\tau_1$. The appropriate solution for x is then

$$x = 1 - (2\nu)^{1/4} \tag{40}$$

Since the mass ratio M_0/M_1, is related to x by Eq. (29), Eq. (40) actually gives the mass ratio for escaping the gravitational field with very small acceleration.

The parameter x is plotted against ν in Fig. 3, using both Eq. (31) with Eq. (35) and Eq. (40). When ν approaches zero, x approaches 1.

Insert for p. 11.

¶ When the acceleration factor ν is very large, the thrust force acts like an impulse. Since the thrust is in the circumferential direction, the rocket action only produces an increase in the circumferential velocity with practically no change in the radial position. The initial circumferential velocity is $\sqrt{g r_0}$, the required circumferential velocity for escape is $\sqrt{2 g r_0}$. Thus the increase of velocity produced by the rocket action is $(\sqrt{2}-1)\sqrt{g r_0}$. This explains the asymptotic value of x for very large ν.

When γ is very large, χ approaches $\sqrt{2} - 1$. As γ increases, χ and hence the mass ratio M_0/M_1, decrease monotonically. Therefore, same as the result for purely radial thrust, there is a strong influence of the magnitude of acceleration on the required mass ratio. However as far as decreasing the mass ratio is concerned, there is no appreciable advantage in using γ greater than 1/2.

→ Insert.

Discussion

By comparing Fig. 2 with Fig. 3, it is apparent that the radial thrust is much less efficient than the circumferential thrust for take-off from the satellite orbit. For large thrusts, the value of log (M_0/M_1) for radial thrust is more than twice that for circumferential thrust. Furthermore, in case of radial thrust, the ratio of thrust to the instantaneous mass, if maintained constant, must be larger than $g/8$. In case of circumferential thrust, no such limit exist. Therefore circumferential thrust is definitely preferred.

The quantity $c \log(M_0/M_1)$ is a measure of the performance or the capability of the vehicle. It has the dimension of a velocity and is actually the increase of velocity which the vehicle is capable of in a space without gravitation. This quantity is conveniently called the characteristic velocity of the vehicle. Let this be denoted by V. Then for the case of circumferential thrust, Eq. (29) gives

$$V = c \log(M_0/M_1) = \sqrt{g r_0}\, x = \frac{S}{\sqrt{2\lambda}}\, x \qquad (41)$$

where S is the "escape velocity" from the surface of the earth and λ is the ratio of the radii of the satellite orbit and the earth. S is equal to 11.2 km/sec. Fig. 3 then shows that by decreasing the acceleration from

1/2 to 1/3000 g, χ , hence the required characteristic velocity V , will increase by a factor of two. This is a very important point for the designers of space ships.

REFERENCES

1. "Interplanetary Travel between Satellite Orbits" by L. Spitzer, Jr. Journal of the American Rocket Society, Vol. 22, pp. 92-96 (1952).

2. "Interorbital Transport Techniques" by H. Preston - Thomas. Journal of the British Interplanetary Society, Vol. 11, pp. 173-193 (1952).

3. "Man on the Moon, the Journey" by W. von Braun. Collier's, Oct. 18, 1952, p. 52.

Double spacing

Single spacing

Single spacing

Figure Captions

Fig. 1 Take-Off from the Satellite Orbit with Thrust in the Plane of Satellite Orbit

Double spacing

Fig. 2 Mass Ratio Factor $\frac{c}{\sqrt{g r_0}} \log (M_0/M_1)$ against Acceleration Factor μ for Radial Thrust. c, Effective Exhaust Velocity; g, Gravity at the Satellite Orbit of Radius r_0; M_0, Initial Mass; M_1, Final Mass; μ, the Ratio of Instantaneous Thrust per unit Mass and g.

Fig. 3 Mass Ratio Factor $\frac{c}{\sqrt{g r_0}} \log (M_0/M_1)$ against Acceleration Factor ν for Circumferential Thrust. c, Effective Exhaust Velocity; g, Gravity at the Satellite Orbit of Radius r_0; M_0, Initial Mass; M_1, Final Mass; ν, the Ratio of Instantaneous Thrust per unit Mass and g.

AMERICAN ROCKET SOCIETY, INC.



29 WEST 39TH STREET
NEW YORK 18, N. Y.

Department Aeronautical Engineering
Princeton University
Princeton New Jersey

December 4, 1952

Prof. H. S. Tsien
California Institute of Technology
1201 East California Street
Pasadena 3, California

Dear Tsien:

I have read your paper on "Take-off from Satellite Orbit". I found no reason to suggest any changes and I see no need to seek additional reviews, so I have released it to the New York Office for publication. It will probably appear in the March-April issue of the Journal. It is a rather interesting contribution.

Thank you for your evaluation of the Feldman paper. We are going ahead to publish it.

With best regards,

Sincerely yours,

Martin Summerfield

Martin Summerfield
Editor-in-Chief

MS:edc

Section 7

Circumferential Acceleration

1

<u>Circumferential Acceleration</u>

$$\frac{d}{dt}\left(r^2 \frac{d\phi}{dt}\right) = \Theta r$$

$$\frac{d^2r}{dt^2} = r\left(\frac{d\phi}{dt}\right)^2 - g\frac{r_0^2}{r^2}$$

$$\left(r^3 \frac{d^2r}{dt^2} + g r_0^2 r\right)^{\frac{1}{2}} = r^2 \frac{d\phi}{dt}$$

$$\boxed{\frac{d}{dt}\left(r^3 \frac{d^2r}{dt^2} + g r_0^2 r\right)^{\frac{1}{2}} = \Theta r}$$

$$r = r_0\left[1 + a_3\left(\frac{g}{r_0}\right)^{3/2} t^3 + a_4\left(\frac{g}{r_0}\right)^2 t^4 + a_5\left(\frac{g}{r_0}\right)^{5/2} t^5 + a_6\left(\frac{g}{r_0}\right)^3 t^6 + \cdots\right]$$

$$\frac{d^2r}{dt^2} = g\left[6a_3\left(\frac{g}{r_0}\right)^{1/2} t + 12a_4\left(\frac{g}{r_0}\right) t^2 + 20a_5\left(\frac{g}{r_0}\right)^{3/2} t^3 + 30a_6\left(\frac{g}{r_0}\right)^2 t^4 + \cdots\right]$$

$$r^3 = r_0^3\left[1 + 3a_3\left(\frac{g}{r_0}\right)^{3/2} t^3 + \cdots\right]$$

$$r^3\frac{d^2r}{dt^2} = g r_0^3\left[6a_3\left(\frac{g}{r_0}\right)^{1/2} t + 12a_4\left(\frac{g}{r_0}\right) t^2 + 20a_5\left(\frac{g}{r_0}\right)^{3/2} t^3 + (30a_6 + 18a_3^2)\left(\frac{g}{r_0}\right)^2 t^4 + \cdots\right]$$

$$g r_0^2 r = g r_0^3\left[1 \qquad + a_3\left(\frac{g}{r_0}\right)^{3/2} t^3 + a_4 \qquad \left(\frac{g}{r_0}\right)^2 t^4 + \cdots\right]$$

$$r^3\frac{d^2r}{dt^2} + g r_0^2 r = g r_0^3\left[1 + 6a_3\left(\frac{g}{r_0}\right)^{1/2} t + 12a_4\left(\frac{g}{r_0}\right) t^2 + (20a_5 + a_3)\left(\frac{g}{r_0}\right)^{3/2} t^3 + (a_4 + 30a_6 + 18a_3^2)\left(\frac{g}{r_0}\right)^2 t^4 \cdots\right]$$

$$\left(r^3\frac{d^2r}{dt^2} + g r_0^2 r\right)^{\frac{1}{2}} = r_0\sqrt{g\, r_0}\left[1 + 3a_3\left(\frac{g}{r_0}\right)^{1/2} t + 6a_4\left(\frac{g}{r_0}\right) t^2 + \left(10a_5 + \frac{a_3}{2}\right)\left(\frac{g}{r_0}\right)^{3/2} t^3 + \left(\frac{a_4}{2} + 15a_6 + 9a_3^2\right)\left(\frac{g}{r_0}\right)^2 t^4 + \cdots\right.$$

$$- \frac{1}{8} 36a_3^2\left(\frac{g}{r_0}\right) t^2 - \frac{1}{8} 144 a_3 a_4\left(\frac{g}{r_0}\right)^{3/2} t^3 - \frac{1}{8}\left[144a_4^2 + 12a_3(20a_5 + a_3)\right]\left(\frac{g}{r_0}\right)^2 t^4 -$$

$$+ \frac{8}{16} 27 a_3^3\left(\frac{g}{r_0}\right)^{3/2} t^3 + \frac{8}{16} 27a_3^2 \cdot 6a_4 \left(\frac{g}{r_0}\right)^2 t^4 \cdots$$

$$\left. - \frac{5\times16}{4\times32} 81\, a_3^4 \left(\frac{g}{r_0}\right)^2 t^4 \cdots\right]$$

2

Let $\theta = ng$

$$n\left[1 + \cdots + a_3\left(\frac{g}{r_0}\right)^{3/2} t^3 + \cdots\right]$$

$$= 3a_3 + 2\left[6a_4 - \frac{9}{2}a_3^2\right]\left(\frac{g}{r_0}\right)^{1/2} t + 3\left[10a_5 + \frac{a_3}{2} - 18a_3a_4 + \frac{27}{2}a_3^3\right]\left(\frac{g}{r_0}\right) t^2$$

$$+ 4\left[\frac{a_4}{2} + 15a_6 + 9a_3^2 - 18a_4^2 - \frac{3}{2}a_3(20a_5 + a_3) + 81 \cdot a_3^2 a_4 - \frac{5 \times 81}{8} a_3^4\right]\left(\frac{g}{r_0}\right)^{3/2} t^3 + \cdots$$

Thus $n = 3a_3$, $\qquad \underline{a_3 = \frac{n}{3}}$

$6a_4 = \frac{9}{2}a_3^2 \qquad \underline{a_4 = \frac{n^2}{12}}$

$$a_5 = -\frac{a_3}{20} + \frac{18}{10}a_3a_4 - \frac{27}{20}a_3^3 = -\frac{n}{60} + n^3\frac{18}{10}\frac{1}{3}\frac{1}{12} - n^3\frac{27}{20}\frac{1}{27}$$

$$\underline{a_5 = -\frac{n}{60}}$$

$$\frac{n^2}{12} = \frac{n^2}{24} + 15a_6 + n^2 - 18\frac{n^4}{144} - \frac{n}{2}\left(-\frac{n}{3} + \frac{n}{3}\right) + 9n^2\frac{n^2}{12} - \frac{5n^4}{8}$$

$15a_6 = -\frac{23}{24}n^2 \qquad \underline{a_6 = -\frac{23n^2}{15 \times 24}}$

$$\boxed{r = r_0\left[1 + \frac{n}{3}\tau^3 + \frac{n^2}{12}\tau^4 - \frac{n}{60}\tau^5 - \frac{23n^2}{15 \times 24}\tau^6 + \cdots\right], \quad \tau = \sqrt{\frac{g}{r_0}}\,t}$$

$$\frac{d}{dt} = \sqrt{\frac{g}{r_0}}\frac{d}{d\tau}$$

$$\boxed{u = \frac{dr}{dt} = \sqrt{gr_0}\left[n\tau^2 + \frac{n^2}{3}\tau^3 - \frac{n}{12}\tau^4 - \frac{23}{60}n^2\tau^5 + \cdots\right]}$$

$$u^2 = gr_0\left[n^2\tau^4 + \frac{2}{3}n^3\tau^5 + \left(\frac{n^4}{9} - \frac{n^2}{6}\right)\tau^6 + \cdots\right]$$

$$r^2\left(\frac{d\theta}{dt}\right) = r_0\sqrt{gr_0} + nr_0\sqrt{gr_0}\left[\tau + \frac{n}{12}\tau^4 + \frac{n^2}{60}\tau^5 - \frac{n}{360}\tau^6 + \cdots\right]$$

$$\boxed{r^2\left(\frac{d\theta}{dt}\right) = r_0\sqrt{gr_0}\left[1 + n\tau + \frac{n^2}{12}\tau^4 + \frac{n^3}{60}\tau^5 - \frac{n^2}{360}\tau^6 + \cdots\right]}$$

$$\left(r^2\frac{d\theta}{dt}\right)^2 = r_0^3 g\Big[1 + n\tau + \quad + \quad + \frac{n^2}{12}\tau^4 + \frac{n^3}{60}\tau^5 - \frac{n^2}{360}\tau^6 + \cdots$$
$$+ n\tau + n^2\tau^2 \qquad + \frac{n^3}{12}\tau^5 + \frac{n^4}{60}\tau^6 + \cdots$$
$$+ \frac{n^2}{12}\tau^4 + \frac{n^3}{12}\tau^5 +$$
$$+ \frac{n^3}{60}\tau^5 + \frac{n^4}{60}\tau^6 + \cdots$$
$$- \frac{n^2}{360}\tau^6 + \cdots$$

$$= r_0^3 g\left[1 + 2n\tau + n^2\tau^2 + \frac{n^2}{6}\tau^4 + \frac{n^3}{5}\tau^5 - \frac{n^2}{180}(1 - 6n^2)\tau^6 + \cdots\right]$$

$$(ru)^2 = r_0^3 g\left[1 + \frac{2}{3}n\tau^3 + \cdots\right]\left[n^2\tau^4 + \frac{2}{3}n^3\tau^5 - \frac{n^2}{6}\left(1 - \frac{2}{3}n^2\right)\tau^6 + \cdots\right]$$

$$= r_0^3 g\left[n^2\tau^4 + \frac{2}{3}n^3\tau^5 - \frac{n^2}{6}\left(1 - \frac{2}{3}n^2\right)\tau^6 + \cdots\right]$$

$$r^2\left[u^2 + v^2\right] = r_0^3 g\left[1 + 2n\tau + n^2\tau^2 + \frac{7}{6}n^2\tau^4 + \frac{13}{15}n^3\tau^5 + \left\{-\frac{31}{180}n^2 + \frac{13}{90}n^4\right\}\tau^6 + \cdots\right]$$

$$-2gr_0^2 r = r_0^3 g\left[-2 - \frac{2}{3}n\tau^3 - \frac{n^2}{6}\tau^4 + \frac{n}{30}\tau^5 + \frac{23}{15\times 12}n^2\tau^6 \cdots\right]$$

τ_1 is then given by

$$0 = -1 + 2n\tau_1 + n^2\tau_1^2 - \frac{2}{3}n\tau_1^3 + n^2\tau_1^4 + \frac{n}{30}(1 + 26n^2)\tau_1^5$$
$$+ \left\{-\frac{8}{180}n^2 + \frac{13}{90}n^4\right\}\tau_1^6 + \cdots$$

$$n\tau_1 = x$$

$$1 = 2x + x^2 - \frac{2}{3}\frac{x^3}{n^2} + \frac{x^4}{n^2} + \frac{x^5}{30n^4} + \frac{13}{15}\frac{x^5}{n^2} - \frac{1}{180}\frac{x^6}{n^4} + \frac{13}{90}\frac{x^6}{n^2} \cdots$$

$$x = x^{(0)} + \frac{1}{n^2}x^{(1)} + \frac{1}{n^4}x^{(2)} + \cdots$$

$$x^2 = x^{(0)^2} + \frac{2}{n^2}x^{(0)}x^{(1)} + \frac{1}{n^4}\left(x^{(1)^2} + 2x^{(0)}x^{(2)}\right) + \cdots$$

$$x^3 = x^{(0)^3} + \frac{3}{n^2}x^{(0)^2}x^{(1)} + \cdots$$

$$x^4 = x^{(0)^4} + \frac{4}{n^2}x^{(0)^3}x^{(1)} + \cdots$$

$$x^5 = x^{(0)^5} + \frac{5}{n^2}x^{(0)^4}x^{(1)} + \cdots$$

$$x^6 = x^{(0)^6} + \frac{6}{n^2}x^{(0)^5}x^{(1)} + \cdots$$

$$1 = 2x^{(0)} + x^{(0)^2} + \frac{1}{n^2}\left\{2x^{(1)} + 2x^{(0)}x^{(1)} - \frac{2}{3}x^{(0)^3} + x^{(0)^4} + \frac{13}{15}x^{(0)^5} + \frac{13}{90}x^{(0)^6}\right\}$$

$$+ \frac{1}{n^4}\Big\{2x^{(2)} + x^{(1)^2} + 2x^{(0)}x^{(2)} - \frac{2}{3}3x^{(0)^2}x^{(1)} + 4x^{(0)^3}x^{(1)}$$

$$+ \frac{1}{30}x^{(0)^5} + \frac{13}{15}5x^{(0)^4}x^{(1)} - \frac{1}{180}x^{(0)^6} + \frac{13}{90}6x^{(0)^5}x^{(1)}\Big\}$$

$$\boxed{x^{(0)} = \sqrt{2} - 1}$$

$$Mng = -c\frac{dM}{dt}$$

$$\log\frac{M_0}{M_1} = \frac{1}{c}ngt_1 = \frac{\sqrt{gr_0}}{c}n\tau_1$$

$$\boxed{\log\frac{M_0}{M_1} = \frac{\sqrt{gr_0}}{c}x}$$

(5)

$$2(1+x^{(0)})x^{(1)} = \frac{2}{3}x^{(0)^3} - x^{(0)^4} - \frac{13}{15}x^{(0)^5} - \frac{13}{90}x^{(0)^6}$$

-3+4

$$\boxed{x^{(1)} = \frac{1}{2\sqrt{2}}\left\{\frac{2}{3}x^{(0)^3} - x^{(0)^4} - \frac{13}{15}x^{(0)^5} - \frac{13}{90}x^{(0)^6}\right\}}$$

$$\boxed{x^{(2)} = \frac{1}{2\sqrt{2}}\left\{-x^{(1)^2} + 2x^{(0)^2}x^{(1)} - 4x^{(0)^3}x^{(1)} - \frac{1}{30}x^{(0)^6} - \frac{13}{3}x^{(0)^4}x^{(1)} + \frac{8}{180}x^{(0)^6} - \frac{13}{15}x^{(0)^5}x^{(1)}\right\}}$$

$$x^{(0)} = \sqrt{2}-1 = 0.41421 \quad , \quad \sqrt{2} = 1.41421$$

$$\frac{1}{\sqrt{2}-1} = \sqrt{2}+1$$

$$-\frac{13}{15}x^{(0)^5} - \frac{13}{90}x^{(0)^6} = -\frac{13}{15}x^{(0)^5}\left(1+\frac{1}{6}x^{(0)}\right) = -0.92650\,x^{(0)^5} = -0.011297$$

$$x^{(0)^2} = 0.171570 \quad , \quad x^{(0)^3} = 0.071066$$

$$x^{(0)^4} = 0.029436 \quad , \quad x^{(0)^5} = 0.012193$$

$$x^{(1)} = \frac{1}{2.82842}(0.006644) = 0.002349$$

0.0003244

$$x^{(2)} = \frac{1}{2.82842}\left\{-0.000005518 + 0.0008060 \times 0.17158 - \frac{13}{3} \times 0.029436 \times 0.002349 \times 1.08284 + \frac{1}{90} \times 0.071066^2\right\}$$

0.0000561

$$= -0.00004791$$

n	x
∞	0.41421
1	0.41651
$1/\sqrt{10}$	0.43391

$$x = 0.41421 + \frac{0.002349}{n^2} - \frac{0.00004791}{n^4} \cdots$$

$$= 0.41421\left(1 + \frac{0.005671}{n^2} - \frac{0.0001157}{n^4} - \cdots\right)$$

For the case $n \ll 1$, then

$$r^3 \frac{d^2r}{dt^2} \ll g r_0^2 r$$

So as a first approximation,

$$r_0 \sqrt{g} \frac{dr^{1/2}}{dt} = n g r$$

$$\frac{1}{2} r_0 \sqrt{g} \frac{dr}{r^{3/2}} = n g dt$$

$$r_0 \sqrt{g} \left\{ \frac{1}{r_0^{1/2}} - \frac{1}{r^{1/2}} \right\} = n g t$$

Then $\quad \frac{1}{r_0^{1/2}} - \frac{1}{r^{1/2}} = n \frac{1}{r_0^{1/2}} \sqrt{\frac{g}{r_0}}\, t$

$$\frac{1}{r_0^{1/2}} \left(1 - n \sqrt{\frac{g}{r_0}}\, t \right) = \frac{1}{r^{1/2}}$$

$$r = r_0 \frac{1}{\left(1 - n\sqrt{\frac{g}{r_0}}\, t\right)^2}$$

$$\frac{dr}{dt} = \sqrt{g r_0} \frac{2n}{\left(1 - n\sqrt{\frac{g}{r_0}}\, t\right)^3}$$

$$r^2 \frac{d\theta}{dt} = r_0^2 \sqrt{\frac{g}{r_0}} + n g \int_0^t r_0 \frac{dt}{\left(1 - n\sqrt{\frac{g}{r_0}}\, t\right)^2}$$

$$= r_0 \sqrt{g r_0} \left\{ 1 + \int_0^{n\sqrt{\frac{g}{r_0}}\, t} \frac{d\xi}{(1-\xi)^2} \right\}$$

$$= r_0 \sqrt{g r_0} \frac{1}{1 - n\sqrt{\frac{g}{r_0}}\, t}$$

$$r \frac{d\theta}{dt} = \sqrt{g r_0} \left(1 - n\sqrt{\frac{g}{r_0}}\, t\right)$$

At $t = t_1$ $\qquad n\sqrt{\frac{g}{r_0}}\,t_1 = n\tau_1 = x$ $\qquad$ 7

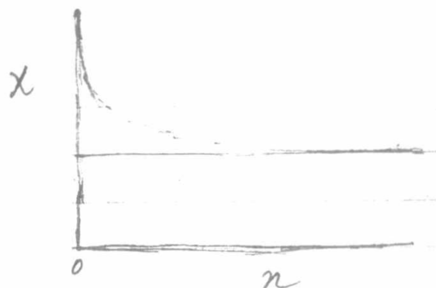
$$0 = \left[\left(\frac{dr}{dt}\right)^2 + \left(r\frac{d\theta}{dt}\right)^2\right] - 2\frac{g r_0^2}{r}$$

$$0 = \frac{4n^2}{(1-x)^6} + (1-x)^2 - 2(1-x)^2$$

$$4n^2 = (1-x)^8$$

$$1 - x = 2^{1/4} n^{1/4}$$

$$\boxed{x = 1 - (2n)^{1/4}}$$



$$r^3\frac{d^2r}{dt^2} = r_0^4 \frac{1}{(1-\tau)^6}\; 6\, \frac{n^2 \frac{g}{r_0}}{(1-\tau)^4} \quad , \quad \frac{d^2r}{dt^2} = g\,\frac{n^2}{(1-\tau)^4}$$

$$g r_0^2 r = g r_0^3 \frac{1}{(1-\tau)^2}$$

$$r^3\frac{d^2r}{dt^2} \Big/ g r_0^2 r = \frac{6n^2}{(1-\tau)^8} \longrightarrow \frac{3}{2}$$

Circumferential Acceleration

$$\frac{d}{dt}\left(r^2 \frac{d\theta}{dt}\right) = \Theta r$$

$$\frac{d^2 r}{dt^2} = r\left(\frac{d\theta}{dt}\right)^2 - g\frac{r_0^2}{r}$$

$$\left(r^3 \frac{d^2 r}{dt^2} + g r_0^2 r\right)^{\frac{1}{2}} = r^2 \frac{d\theta}{dt}$$

$$\boxed{\frac{d}{dt}\left(r^3 \frac{d^2 r}{dt^2} + g r_0^2 r\right)^{\frac{1}{2}} = \Theta r}$$

$$r = r_0\left[1 + a_3\left(\frac{g}{r_0}\right)^{3/2} t^3 + a_4\left(\frac{g}{r_0}\right)^2 t^4 + a_5\left(\frac{g}{r_0}\right)^{5/2} t^5 + \cdots\right]$$

$$\frac{d^2 r}{dt^2} = r_0\left[6a_3\left(\frac{g}{r_0}\right)^{3/2} t + 12a_4\left(\frac{g}{r_0}\right)^2 t^2 + 20a_5\left(\frac{g}{r_0}\right)^{5/2} t^3 + \cdots\right]$$

$$r^3 = r_0^3\left[1 + \cdots\right]$$

$$r^3 \frac{d^2 r}{dt^2} = r_0^3 g\left[6a_3\left(\frac{g}{r_0}\right)^{\frac{1}{2}} t + 12a_4\left(\frac{g}{r_0}\right) t^2 + 20a_5\left(\frac{g}{r_0}\right)^{3/2} t^3 + \cdots\right]$$

$$g r_0^2 r = r_0^3 g\left[1 + a_3\left(\frac{g}{r_0}\right)^{3/2} t^3 + \cdots\right]$$

$$r^3 \frac{d^2 r}{dt^2} + g r_0^2 r = r_0^3 g\left[1 + 6a_3\left(\frac{g}{r_0}\right)^{\frac{1}{2}} t + 12a_4\left(\frac{g}{r_0}\right) t^2 + (20a_5 + a_3)\left(\frac{g}{r_0}\right)^{3/2} t^3 + \cdots\right]$$

$$\left(r^3 \frac{d^2 r}{dt^2} + g r_0^2 r\right)^{\frac{1}{2}} = r_0^{3/2}\sqrt{g}\left[1 + 3a_3\left(\frac{g}{r_0}\right)^{\frac{1}{2}} t + 6a_4\left(\frac{g}{r_0}\right) t^2 + \left(10a_5 + \frac{a_3}{2}\right)\left(\frac{g}{r_0}\right)^{3/2} t^3 + \cdots\right.$$
$$- \frac{1}{8} 36 a_3^2 \left(\frac{g}{r_0}\right) t^2 - \frac{1}{8} 144 a_3 a_4 \left(\frac{g}{r_0}\right)^{3/2} t^3 + \cdots$$
$$\left. + \frac{1}{16} 6^3 a_3^3 \left(\frac{g}{r_0}\right)^{3/2} t^3 + \cdots\right]$$

$\Theta = ng$

$$n[1 + \cdots] = 3a_3 + 2\left(6a_4 - \frac{9}{2}a_3^2\right)\left(\frac{g}{r_0}\right)^{1/2} t$$

$$+ 3\left[10a_5 + \frac{a_3}{2} - 18a_3a_4 + \frac{27}{2}a_3^3\right]\left(\frac{g}{r_0}\right)t^2 +$$

$$3a_3 = n, \qquad a_3 = n/3$$

$$a_4 = \frac{9}{12}a_3^2 = \frac{n^2}{12}$$

$$a_5 = -\frac{a_3}{20} + \frac{9}{5}a_3a_4 - \frac{27}{20}a_3^3$$

$$= -\frac{n}{60} + \frac{9}{5}\frac{n^3}{36} - \frac{27}{20}\frac{n^3}{27} = -\frac{n}{60}$$

$$\boxed{\frac{r}{r_0} - 1 = \frac{n}{3}\left(\frac{g}{r_0}\right)^{3/2} t^3 + \frac{n^2}{12}\left(\frac{g}{r_0}\right)^2 t^4 - \frac{n}{60}\left(\frac{g}{r_0}\right)^{5/2} t^5 + \cdots}$$

$$\boxed{u = \frac{dr}{dt} = \sqrt{gr_0}\left[n\left(\frac{g}{r_0}\right)t^2 + \frac{n^2}{3}\left(\frac{g}{r_0}\right)^{3/2} t^3 - \frac{n}{12}\left(\frac{g}{r_0}\right)^2 t^4 \cdots\right]}$$

$$-r_0^2\left(\frac{d\theta}{dt}\right)_0 + r^2\frac{d\theta}{dt} = ng\int_0^t r\,dt = ngr_0\left[t + \frac{1}{4}a_3\left(\frac{g}{r_0}\right)^{3/2} t^4 + \frac{1}{5}a_4\left(\frac{g}{r_0}\right)^2 t^5\right.$$

$$\left. + \frac{1}{6}a_5\left(\frac{g}{r_0}\right)^{2.5} t^6 + \cdots\right]$$

$$r^2\frac{d\theta}{dt} = r_0^2\sqrt{\frac{g}{r_0}}\left[1 + n\left(\frac{g}{r_0}\right)^{1/2} t + \frac{n}{12}\left(\frac{g}{r_0}\right)^2 t^4 + \frac{n^2}{60}\left(\frac{g}{r_0}\right)^{5/2} t^5 - \frac{n}{360}\left(\frac{g}{r_0}\right)^3 t^6 + \cdots\right]$$

$$r = r_0\left[1 + \frac{n}{3}\left(\frac{g}{r_0}\right)^{3/2} t^3 + \frac{n^2}{12}\left(\frac{g}{r_0}\right)^2 t^4 - \frac{n}{60}\left(\frac{g}{r_0}\right)^{5/2} t^5 + \cdots\right]$$

$$r\frac{d\theta}{dt} = \sqrt{gr_0}\left[1 + n\left(\frac{g}{r_0}\right)^{1/2} t - \frac{n}{3}\left(\frac{g}{r_0}\right)^{3/2} t^3 + \frac{n(4-n)}{12}\left(\frac{g}{r_0}\right)^2 t^4 \cdots\right]$$

2) Case $R = 0$

$$\frac{d}{dt}\left(r^2 \frac{d\theta}{dt}\right) = \Theta r$$

$$r^2 \frac{d\theta}{dt} = r_0^2 \left(\frac{d\theta}{dt}\right)_0 + \int_0^t \Theta r \, dt$$

$$\frac{d^2 r}{dt^2} = \frac{1}{r^3}\left\{ r_0^2 \left(\frac{d\theta}{dt}\right)_0 + \int_0^t \Theta r \, dt \right\}^2 - g \frac{r_0^2}{r^2}$$

But $\quad r_0 \left(\frac{d\theta}{dt}\right)_0^2 = g,$

$$\frac{d^2 r}{dt^2} = g \frac{r_0^2}{r^2}\left(\frac{r_0}{r} - 1\right) + 2 \frac{r_0^2 \left(\frac{d\theta}{dt}\right)_0}{r^3} \int_0^t \Theta r \, dt + \frac{1}{r^3}\left[\int_0^t \Theta r \, dt\right]^2$$

So $\quad \frac{d^2 r}{dt^2} = 0 \quad$ at $\quad t = 0, \quad r = r_0.$

Thus

$$(r - r_0) \sim t^3$$

$$\frac{dr}{dt} \sim t^2 \sim (r - r_0)^{2/3}$$

So let

$$\int_0^t \Theta r \, dt = ng \frac{1}{\sqrt{g r_0}} \int_{r_0}^{r} \frac{r \, dr}{\left(\frac{r}{r_0} - 1\right)^{2/3}}$$

$$= n \sqrt{\frac{g}{r_0}} \, r_0^2 \int_1^{r/r_0} \frac{\eta \, d\eta}{(\eta - 1)^{2/3}}$$

$$= n \sqrt{\frac{g}{r_0}} \, r_0^2 \left[\frac{3}{4}(\eta - 1)^{4/3} + 3(\eta - 1)^{1/3}\right]_1^{r/r_0}$$

$$= n \sqrt{\frac{g}{r_0}} \, r_0^2 \left[\frac{3}{4}\left(\frac{r}{r_0} - 1\right)^{4/3} + 3\left(\frac{r}{r_0} - 1\right)^{1/3}\right]$$

$$r_0^2 \left(\frac{d\theta}{dt}\right)_0 = r_0^2 \sqrt{\frac{g}{r_0}}$$

$$\frac{1}{2}\frac{du^2}{dr} = g\frac{r_0^2}{r^2}\left(\frac{r_0}{r}-1\right) + 2ng\left(\frac{r_0}{r}\right)^3\left[\frac{3}{4}\left(\frac{r}{r_0}-1\right)^{4/3} + 3\left(\frac{r}{r_0}-1\right)^{1/3}\right]$$

$$+ n^2 g\left(\frac{r_0}{r}\right)^3\left[\frac{3}{4}\left(\frac{r}{r_0}-1\right)^{4/3} + 3\left(\frac{r}{r_0}-1\right)^{1/3}\right]^2$$

$$= g\left[\frac{r_0^3}{r^3} - \frac{r_0^2}{r^2} + \frac{3n}{2}\left(\frac{r_0}{r}\right)^3\left(\frac{r}{r_0}-1\right)^{4/3} + 6n\left(\frac{r_0}{r}\right)^3\left(\frac{r}{r_0}-1\right)^{1/3}\right.$$

$$\left. + n^2\frac{9}{16}\left(\frac{r_0}{r}\right)^3\left(\frac{r}{r_0}-1\right)^{8/3} + n^2\frac{9}{2}\left(\frac{r_0}{r}\right)^3\left(\frac{r}{r_0}-1\right)^{5/3} + n^2 9\left(\frac{r_0}{r}\right)^3\left(\frac{r}{r_0}-1\right)^{2/3}\right]$$

$$\boxed{\frac{1}{2}u^2 = g r_0\int_1^{r/r_0}\left[\frac{1}{\eta^3} - \frac{1}{\eta^2} + \frac{3n}{2}\frac{1}{\eta^3}(\eta-1)^{4/3} + 6n\frac{1}{\eta^3}(\eta-1)^{1/3} + \frac{9}{16}n^2\frac{1}{\eta^3}(\eta-1)^{8/3} + \frac{9}{2}n^2\frac{1}{\eta^3}(\eta-1)^{5/3} + 9n^2\frac{1}{\eta^3}(\eta-1)^{2/3}\right]d\eta}$$

$$\int_1^{r/r_0}\frac{d\eta}{\eta^3}(\eta-1)^{1/3} = \int_1^{r/r_0}\frac{d\eta}{\eta^{8/3}}\left(1-\frac{1}{\eta}\right)^{1/3}$$

$$\frac{1}{\eta} = \zeta \qquad -\frac{1}{\eta^2}d\eta = d\zeta$$

$$= \int_{r_0/r}^{1}\zeta^{2/3}(1-\zeta)^{1/3}d\zeta = \int_0^1\zeta^{2/3}(1-\zeta)^{1/3}d\zeta - \int_0^{r_0/r}\zeta^{2/3}(1-\zeta)^{1/3}d\zeta$$

$$= \int_0^1\zeta^{5/3-1}(1-\zeta)^{4/3-1}dt - \int_0^{r_0/r}\zeta^{2/3}(1-\zeta)^{1/3}d\zeta$$

$$= \frac{\Gamma\left(\frac{5}{3}\right)\Gamma\left(\frac{4}{3}\right)}{2} - \int_0^{r_0/r}\zeta^{2/3}(1-\zeta)^{1/3}d\zeta$$

$$= \frac{2}{3}\frac{1}{3}\frac{1}{2}\Gamma\left(1-\frac{1}{3}\right)\Gamma\left(\frac{1}{3}\right) - \int_0^{r_0/r}\zeta^{2/3}(1-\zeta)^{1/3}d\zeta$$

9

$$\int_1^{r/r_0} \frac{d\eta}{\eta^3}(\eta-1)^{1/3} = \frac{\pi}{9\sin\frac{\pi}{3}} - \int_0^{r_0/r} \zeta^{2/3}(1-\zeta)^{1/3} d\zeta$$

$$\int_1^{r/r_0} \frac{d\eta}{\eta^3}(\eta-1)^{4/3} = \int_{r_0/r}^{1} \zeta^{-1/3}(1-\zeta)^{4/3} d\zeta$$

$$= \int_0^{1} \zeta^{2/3-1}(1-\zeta)^{7/3-1} d\zeta - \int_0^{r_0/r} \zeta^{-1/3}(1-\zeta)^{4/3} d\zeta$$

$$\int_1^{r/r_0} \frac{d\eta}{\eta^3}(\eta-1)^{4/3} = \frac{2}{9}\frac{\pi}{\sin\frac{\pi}{3}} - \int_0^{r_0/r} \zeta^{-1/3}(1-\zeta)^{1/3} d\zeta + \int_0^{r_0/r} \zeta^{2/3}(1-\zeta)^{1/3} d\zeta$$

$$\int_1^{r/r_0} \frac{d\eta}{\eta^3}(\eta-1)^{2/3} = \int_{r_0/r}^{1} \zeta^{1/3}(1-\zeta)^{2/3} d\zeta \qquad (4/3-1,\ 5/3-1)$$

$$\int_1^{r/r_0} \frac{d\eta}{\eta^3}(\eta-1)^{2/3} = \frac{\pi}{9\sin\frac{\pi}{3}} - \int_0^{r_0/r} \zeta^{1/3}(1-\zeta)^{2/3} d\zeta$$

$$\int_1^{r/r_0} \frac{d\eta}{\eta^3}(\eta-1)^{5/3} = \int_{r_0/r}^{1} \zeta^{-2/3}(1-\zeta)^{5/3} d\zeta \qquad (1/3-1,\ 8/3-1)$$

$$\int_1^{r/r_0} \frac{d\eta}{\eta^3}(\eta-1)^{5/3} = \frac{5}{9}\frac{\pi}{\sin\frac{\pi}{3}} - \int_0^{r_0/r} \zeta^{-2/3}(1-\zeta)^{2/3} d\zeta + \int_0^{r_0/r} \zeta^{1/3}(1-\zeta)^{2/3} d\zeta$$

$$\int_1^{r/r_0} \frac{d\eta}{\eta^3}(\eta-1)^{8/3} = \int_1^{r/r_0} \eta^{-\frac{1}{3}} d\eta \left(1-\frac{1}{\eta}\right)^{8/3}$$

$$= \left[\frac{3}{2}\eta^{2/3}\left(1-\frac{1}{\eta}\right)^{8/3}\right]_1^{r/r_0} - \frac{3}{2}\frac{8}{3}\int_1^{r/r_0} \eta^{2/3}\left(1-\frac{1}{\eta}\right)^{5/3} d\left(-\frac{1}{\eta}\right)$$

$$= \frac{3}{2}\left(\frac{r}{r_0}\right)^{2/3}\left(1-\frac{r_0}{r}\right)^{8/3} - 4\int_{r_0/r}^{1} \zeta^{-2/3}(1-\zeta)^{5/3} d\zeta$$

$$\boxed{\int_1^{r/r_0} \frac{d\eta}{\eta^3}(\eta-1)^{8/3} = \frac{3}{2}\left(\frac{r}{r_0}\right)^{2/3}\left(1-\frac{r_0}{r}\right)^{8/3} - \frac{20}{9}\frac{\pi}{\sin\frac{\pi}{3}} + 4\int_0^{r_0/r} \zeta^{-2/3}(1-\zeta)^{5/3} d\zeta}$$

$$\frac{\pi}{\sin\frac{\pi}{3}} = \frac{2\pi}{\sqrt{3}}$$

$$\frac{1}{2}u^2\frac{1}{g r_0} = \frac{1}{2}\left(1-\frac{r_0^2}{r^2}\right) - \left(1-\frac{r_0}{r}\right) + \frac{3n}{2}\left[\frac{4\pi}{9\sqrt{3}} - f_1\left(\frac{r_0}{r}\right)\right]$$

$$+ 6n\left[\frac{2\pi}{9\sqrt{3}} - f_2\left(\frac{r_0}{r}\right)\right]$$

$$+ \frac{9}{16}n^2\left[\frac{3}{2}\left(\frac{r}{r_0}\right)^{2/3}\left(1-\frac{r_0}{r}\right)^{8/3} - \frac{40\pi}{9\sqrt{3}} + 4f_3\left(\frac{r_0}{r}\right)\right]$$

$$+ \frac{9}{2}n^2\left[\frac{10\pi}{9\sqrt{3}} - f_3\left(\frac{r_0}{r}\right)\right] + 9n^2\left[\frac{2\pi}{9\sqrt{3}} - f_4\left(\frac{r_0}{r}\right)\right]$$

$$\boxed{\begin{aligned} f_1\left(\frac{r_0}{r}\right) &= \int_0^{r_0/r} \zeta^{-1/3}(1-\zeta)^{4/3} d\zeta \\ f_2\left(\frac{r_0}{r}\right) &= \int_0^{r_0/r} \zeta^{2/3}(1-\zeta)^{1/3} d\zeta \\ f_3\left(\frac{r_0}{r}\right) &= \int_0^{r_0/r} \zeta^{-2/3}(1-\zeta)^{5/3} d\zeta \\ f_4\left(\frac{r_0}{r}\right) &= \int_0^{r_0/r} \zeta^{1/3}(1-\zeta)^{2/3} d\zeta \end{aligned}}$$

$$\frac{u^2}{2gr_0} = -\frac{1}{2}\left(1-\frac{r_0}{r}\right)^2 + n\left[\frac{2\pi}{\sqrt{3}} - \frac{3}{2}f_1\left(\frac{r_0}{r}\right) - 6f_2\left(\frac{r_0}{r}\right)\right]$$
$$+n^2\left[\frac{27}{32}\left(\frac{r}{r_0}\right)^{2/3}\left(1-\frac{r_0}{r}\right)^{8/3} + \frac{9\pi}{2\sqrt{3}} - \frac{9}{4}f_3\left(\frac{r_0}{r}\right) - 9f_4\left(\frac{r_0}{r}\right)\right]$$

$$\frac{u}{\sqrt{2gr_0}} = \left\{n^2\left[\frac{27}{32}\left(\frac{r}{r_0}\right)^{2/3} \quad\right] + n\left[\ - \ - \ \right] - \frac{1}{2}\left(1-\frac{r_0}{r}\right)^2\right\}$$

$$\frac{\Theta r}{u} = \frac{ng}{\sqrt{gr_0}}\,\frac{r}{\left(\frac{r}{r_0}-1\right)^{2/3}}$$

$$\Theta = ng\left(\frac{r}{r_0}-1\right)^{-2/3}\left\{n^2\left[\frac{27}{16}\left(\frac{r}{r_0}\right)^{2/3}\left(1-\frac{r_0}{r}\right)^{8/3} + \frac{9\pi}{\sqrt{3}} - \frac{9}{2}f_3\left(\frac{r_0}{r}\right) - 18f_4\left(\frac{r_0}{r}\right)\right]\right.$$
$$\left. + n\left[\frac{4\pi}{\sqrt{3}} - 3f_1\left(\frac{r_0}{r}\right) - 12f_2\left(\frac{r_0}{r}\right)\right] - \left(1-\frac{r_0}{r}\right)^2\right\}^{1/2}$$

$$\left[u^2 + r^2\left(\frac{d\theta}{dt}\right)^2\right] - 2g\frac{r_0^2}{r} = 0 \qquad \text{at } r = r_1$$

$$r\left[r\left(\frac{d\theta}{dt}\right)^2 - g\frac{r_0^2}{r^2}\right] - g\frac{r_0^2}{r}$$

$$= rg\left[\frac{r_0^3}{r^3} - 2\frac{r_0^2}{r^2} + \frac{3n}{2}\left(\frac{r_0}{r}\right)^3\left(\frac{r}{r_0}-1\right)^{4/3} + 6n\left(\frac{r_0}{r}\right)^3\left(\frac{r}{r_0}-1\right)^{1/3}\right.$$
$$\left. + n^2\frac{9}{16}\left(\frac{r_0}{r}\right)^3\left(\frac{r}{r_0}-1\right)^{8/3} + n^2\frac{9}{2}\left(\frac{r_0}{r}\right)^3\left(\frac{r}{r_0}-1\right)^{5/3} + n^2\, 9\left(\frac{r_0}{r}\right)^3\left(\frac{r}{r_0}-1\right)^{2/3}\right]$$

$$0 = -\left(1-\frac{r_0}{r}\right)^2 + n\left[\frac{4\pi}{\sqrt{3}} - 3f_1\left(\frac{r_0}{r}\right) - 12 f_2\left(\frac{r_0}{r}\right)\right] + n^2\left[\frac{27}{16}\left(\frac{r}{r_0}\right)^{2/3}\left(1-\frac{r_0}{r}\right)^{8/3} + \frac{9\pi}{\sqrt{3}}\right.$$

$$\left. - \frac{9}{2} f_3\left(\frac{r_0}{r}\right) - 18 f_4\left(\frac{r_0}{r}\right)\right]$$

$$+ \left(\frac{r_0}{r}\right)^2 - 2\left(\frac{r_0}{r}\right) + n\left[\frac{3}{2}\left(\frac{r_0}{r}\right)^2\left(\frac{r}{r_0}-1\right)^{4/3} + 6\left(\frac{r_0}{r}\right)^2\left(\frac{r}{r_0}-1\right)^{1/3}\right] + n^2\left[\frac{9}{16}\left(\frac{r_0}{r}\right)^2\left(\frac{r}{r_0}-1\right)^{8/3}\right.$$

$$\left. + \frac{9}{2}\left(\frac{r_0}{r}\right)^2\left(\frac{r}{r_0}-1\right)^{5/3} + 9\left(\frac{r_0}{r}\right)^2\left(\frac{r}{r_0}-1\right)^{2/3}\right]$$

$$\boxed{\begin{aligned} 1 = {} & n\left[\frac{4\pi}{\sqrt{3}} - 3f_1\left(\frac{r_0}{r}\right) - 12 f_2\left(\frac{r_0}{r}\right) + \frac{3}{2}\left(\frac{r_0}{r}\right)^{2/3}\left(1-\frac{r_0}{r}\right)^{4/3} + 6\left(\frac{r_0}{r}\right)^{5/3}\left(1-\frac{r_0}{r}\right)^{1/3}\right] \\ & + n^2\left[\frac{27}{16}\left(\frac{r}{r_0}\right)^{2/3}\left(1-\frac{r_0}{r}\right)^{8/3} + \frac{9\pi}{\sqrt{3}} - \frac{9}{2} f_3\left(\frac{r_0}{r}\right) - 18 f_4\left(\frac{r_0}{r}\right)\right. \\ & \left. + \frac{9}{16}\left(\frac{r}{r_0}\right)^{2/3}\left(1-\frac{r_0}{r}\right)^{8/3} + \frac{9}{2}\left(\frac{r_0}{r}\right)^{1/3}\left(1-\frac{r_0}{r}\right)^{5/3} + 9\left(\frac{r_0}{r}\right)^{4/3}\left(1-\frac{r_0}{r}\right)^{2/3}\right] \end{aligned}}$$

$$M\Theta = -c\,\frac{dM}{dt}$$

$$-\frac{dM}{M} = \frac{1}{c}\,\Theta\, dt$$

$$\log\frac{M_0}{M_1} = \frac{1}{c}\int_{r_0}^{r_1}\frac{\Theta\, dr}{\left(\frac{dr}{dt}\right)}$$

$$= \frac{ng}{c\sqrt{g r_0}}\int_{r_0}^{r_1}\frac{dr}{\left(\frac{r}{r_0}-1\right)^{2/3}}$$

$$= \frac{n}{c}\sqrt{g r_0}\int_1^{r_1/r_0}\frac{d\eta}{(\eta-1)^{2/3}} = \boxed{\frac{3n}{c}\sqrt{g r_0}\left(\frac{r_1}{r_0}-1\right)^{1/3} = \log\frac{M_0}{M_1}}$$

［Ｇｅｎｅｒａｌ Ｉｎｆｏｒｍａｔｉｏｎ］
书名＝钱学森力学手稿　　９
作者＝钱学森著
页数＝１９２
ＳＳ号＝１３２９５５５９
出版日期＝２０１３．０２

前言

目录